UNIVERSITÀ DEGLI STUDI DI UDINE

Dipartimento di Scienze Mediche e Biologiche

CORSO DI DOTTORATO DI RICERCA IN SCIENZE E TECNOLOGIE CLINICHE
XXVIII CICLO

TESI DI DOTTORATO DI RICERCA

CDK6 controls platinum sensitivity *via* the regulation of FOXO3/ATR: a new actionable pathway for ovarian cancer patients

DOTTORANDA
Dott.ssa Alessandra Dall'Acqua

RELATORE
Prof. Francesco Curcio

CORRELATORI
Dott. Gustavo Baldassarre
Dott.ssa Monica Schiappacassi

COORDINATORE
Prof. Giuseppe Damante

Anno Accademico 2014/2015

This PhD work was done
at Centro di Riferimento Oncologico (CRO, National Cancer Institute)
of Aviano, in the Division of Experimental Oncology 2
directed by Dr. Gustavo Baldassarre.

TABLE OF CONTENTS

ABSTRACT

High Grade Epithelial Ovarian Cancers (HGEOCs) consist in a heterogeneous group of tumors. Late diagnosis and drug-resistant recurrences make HGEOCs the most aggressive among the gynecological malignancies. The central role played by CDKs (Cyclin-Dependent Kinase) in several cellular mechanisms, such as control of cell cycle progression, DNA repair, transcription and apoptosis, make them attractive targets to overcome drug-resistance in HGEOCs. Using the RNA interference technology (targeting 23 members of the CDKs family) we performed a functional genomic screening by which we have identified CDK6 as the CDK most significantly involved in platinum sensitivity. The effect of CDK6 silencing on the sensitivity to both carboplatinum (CBDCA) and cisplatin (CDDP) was confirmed in a panel of EOC cell lines using multiple shRNAs. Next, the use of CDK6 dominant negative $CDK6^{D163N}$ and constitutively active $CDK6^{R31C}$ mutants demonstrated that CDK6 kinase activity is necessary to protect from platinum-induced death. Accordingly, an orally active CDK4/CDK6 inhibitor, PD 0332991, was able to sensitize EOC cells to CBDCA or CDDP treatment both *in vitro* and *in vivo*, in a CDK6-dependent and CDK4-independent manner. To understand the molecular mechanism whereby CDK6 regulates platinum-induced cell death in HGEOC we focused on CDK6 specific phosphorylation targets demonstrating that the transcription factor FOXO3 is a relevant downstream target of CDK6. FOXO3a downregulation sensitizes HGEOC cells to platinum while FOXO3a overexpression in CDK6 silenced cells was able to rescue the effect of CDK6 silencing on platinum-induced cell death. Functional and biochemical analyses showed that upon platinum exposure, Cyclin D3-CDK6 complex binds and phosphorylates FOXO3 on Serine 325, preventing FOXO3 degradation and promoting FOXO3 nuclear translocation. We showed that CDK6/FOXO3 axis is necessary to control the DNA damage response in HGEOC cells through the regulation of ATR/CHK1 pathway, and using a chromatin immunoprecipitation approach we demonstrated that FOXO3 binds the ATR promoter confirming the role of FOXO3 and CDK6 as upstream mediators of ATR transcription upon DNA damage. Accordingly, the silencing of both CDK6 or FOXO3 induced ATR downregulation, decreased CHK1 phosphorylation and increased platinum dependent-cell death via the induction of the so-called Premature Chromosome Condensation (PCC) mechanism by which cells undergo to death when the ATR/CHK1 pathway is inhibited. In accord with these findings, high CDK6 and FOXO3 expression levels predict poor survival of EOC patients further increasing the translational relevance of this work. Therefore, CDK6 represents an actionable target that could be exploited to improve platinum efficacy in HGEOC patients.

INTRODUCTION

1. 1 Epithelial Ovarian Cancers (EOCs)

Epithelial Ovarian Cancers (EOCs) represent the fourth commonest cause of female cancer death in the developed world and the estimated annual incidence of this disease worldwide is just over 220.000 individuals (Jayson et al., 2014). In the 75% of the cases EOCs are spread out into the peritoneal cavity at the time of diagnosis and for this reason they are described in literature as "silent killer". The International Federation of Gynecology and Obstetrics (FIGO) has recently updated the staging system and proposes a four-steps staging for EOCs: I) Disease limited to ovaries only; II) Disease extended to pelvis, affecting tubes and uterus; III) Disease spread to the abdominal cavity and lymph nodes; IV) Distant metastasis (Prat, 2015). Molecular and morphological analysis divide EOCs in two main categories (type I and type II) specified by different driver mutations and different prognoses (Jayson et al., 2014; Lim and Oliva, 2013; Shih and Kurman, 2004). Type I ovarian tumors, that include low-grade serous, mucinous, endometrioid, malignant Brenner tumor and clear cell tumors develop in a stepwise manner from well-recognized precursors and show more indolent behavior with low proliferative index throughout their course. They are associated with distinct molecular changes such as mutation in BRAF and KRAS for serous tumors, KRAS for mucinous tumors and β -catenin and PTEN mutations for endometrioid tumors (Cancer Genome Atlas Research Network, 2011; Jayson et al., 2014). The largest type II group composed by high-grade epithelial ovarian cancers (HGEOCs), includes high-grade serous, high-grade endometrioid and undifferentiated tumors that are rarely associated with a morphologically recognizable precursor lesion. These types of tumors present as clinically aggressive neoplasms that spread rapidly, metastasize early and are highly aggressive. They are characterized by genomic instability, DNA copy number abnormalities and distinct recurrent mutation in p53, BRCA1, BRCA2, NF1 and RB1. Moreover homologous recombination repair pathways are defective in roughly 50% of HGSOC (High-Grade Serous Ovarian Cancer) and NOTCH and FOXM1 signaling are implicated in the pathophysiology of serous tumors (Cancer Genome Atlas Research Network, 2011; Jayson et al., 2014; Patch et al., 2015). Standard of care for patients combines radical surgery followed by platinum-based chemotherapy. Surgery that includes a total hysterectomy, bilateral salpingo-oophorectomy, tumor debulking and omentectomy has the purpose to provide a histopathological diagnosis and to establish the FIGO stage. The standard chemotherapy is based on platinum drug (cisplatin or carboplatin) in association with a second compound (i.e. taxanes). The anticancer activity exploited by platinum results in an interlaced signaling pathway that plays its action both in the nucleus and cytoplasm. Yet, the cytotoxic effect seems to be primarily due to cross-linking within and between DNA strands and subsequent single-

strand and double-strand breaks. The double-strand breaks require repair by the error-prone non-homologous end-joining pathway (G1 phase) or conservative repair through error-free homologous recombination (S and G2 phase) (Cooke and Brenton, 2011). A limited DNA damage results in cell cycle arrest in S and G2 phases with the aim to re-establish DNA integrity and to prevent potentially abortive or abnormal mitosis. On the contrary, when DNA damage is extended, cells are driven to apoptosis as a consequence of tumor suppressor p53 activation. The activation of p53, in turn, leads to transcriptional upregulation of pro-apoptotic proteins such as BAX, BAK, CD95 and TRAIL and downregulation of anti-apoptotic molecules such as BCL2, BCL-X and IAPs (Agarwal and Kaye, 2003; Galluzzi et al., 2012). In the last 20 years, only marginal improvement in terms of treatment efficacy has been observed and nearly all patients with advanced stages develop treatment-resistant disease in the 80% of the cases (Jayson et al., 2014).

1.1.1 Platinum-Resistance

Platinum resistance, acquired or intrinsic, underscores a variety of explanations including host environmental factors, genetic or epigenetic alterations as well as inaccessibility of drugs in cancer cells (Figure 1). During the last years several groups have explored the complexity of mechanisms behind the development of platinum resistance supported by whole genome sequencing data (Cancer Genome Atlas Research Network, 2011; Castellarin et al., 2013; Patch et al., 2015; Ross et al., 2013). Recently, Patch and collegues observed a range of molecular changes associated with acquired chemo-resistance that occurs under the selective pressure of platinum treatment in HGEOC. In particular reversion of BRCA1 and BRCA2 mutational status (in BRCA1 and BRCA2 deficient tumors), changes in promoter methylation in BRCA genes, structural rearrangements in tumor tissue and up-regulation of transporters that mediate the efflux of many chemotherapeutic agents were the principal findings (Patch et al., 2015). These evidences support the idea that despite their initial sensitivity to platinum some cells adapt to prevent death and continue to survive. Conversely, intrinsic drug resistance assumes that in all HGEOC a small population of platinum-resistant cancer cells exists before treatment and emerges once treatment has killed their platinum-sensitive counterpart. This results in re-growth of the tumor and low probability that will respond to further treatment with platinum drugs. Pre-existing resistance cancer cells could also explain high rates of relapse, dominated especially by a platinum refractory phenotype (Cooke and Brenton, 2011; Holmes, 2015). Clinical evidences support the theory of clonal selection for drug resistance in several cancers. For instance, point mutations in small numbers of tumor cells present at time of diagnosis in some cases of acute lymphocytic leukemia (ALL) and chronic myeloid leukemia (CML) confer resistance to imatinib (Cooke and Brenton,

2011). Genomic studies show amplification of CCNE1 gene as an early event that confers platinum resistance in ovarian cancer (Bowtell et al., 2015; Cancer Genome Atlas Research Network, 2011; Patch et al., 2015). Moreover, in HGEOC a whole exome analysis on tumors samples (Castellarin et al., 2013) revealed that the majority of mutations found in a group of relapsed patients were already present in the primary samples, supporting the idea that recurrent HGEOC arise from multiple resistant clones pre-existing at the beginning of cancer development. These findings indicate that a successful treatment of chemo-resistant or relapsed patients can be likely hampered by the clonal feature of the disease in which sensitive and resistant subclones pre-exist from early events of tumor development.

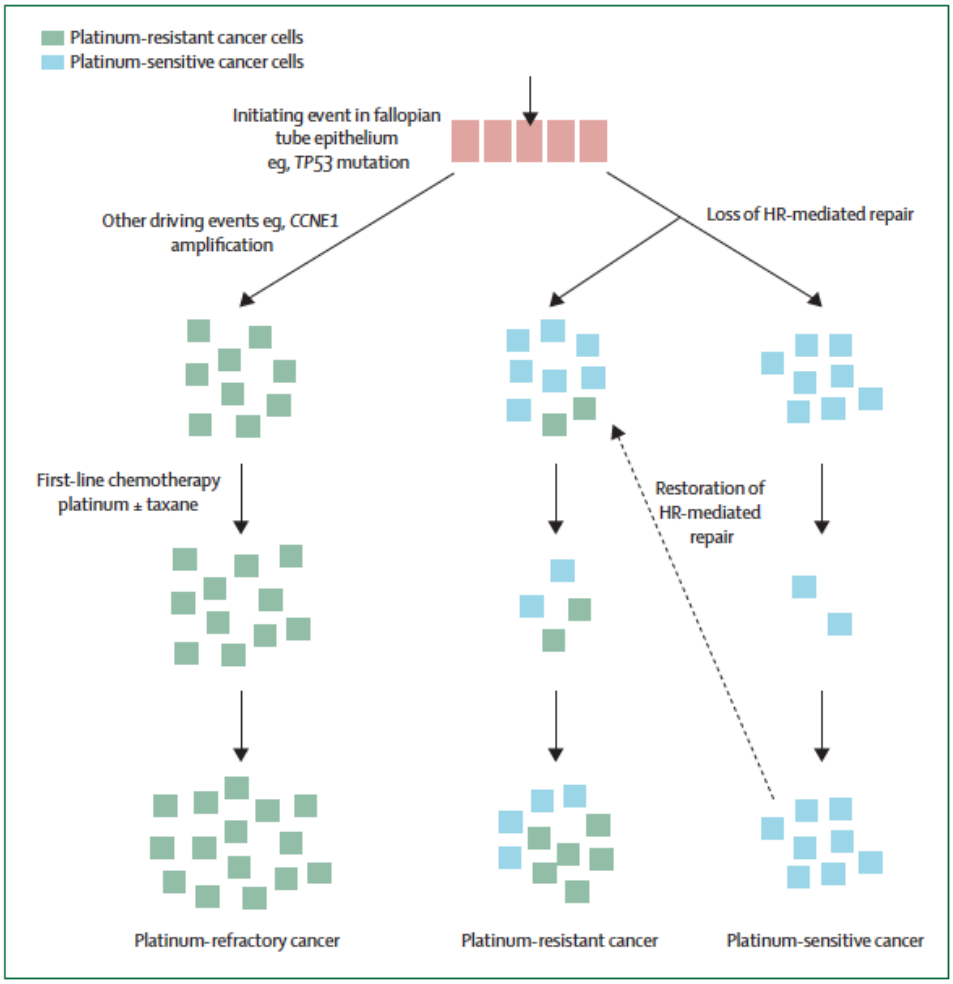

Figure 1: Model of intrinsic or acquired chemo-resistance in HGEOC. As indicated by the green squares platinum resistant cells exist before treatment and emerge once treatment has killed their platinum-sensitive counterpart. (Cooke and Brenton, 2011).

Furthermore, relapsed chemo-resistance HGEOCs lacking recurrent actionable mutations suggest that the prevention of clinical relapse rather than design of specific personalized therapy in relapsed patients should be pursued to improve patient' survival. Interestingly, a distinct subgroup of HGEOC, represented by patients carrying BRCA1/2 mutations, is particularly sensitive to platinum and usually displays a better prognosis (Cancer Genome Atlas Research Network, 2011; Jayson et al., 2014; Patch et al., 2015). Clinical evidences demonstrated that HGEOC patients carrying BRCA1/2 mutations could benefit from the use of specific targeted therapies (i.e. PARP inhibitors) used alone (Audeh et al., 2010; Chan and Mok, 2010; Kaufman et al., 2014) or especially in combination with platinum (Oza et al., 2015), supporting the use of combination therapies (i.e. a targeted agent plus traditional chemotherapy) as a valid therapeutic approach in selected groups of EOC patients.

1.2 Functional Genomic

Functional genomic is an interesting approach to identify new druggable targets to overcome drug resistance in several type of tumors and especially in ovarian cancer. Functional genomic experiments typically utilizes large-scale, high-throughput assays to measure and track many genes or proteins in parallel under different experimental or environmental conditions. Two are the traditional approaches in functional genomic. Forward genetics starts with a phenotype of interest, for instance obtained by screening a collection of mutants, and aims to identify the responsible gene. Conversely, reverse genetics takes a defined mutant, for example a knockout mouse, and looks for the functional consequence of this genetic change (Nijman, 2015). The genetic concept of synthetic lethality, in which the silencing of multiple genes or the combination between gene depletion and drug treatment results in cell death, provides in fact a powerful tool to design novel therapeutic strategies to kill cancer cells (Lord and Ashworth, 2013). Using the RNA Interference technology (RNAi) it has become feasible to systematically identify synthetic lethal interactions in human cells, and a variety of different screening strategies are applied nowadays (Pathak et al., 2014; Sethi et al., 2012; Tan et al., 2013). The main advantage of genome-wide RNAi screening is their ability to discover previously uncharacterized or unsuspected genes whose silencing induces changes in cell viability in term of death or survival. They require high-throughput tools such as liquid handling robot, data acquisition platforms, complex computational analyses and a set of constructs to target specific pathways (i.e. shRNA or siRNA libraries) and can be performed in a single well or in pooled format (Alvarez-Calderon et al., 2013). Most of the chemical genetic screens using RNAi have been made to identify suppressors or enhancers of anticancer agents. Such modifiers may serve as biomarkers to guide therapeutic response or may themselves be drug targets

that can potentially be employed in combination through a mechanism of synthetic lethality. This is particularly important in cancer: a combination between two compounds with different cellular targets may give the possibility to overcome treatment resistance and taking advantage from drugs with synergistic activity is possible to use lower drug concentration to achieve the same biological effect, thereby limiting side effects (Nijman, 2015).

1.3 Cell Cycle

The term “cell cycle” describes a series of tightly integrated events by which cells grow and proliferate. Cell cycle governs the transition from a quiescent status (G0) to cell proliferation and through its checkpoints controls the fidelity of the genetic transcript (Schwartz and Shah, 2005). It is in fact largely accepted that is essential for their survival that the two daughter cells receive a full complement of all the organelles and a copy of the genome correctly duplicated. Several mechanisms ensure that S phase is completed before mitosis begins and that M phase started only if the DNA has been faithfully replicated. This is possible since two Gap phases (the G1 separating the M and S phases, and the G2 between the S and M phases) are present in somatic cells and dictate the timing of cell division during which the control mechanisms principally act. Healthy cells need to decide when to divide and when to remain in quiescent status: the re-entry into the cells cycle is promoted by stimuli derived from the local microenvironment such as exposure to nutrients and mitogen activation. When cells are stimulated to enter the cycle (G1), they generally have to overcome a transition point beyond which cell progression through the cell cycle is independent of external stimuli. Once the cell had passed the restriction point it is irreversibly committed to complete cell division even if growth factor stimulation is removed. After DNA duplication (S phase), cells prepare themselves for mitosis. In G2 phase in fact, cells control that DNA has been faithful duplicated and check the internal signaling events necessary for a successful division. Several signaling pathways monitor the integrity of microtubule function to ensure the fidelity of chromosome segregation. Regulation by growth factors would be damaging for a cell, and consequently, mitosis is a growth factors-independent phase of the cell cycle. As cells exit mitosis, the cell cycle is reset, allowing the establishment of a new, competent replication state in G0 or G1 phases.

1.3.1 Cyclins and Cyclin-Dependent Kinases (CDKs)

Progression through the cell cycle is orderly driven by Cyclin-Dependent Kinases (CDKs) activity (Figure 2). CDKs that belong to serine and threonine kinases family are relatively stable and long half-life proteins whose activity depends on associations with Cyclins. Whereas Cyclins expression is regulated through the cell cycle in various ways, CDKs' activity is strictly correlated with the binding to a specific Cyclin (Belletti et al., 2005). Cyclin are expressed or are present at stable levels at different times; they are differentially sensitive to cell-cycle-regulated inhibitors; they are differentially restricted to specific subcellular locations; or they bind specifically to only some phosphorylation targets. Cyclins and CDKs are further regulated by the binding of specific CDK inhibitor proteins (CKIs) (Nigg, 2001). These inhibitors can be divided into two groups. The first INK4 group (Inhibitors of CDK4), includes p15, p16, p18 and p19 and they specifically inhibit the catalytic subunit of CDK4 and CDK6 but not the catalytic domain of other CDKs or Cyclins. In the second group, Cip/Kip inhibitors such as p21, p27, p57 affect the activity of Cyclin D, E and A-dependent kinases (Sherr and Roberts, 1999). Active complexes Cyclin-CDK phosphorylate a large number of biological substrates allowing the cell to move to the next phase of the mitotic cycle and at the same time preventing the exit. The transition through each phase of cell cycle is carried out only after the formation of the specific Cyclin-CDK complex and is followed by the fast degradation of the same, mainly due to Cyclin ubiquitin-mediated degradation (Belletti et al., 2005). Restriction point control is mediated by two families of enzymes: Cyclin D- and E-dependent kinases. The D-type Cyclins (D1, D2, and D3) interact combinatorially with two distinct catalytic partners: CDK4 and CDK6. In contrast, the loss of expression of Cyclin D constitutes a signal that forces the cell to exit from the mitotic cycle and to enter the G0. This represents a key relationship between the extracellular signaling and the machinery of the cell cycle. The activation of CDK4/6 is essential for passing the restriction point, in fact it induces the phosphorylation of retinoblastoma protein (pRB1) reducing its activity of transcriptional repressor. RB1 belongs to the tumor suppressor gene family and interacting with E2F transcription factors inhibits their activity. RB1 phosphorylation leads to the release of the transcription factor E2F, which activates a cascade of transcriptional events whose products are the limiting factor for progression through the G1 phase and the beginning of S phase (Cyclin E, CDK2, E2F, DNA Pol-α and c-Myc). This event is therefore necessary to trigger a positive feedback loop to phosphorylate RB1: the initial phosphorylation of RB1 allows transcription of cyclin E and the generation of Cyclin E-CDK2 in late G1, which catalyzes further phosphorylation of RB1.

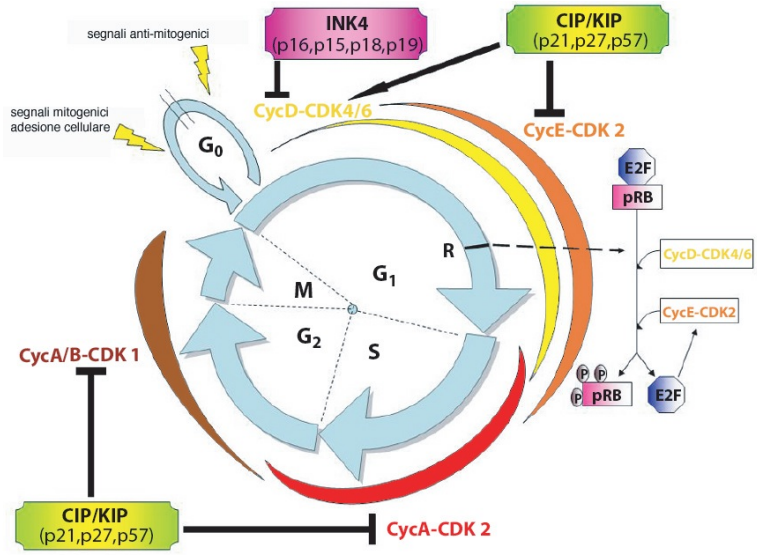

Figure 2: Schematic representation of cell cycle. Mitogenic stimuli induce cell cycle progression from G0 to G1, inducing the expression of the D-type Cyclins and a lowering of p27 expression. The subsequent activation of the Cyclin-CDK complex allows the cell to pass the restriction point (R) during the G1-S transition, due to inactivation of the protein pRB following its hyper-phosphorylation by CDK, and thus complete mitotic cycle (Belletti et al., 2005).

At this point, the progression through the cell cycle becomes independent from Cyclin D-CDK4/6 complexes. Cyclin E-CDK2 complexes also phosphorylate other substrates participating in different cellular functions and necessary for the progression towards the S phase. After a peak of activity of the Cyclin E-CDK2 complex during the G1/S transition, Cyclin E is rapidly degraded and replaced by Cyclin A: in fact, the DNA synthesis requires the activation of Cyclin A-CDK2 complex. Following Cyclin A and B drive the G2/M transition in association with CDK1. After completion of the mitotic cycle, RB1 is dephosphorylated by the phosphatase PP1, now free from inhibition operated by the Cyclin-CDK complexes, allowing the cell to enter a new G1 or G0 phase. In addition to the three interphase CDKs (CDK4, CDK6 and CDK2) and the mitotic CDK1, other CDKs members are involved in cell cycle control. For example CDK5, mostly expressed in neuronal cells, phosphorylates several cytoskeletal proteins eliciting its activity in the post-mitotic phase (Malumbres and Barbacid, 2005). CDK7 exerts its role in CDKs activation in association with Cyclin H (Larochelle et al., 2007), while CDK10 and CDK11 are involved in cell cycle progression by playing different roles during the G2/M transition (Malumbres and Barbacid, 2005). In malignant cells, altered expression of CDKs and their regulators, including overexpression of Cyclins and loss of expression of CDKs inhibitors, results in deregulated CDK activity, giving a selective growth advantage (Shapiro, 2006).

1.3.2 CDKs: not only cell cycle

CDKs control several molecular mechanisms going beyond the properly cell cycle regulation. CDK7, CDK8 and CDK9 are intimately connected with the process of RNA polymerase II dependent transcription, initiation and elongation and each of these kinases is a part of a larger multisubunit complex (Nemet et al., 2014). Also CDK12 and CDK13 play a key role in transcription. In fact, CDK12 and CDK13 participate to alternative splicing regulation (Malumbres and Barbacid, 2009) and in combination with Cyclin K phosphorylate RNA polymerase II on its carboxy-terminal domain (Lim and Kaldis, 2013) controlling the transcription of genes related to DNA damage response and snRNA (small nuclear RNA) respectively (Liang et al., 2015). CDKs play a pivotal role also in DNA replication and DNA Damage Response (DDR) (Falck et al., 2012; Wohlbold and Fisher, 2009; Yata and Esashi, 2009; Zegerman, 2015). CDK2 is strongly correlated to DNA replication: inhibition of CDK2 impairs replication in S phase as determined by retention of PCNA on chromatin, moreover CDK2 activity negatively acts on DNA replication by phosphorylating CIZ1 blocking replisome formation (Copeland et al., 2015). Other CDKs are involved in pre-replication complex formation: CDK4 and CDK6 are important to form the pre-replication complex (pre-RC) in RB-proficient cycling cells, modulating the levels of CDt1 and Cdc6. These two proteins, individually enrolled, are necessary to recruit MCMs proteins (MCM2-7) to complete the pre-replication complex formation. Inhibition of CDK4/CDK6 results in decreased Cdc6 and CDt1 RNA levels, consisting with the idea that they are regulated by E2F (Braden et al., 2008). CDK1 and CDK2 activity is also essential for the proper activation of DDR: they play a crucial role in the choice of Homologous Recombination or Double Strand Breaks repair pathway and in progression during S and G2 phases (Malumbres and Barbacid, 2009; Wohlbold and Fisher, 2009; Yata and Esashi, 2009). Early studies in budding yeast demonstrated that defect in CDK1 activity affects Irradiation-mediated Rad51-foci formation. In human RAD51-foci formation is largely restricted to S and G2 phases and this is impaired by the use of roscovidine, a CDKs inhibitor (Yata and Esashi, 2009). Moreover CDK1 and CDK2 activity is necessary to regulate multiple steps in DDR pathway and in particular controlling CHK1 full activation (Xu et al., 2012). CDK2-dependent phosphorylation on Serine 327 of CtIP is essential for physical interaction between CtIP and BRCA1 promoting HR. On the contrary CDK1 can inhibit HR: CDK1-dependent phosphorylation of BRCA2 on S3291 alters its C-terminal interaction with RAD51, impairing HR pathway. CDKs activity is crucial also for RPA recruitment: ssDNA coating with RPA is reduced following CDK inhibition. (Esashi et al., 2005; Yata and Esashi, 2009). Taken together these observations establish that CDKs play a central role in regulating DDR, but several open questions

remain on the precise role of the different CDKs in this process (Wohlbold and Fisher, 2009) and on their role(s), if any, in regulating the response to platinum.

1.3.3 Cyclin-Dependent Kinase 6 (CDK6)

In 1994 Meyerson and Harlow first investigated the role of PLSTIRE gene product, subsequently renamed CDK6. This gene located into the chromosome 7 codifies for a protein of 34 kDa that share a 71% of amino acid sequence identity with its closest homologue CDK4. It is widely know that CDK4 and CDK6 exert their principal role controlling progression through G1 phase in cell cycle. Yet, they not only phosphorylate RB1 but exert their regulatory effect on other transcriptional programs to govern cell proliferation phosphorylating several targets such as FOXM1 (Anders et al., 2011; Tigan et al., 2015). However several literature data demonstrate that CDK4 and CDK6 differ in tissue-specific functions, expression and contribute differently to tumor development, supporting the idea also for distinct, non-overlapping functions of CDK4 and CDK6. Early experiments in T-cells suggest that cell-type specific expression might explain the need of two Cyclin-Dependent Kinases and several subsequent evidences show that activation of CDK6 preceded CDK4 activation by several hours in T-cells; latter studies also demonstrate the different response of these kinases to p21 inhibitor. Furthermore CDK4 and CDK6 preferentially phosphorylate different residues on RB1 that are threonine 826 and 821 respectively CDK4 and CDK6 also display distinct patterns of sub-cellular localization. In U2OS cells, CDK6 is localized predominantly in the cytoplasm, while in T-cells it was detected both in the nucleus and in the cytoplasm with only the nuclear fraction active as an RB1 phosphorylating kinase (reviewed by Grossel and Hinds, 2006a, 2006b). These evidences in subcellular localization suggest a mechanism for regulating kinase activity, or may be indicative of the presence of cytoplasmic role or substrate(s) of CDK6 as also demonstrated by several targets phosphorylated by CDK6 (Anders et al., 2011; Kohrt et al., 2014). In the last 15 years CDK6 role was extended from the control of cell cycle progression through the G1 phase to more different functions, indicating a cell cycle-independent role of this protein involving or not its kinase activity (Figure 3). In fact recent findings have underlined unexpected functions for CDK6 and suggest a novel role for CDK6 as a transcriptional regulator. CDK6 binds to RUNX1, preventing it from binding to DNA and precluding the formation of transcriptionally active RUNX1/C/EBPa dimers showing an inhibitory activity on myeloid cells differentiation (Placke et al., 2014). CDK6 is also able to regulate transcription independently of its kinase activity, it interacts with STAT3 to control the expression of $p16^{INK4}$. CDK6 binds also to VEGFA promoter, enhancing the transcription of this factor an in

turn promoting angiogenesis (Kollmann et al., 2013). Furthermore the role of CDK6 on the development of hematopoietic lineage cells it is well established by *in vitro* and *in vivo* studies (Hu et al., 2009; Malumbres et al., 2004).

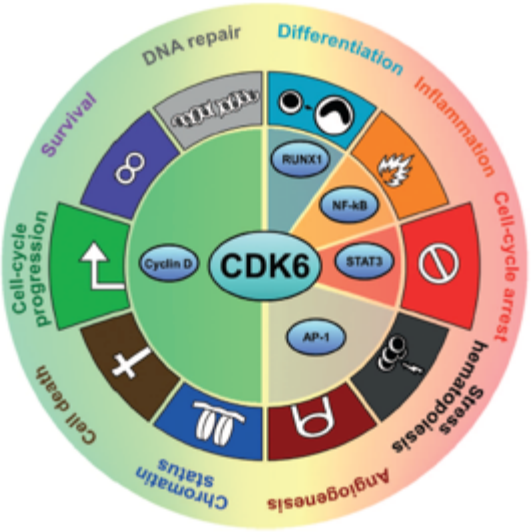

Figure 3: CDK6 functions both as a cell-cycle kinase and as a transcriptional regulator. The figure gives an overview of the network of interaction partners with which CDK6 has been implicated and indicates the outcomes of the interactions. Distinct sets of target genes regulated in either kinase-dependent and kinase-independent manner are responsible for the observed outcomes (Tigan et al., 2015).

Recently it was demonstrated a novel role of CDK6 in hematopoietic and leukemic cells, in particular these findings define CDK6 as an important regulator of stem cell activation and an essential component of a transcriptional complex that suppress EGR1 in Hematopoietic Stem Cells (HSCs) and Leukemia Stem Cells (LSCs) (Scheicher et al., 2014). Analyses of CDK6 and CDK4 expression in tumor samples have confirmed again their discrete and non-overlapping functions: certain types of tumors selectively amplify either CDK4 or CDK6. For instance, CDK4 is specifically mutated in human melanoma, while CDK6 activity was found to be elevated in squamous cell carcinomas, neuroblastoma, leukemia and lymphoma without any alteration on CDK4 (Tigan et al., 2015). Moreover there are indications that chromosomal translocations involving CDK6 locus drive b-lymphoid malignancies (Chen et al., 2009), as well as reports amplifications at this locus in glioblastoma and pancreatic cancer (Waddell et al., 2015; Wiedemeyer et al., 2010). CDK6 has recently been shown to be critical for the progression of mixed lineage leukemia (MLL)-rearranged acute myeloid leukemia and acute lymphoblastic leukemia (Tigan et al., 2015). CDK6 role in several cellular processes both in a cell cycle-dependent and independent manner involving or not its kinase activity and in a way that is not shared with CDK4 makes it a versatile player in transcriptional regulation and differentiation to the

determination of cell fate. Nowadays the myriad of mechanistic studies regarding CDK4/CDK6 deregulation in cancer has led to the development of CDKs inhibitors selective for CDK4 and CDK6 that are under study in numerous clinical trial

AIM OF THE STUDY

High Grade Epithelial Ovarian Cancer (HGEOC) is the most deadly disease among the gynecological malignancies, representing the fourth leading cause of cancer death in women in developed world. In the 75% of the cases HGEOCs are diagnosed at late stage, with tumor already spread throughout the abdominal cavity. Currently, standard therapy for HGEOCs is characterized by optimal surgical debulking followed by platinum-based therapies. Due to the fact that HGEOC is a clonal disease in which platinum-resistant subclones preexist at diagnosis, most of the patients relapse, developing platinum resistant recurrences that compromise their prognosis.

Aimed to figure out new actionable molecular partners that could allow an improvement in platinum response, this PhD work utilized a loss-of-function screening targeting the 23 members of the human Cyclin-Dependent Kinases (CDKs) family to verify the hypothesis that targeting any CDK is possible to improve platinum efficacy in HGEOC. It is well established that CDKs play a central role in several biological processes, for example in the regulation of DNA Damage Response, thus we have chosen them as an interesting target to investigate.

MATERIALS AND METHODS

2.1 Cell lines

MDAH2774 (ATCC CRL-10303), OVCAR8 (NCI 60-0507712), KURAMOCHI (JRCB0098), OVSAHO (JCRB1046), COV362 (ECACC 07071910), OV90 (ATCC CRL-11732), SKOV3 (ATCC HTB-77), Caov-3 (ATCC HTB-75), OVCAR4 (NCI 60 XXX), OVCAR3 (ATCC HTB-161), ES-2 (ATCC CRL-1978), TOV112D (ATCC CRL-11731), TOV21G (ATCC CRL-11730) cells were maintained in RPMI-1640 medium (Sigma-Aldrich Co.) supplemented with 10% heat-inactivated FBS. Immortalized Human Ovarian Epithelial Cells (IHOEC) (abm T1074) were grown in Pigrow I medium supplemented with 10% heat-inactivated FBS. 293FT cells (Invitrogen Inc.) used for lentivirus production and 293 T17 (ATCC) were grown in DMEM supplemented with 10% heat-inactivated FBS (Sigma-Aldrich Co.).

2.2 Reagents

Carboplatin (CBDCA) and cisplatin (CDDP) (TEVA Italia) were used for *in vitro* and *in vivo* experiments. PD 0332991 HCl is a pyridopyrimidine–derived cyclin-dependent kinase 4/6 inhibitor purchased from SelleckChem (S1116), cycloheximide (CHX) was purchased from Sigma and MG132 from Calbiochem.

2.3 Loss-of-function screening

Lentiviral particles were produced on 96-well plates using 293FT cells transfected using FuGENE HD Transfection Reagent with the lentiviral based sh constructs and lentiviral system vectors pLP1, pLP2, and pVSV-G. The sh-CDKs library created was used to perform the loss-of-function screening. On day one 1000 MDAH cells/well cells were seeded in 96-well plates using a robotic liquid handling Hamilton's MICROLAB STARlet. On day two cells were transfected with the specific sh-RNA or the control sh-ctrl. 72 hours post transduction cells were treated with CBDCA 140 μg/ml for 16 hours. Cell viability was evaluated 24 hours after the end of treatment using CellTiter 96 AQueous cell proliferation assay kit (Promega).

2.4 Cell viability and IC50 drugs calculation

HGEOC cells were seeded in 96-well culture plates ($1x10^3$ cells/well) and after 24 hours transduced with lentiviral shRNAs. 72 hours after transduction, plates were treated or not with CBDCA or CDDP for 16 hrs at the indicated concentrations. Cell viability was determined 24 hours after treatment using the CellTiter 96 AQueous cell proliferation assay kit (Promega). In cell

viability assays using platinum and PD0332991 combined treatment HGEOC cells were seeded in 96-well culture plates ($3x10^3$ cells/well) and after 24 hours treated with increasing doses of CBDCA or CDDP for 16 hours and with PD (using a concentration of the half of the IC50 calculated for each cell line) for 24 hours. Cell viability was determined 24 hours after the end of treatment using the CellTiter 96 AQueous cell proliferation assay kit (Promega).

2.5 Generation of platinum- resistant cell lines.

Platinum resistant cell lines were generated by treating for 2 hours MDAH cells with a CDDP dose 10-fold higher than IC50 and followed by a recovery period. After 20 cycles of CDDP treatment the resulting cell lines maintained in drug-free medium were tested and new IC50 was calculated comparing them to MDAH parental cells.

2.6 Vectors, transfections and recombinant viruses

Site directed mutagenesis was used to generate CDK6 and FOXO3 point mutants with commercial kit (QuikChange Site-Directed Mutagenesis Kit from Agilent). pcDNA3 Flag-FOXO3 was a gift from K. Guan (plasmid # 13507 Addgene Inc. Cambridge, Massachusetts). Cells were transfected using FuGENE HD Transfection Reagent (Roche Applied Science, Indianapolis, Indiana). pLKO for control and specific shRNAs were purchased from Sigma-Aldrich Co (See Table 1) (St. Louis, Missouri).

2.7 Colony Assay

MDAH parental cells and MDAH platinum resistant cells were seeded in 6-well plates (400 cells/well) mixing together parental cells and different quantity of platinum resistant cells: 0, 10, 20, 50 and 100% of the total. Cells were treated with CDDP 10 μM for 3 hours and/or with PD0332991 8 μM for 24 hours. Ten days later plates were stained with crystal violet. Plates were then photographed and colonies were counted.

2.8 Growth curve

MDAH and OVCAR8 cells were plated in 6-well plates (50.000/well) and transduced with sh-ctrl or sh-CDK6. Viable cells were counted daily in triplicate for 3 days, by trypan-blue dye exclusion method.

2.9 FACS analysis

MDAH and OVCAR8 cells were plated in 100 mm dish and silenced with sh-ctrl or sh-CDK6. Cells were then collected 72 hours post transduction and fixed in ice-cold 70% ethanol, washed twice in PBS 1x and resuspended in propiudium iodide (50 µg /ml supplemented with 100 µg/ml RNase A in PBS 1x). Stained cells were subjected to FACS analyses with FACScan instrument (BD Biosciences). Distribution of cells in G1, 2 and G2/M phases was calculated using the WinMDI2.8 software.

2.10 SA- β -Galactosidase Staining

MDAH cells were plated in 12-well plates and transduced with sh-ctrl and sh-CDK6. 72 and 96 hours post transduction cells were fixed with 2% formaldehyde and 0,2% glutaraldehyde solution for 20 min at 4°C. Fixed cells then were washed three times with PBS 1x and incubated with X-gal solution (40 mg/ml X-Gal, 2mM MgCl2, 10mM $K4Fe(CN)_6$*3H2O, 10mM $K3Fe(CN)_6$ in PBS 1x) overnight at 37°C; the positive cells turned blue and were scored as β-Gal-positive cells/field using a transmitted light microscopy with a 40x objective in 10 randomly selected fields.

2.11 Immunofluorescence

For immunofluorescence, cells plated on coverslips and fixed in PBS 4% paraformaldehyde (PFA) or tissue sections were stained with primary antibodies: γH2AX (S139), pRB1 (S780) or Ki67 and propidium iodide (5 µg/ml) for nuclear staining as reported (Berton et al., 2014). Stained cells were analyzed using a confocal laser-scanning microscope (TSP2 Leica) interfaced with a Leica DMIRE2 fluorescent microscope or using a Nikon Diaphot 200 epifluorescent microscope. Fluorescence intensity of selected regions of cell was measured with computer-assisted imaging software (LAS, Leica). Alternatively, fluorescence intensity and protein co-localization were studied using the Volocity® software (PerkinElmer).

2.12 Video time-lapse microscopy

For the evaluation of cell viability following CBDCA and PD treatment MDAH cells were seeded in 12-well plate (3×10^4) and transfected with GFP-Histone H1. After 24 hours cells were treated with CBDCA (140 ug/ml) for 16 hours. At the end of CBDCA treatment cells were treated or not with PD (8 uM). Cells were then incubated in the Leica Time Lapse AF6000LX workstation equipped with the Leica DMI 6000 motorized microscope and an environmental chamber for the proper setting of temperature humidity and CO_2 concentration. Images were collected starting at the

end of CBDCA treatment every 5 minutes for 20 hours and used to create a video for the different treatments (Movie 1: CBDCA; Movie 2: PD and Movie 3: CBDCA + PD). For higher magnification, cells were plated on glass bottom dishes (WillCo Wells BV) as previously described (Belletti et al., 2010), treated with CBDCA or CBDCA+PD as reported above and recorded using 63× immersion glycerin objective. Images were taken as described above to obtain Movie 4-CBDCA and Movie 5-CBDCA + PD.

2.13 Preparation of Cell lysates, Immunoblotting, and Immunoprecipitation.

Cell lysates were prepared using cold RIPA lysis buffer (150mM NaCl, 50mM Tris HCl [ph8], 1% Igepal, 0,5% sodium deoxycholate, 0,1% SDS*)* plus a protease inhibitor cocktail (Complete, Roche), 1 mM sodium orthovanadate, and 1 mM dithiothreitol as previously reported (Sonego et al., 2013). Differential extraction of nuclear and cytoplasmic proteins was performed as previously described (Baldassarre et al., 2005; Schiappacassi et al., 2008). Protein concentrations were determined using the Bio-Rad protein assay (Bio-Rad). For immunoblotting, equal concentrations of protein samples were separated by 4–20% SDS-PAGE (Criterion precast gel; Bio-Rad) and transferred to nitrocellulose membranes (Hybond C; Amersham). Immunoprecipitations were performed using 700-800 μg of cell lysate in HNTG buffer (20 mM HEPES, 150 mM NaCl, 10% glycerol, 0.1% Triton X-100) plus 1 μg of the indicated specific primary antibody and incubating overnight at 4°C. The immunocomplexes were precipitated by protein G agarose for another 2 hours at 4°C and separated on SDS-PAGE for western blot analysis. Immunoblotting were performed using the following primary antibodies: goat polyclonal anti-Vinculin (N-19, 1:1000), rabbit polyclonal CDK6 (1:800), goat polyclonal CDK4 (1:400), rabbit polyclonal pRB1 S780 (1:500), rabbit polyclonal PSF (1:800), rabbit polyclonal Luciferase (for IP), goat polyclonal Lamin A (for IP) (Santa Cruz Biotechnology), rabbit monoclonal FOXO3 (1:600), rabbit polyclonal Cyclin D3 (1:500), rabbit polyclonal pCHK1 S296 (1:500), rabbit polyclonal CHK1 (1:500), rabbit monoclonal H2AX (1:500), rabbit polyclonal ATR (1:500) and rabbit polyclonal ATM (1:500) (Cell signalling), rabbit monoclonal Cyclin D1 (1:1000) (Millipore), mouse monoclonal γH2AX (1:500) (Upstate Biotechnology), mouse polyclonal RB1 (BD Biosciences), rabbit polyclonal Actin (1:500), mouse monoclonal Tubulin (1:1000), mouse monoclonal Flag M2, rabbit polyclonal OP18 (1:1000), rabbit polyclonal Actin (1:1000) and V5 and HA agarose conjugated (Sigma-Aldrich Co), mouse GRB2 (1:300) (Transduction Lab), mouse monoclonal GFP (1:500) (Roche). Antibodies were visualized with appropriate horseradish peroxidase-conjugated secondary antibodies (GE Healthcare) for ECL detection (Millipore) or Alexa-conjugated secondary antibodies (Invitrogen) for Odyssey infrared detection (LI-COR Biosciences). Quantification of the immunoblots was done

using the QuantiONE software (Bio-Rad Laboratories) or the Odyssey infrared imaging system (LI-COR Biosciences).

2.14 Recombinant protein production and *in vitro* kinase assay

Production of recombinant proteins was performed by cloning FOXO3 mutants cDNAs in pGEX vector (GE Healthcare) and by transforming E. coli Bl21 pLys bacteria (Agilent) with the expression plasmid. One colony of each bacteria was inoculated into 50 ml of LB-broth with selection and let grow overnight at 37°C. Bacteria culture was diluted 1:10 in LB broth with selection and let grow at 37°C to an OD600 of = 0.9. The expression of recombinant proteins was induced by adding IPTG (Promega) to a final concentration of 1mM and cultures were incubated for additional 4 hours at 37°C. Bacterial pellet was resuspended with 8 ml of ice-cold Lysis Buffer (50mM Tris-HCl [pH 7.5], 100mM NaCl, 5mM $MgCl_2$, 10% glycerol, 0.1% Igepal, 1 mM DTT plus a protease inhibitor cocktail), sonicated (eight 10-sec pulses at 40-50% power, followed by 30-sec rest period on ice) and centrifuged at 4000 rpm for 20 minutes at 4°C. The supernatant was transferred to a fresh tube, 1 ml of glutathione-Sepharose beads (GE Healthcare) was added and samples were kept overnight at 4°C under rotation. Samples were centrifuged 5 minutes at 1300 rpm and supernatant was discarded. Beads were washed three times with 8 ml of ice-cold PBS at 4°C. To elute fusion proteins, 1 ml of elution buffer (50mM Tris-HCl [pH 8] containing 10mM reduced glutathione (Sigma) and protease inhibitors) was added to beads. Three elutions were collected. Protein concentrations were determined using the Bio-Rad protein assay (Bio-Rad) and 4 μg of each protein was used to perform *in vitro* kinase assay. FOXO3a full-length GST-tagged recombinant protein was purchased from Abnova and produced in wheat germ host. *In vitro* kinase assays were performed incubating 800 ng of recombinant Cyclin D3-CDK6 (SignalChem) or Cyclin D1-CDK4 (SignalChem) with 5 ug of FOXO3 or RB recombinant proteins as substrate and 1.5 uCi of [γ -^{32}P]ATP (PerkinElmer Life Sciences) at 30°C for 30 minutes

2.15 Protein stability

MDAH cells transduced with sh-ctrl or sh-CDK6 were treated or not with CDDP for 3 hours (50 μM) and then released in Cycloheximide (CHX, Sigma, 10 μM) containing medium for 2, 4, 6 or 8 hours. The expression of FOXO3 was then evaluated by western blot. Stability of FOXO3 mutants was performed transfecting MDAH FOXO3-sh2 stable cells with GFP-FOXO3^{WT}, GFP-FOXO3^{S325A} or GFP-FOXO3^{S325E}. 48 hours after transfection cells were treated or not with CDDP for 3 hours (50 μM) and then released in CHX (10 μM) containing medium for 2, 4, 6 or 8 hours. At

the end of CHX treatment cells were harvested and cell lysates were prepared using cold RIPA lysis buffer as already described.

2.16 Ubiquitination assay

Ubiquitination assay on FOXO3 mutants was performed by co-transfecting 293 T17 cells with GFP-FOXO3^{WT}, GFP-FOXO3^{S325A}, GFP-FOXO3^{S325E} or GFP-empty vector and HA-Ubiquitin. 48 hours after transfection cells were treated with CDDP (50 μM) and MG132 (Calbiochem, 10μg/ml) for 3 hours and cell lysates were prepared using cold RIPA lysis buffer as already described. Immunoprecipitations were performed using 500 μg of cell lysate using an anti-HA antibody. Co-immunoprecipitated proteins were then analyzed by western blot using an anti-EGFP antibody.

2.17 Mitotic Spreads

MDAH cells were transduced with sh-ctrl or sh-CDK6. After 48 or 72 hours from transduction cells were harvested and mitotic spreads protocol was performed. Cell pellet was resuspended with 5 ml of KCl 75 mM solution and incubated 10 minutes at 37°C. Cells were centrifuged and the pellet resuspended with 5 ml of 5% acetic acid solution (Ibraimov's solution). Cells were centrifuged and the pellet resuspended with 5 ml of methyl alcohol: acetic acid (3:1) solution (Fixative solution). Cells were centrifuged again and repeated the steps with Ibraimov's and fixative solution. The pellet was then resuspended in 300 μl of Fixative solution and 10 μl of the cell suspension was dropped from a height of 10 cm onto a glass slide and allowed to dry. DAPI solution (Fluoroshield ^{TM} with DAPI, Sigma-Aldrich) was spotted onto the slide and a coverslip was placed above it. A fluorescence microscope was used to count mitotic cells that had characteristic features of either a normal mitosis or PCC. At least 100 nuclei were analyzed in each condition.

2.18 Chromatin immunoprecipitation assays

After formaldehyde 37% treatment (10 min room temperature), chromatin was isolated from MDAH cells using a specific lysis buffer (5 mM PIPES pH 8.0, 85 mM KCL, 0.5% Nonidet P-40) and nuclei lysis buffer (50mM Tris-HCL pH 8.0, 10mM EDTA, 1% SDS), supplemented with protease inhibitor cocktail (Roche). After sonication (six 10-sec pulses at 30% power, followed by 30-sec rest period on ice) chromatin was pre-cleared by adding 50 μl protein A/agarose and kept for 4 hours at 4°C on a rotating plate. The supernatant containing 100 μg of chromatin was immunoprecipitated by adding the specific antibody (FLAG, FOXO3 or Luciferase and Large T

antigen as [non related IgG controls]) and kept overnight at 4°C under rotation. Then protein A-agarose beads were added for 2 hrs at 4°C. Beads were washed four times with high-salt wash buffer (50mM HEPES pH 7.9, 500mM NaCl, 1mM EDTA, 0,1% Triton X-100, 0,1% deoxycholate) and twice with TE. At the end the resin was resuspended in elution buffer (50mM Tris-HCl pH 8.0, 10 mM EDTA, 1% SDS) supplemented with 1µl of proteinase K (20 ug/ul) and incubated for 2 h at 55°C and then overnight at 65°C. DNA was purified by standard phenol:chloroform protocol and 15 ng were used to perform qRT-PCR.

2.19 qRT-PCR

Cells were treated as indicated and RNA was extracted at different time points using Trizol reagent (Invitrogen). Total RNA was quantified using the NanoDrop instrument (Thermo Fisher Scientific Inc., USA) and retro-transcribed using the AMV reverse transcriptase according to the manufacturers' instructions (Promega). Absolute quantification was evaluated by qRT-PCR, using SYBR green dye-containing reaction buffer (Real SG Master Mix 5x, Experteam) and running the reactions in the MyiQ2 Two Color Real-time PCR Detection System (Biorad). Data normalization was performed using Pol2A and GAPDH as housekeeping genes and relative expression was calculated using the mRNA concentration.

2.20 Tumor xenograft studies in nude mice

All animal experiments were performed following validated procedures (Sonego et al., 2013; Vecchione et al., 2013). MDAH xenografts were established by subcutaneously injection of $2x10^6$ cells in 0.1 ml PBS in both flanks of female athymic nude mice (Harlan Laboratories, 8 weeks-old). When tumors were 40-60 mm^3 the animals were randomly divided into groups according to experimental design. Mice were also treated with 4 intraperitoneal injections of carboplatin (20mg/Kg/dose) performed every 2 days. Tumor size was measured 3 times a week and volume was calculated (0.5 x length x width2). PD0332991 was dissolved in sodium lactate buffer (50 mmol/l, pH 4) and was given daily at 150 mg/kg by gavage for one week (5 doses). Control mice received the same amount of sodium lactate buffer solution. Animals were sacrificed 4 days after the end of each treatment. Explanted tumors were formalin-fixed and included in paraffin. Immunofluorescence on explanted tumors was performed by staining slides with pRB1 (S780), γH2AX (S139) and proliferation marker Ki67. MDAH pre-transduced xenografts were established by silencing cells with sh-ctrl or sh-CDK6, 48 hours post transduction $2x10^6$ cells were injected in 0.1 ml PBS in right (sh-ctrl) and left (sh-CDK6) flanks of female athymic nude mice. When tumors were 40-60 mm^3 the animals were treated with CBDCA (20mg/Kg/dose) performed every 2 days

for a total of 4 doses. Tumor size was with a caliper and volume was calculated (0.5 x length x width^2). Animals were sacrificed 7 days after the end of treatment.

2.21 Primary EOC collection and analyses

Human EOC samples were collected by CRO institutional Biobank, immediately frozen and stored in liquid nitrogen until needed. Informed consent was obtained from all patients. The CRO-IRB (Internal Review Board) approved this study. Frozen EOC samples were lysed in RIPA buffer as previously reported (Sonego et al., 2013) and 40 µg of total proteins were analyzed by western blot. Tissue micro-array (TMA) was built taking the most representative areas from each single case. Whole hematoxylin and eosin stained (H&E) section from each tumor block was carefully examined by the pathologist. The selected areas of interest presented more than 50% of cancer cells, without necrosis. Two cores (1 mm) were collected from each of the eligible tumor blocks and arrayed into a recipient paraffin block (35 mm×20 mm) using a semiautomatic tissue arrayer instrument (Galileo CK3500 TMA, ISENET, Milan, Italy). The presence of tumor cells on the arrayed specimens was verified using H&E staining. For IHC antigen retrieval was performed in Citrate buffer 10 mM pH6 at 96°C for 15. TMA sections were stained with primary rabbit anti-CDK6 (C21, Santa Cruz 1:800) followed by Biotinylated goat anti-rabbit/anti-mouse IgG (Dako LSAB2 System). IHC reaction was interpreted by an expert pathologist and the final intensity score was obtained taking into account the percentage of positive cells (score 0-4) and the intensity of the staining (score 1-3) as previously reported (Canzonieri et al., 2012). Scores <6 were coded as "low/moderate", >6 as "high".

2.22 Statistical analyses

The computer software PRISM (version 4, GraphPad, Inc.) was used to make graphs in all statistical analyses. In all experiments, differences were considered significant when p was ≤0.05 and statistical significance was indicated with: * $p < 0.05$, ** $p < 0.01$, *** $p < 0.001$, **** $p < 0.0001$. Statistical analyses included paired and un-paired t-tests, Mann-Whitney un-paired t-test and Kaplan-Meier test used as appropriate and as described in each figure. Statistical analyses were performed in part using the on line tool OVMARK (http://glados.ucd.ie/OvMark/index.html) using a median cutoff and analyzing all the available dataset for each specific gene analyzed (i.e. CDK4, CDK6 and FOXO3). The Log-rank test was employed to determine the significance of the association between CDK4, CDK6 and FOXO3 expression and overall survival. The Kaplan-Meyer method was used to generate survival curves. The Spearman's rank-order correlation test

was applied to measure the strength of the association between CDK6, ATR, FOXO3 and CyclinD3 expression.

	sh-RNA	*Name*	*TRC number*
NM_001786	CDK1 sh1	Cyclin–dependent kinase 1	TRCN0000000583
NM_001798	CDK2 sh1	Cyclin-dependent kinase 2	TRCN0000000587
	CDK2 sh2	Cyclin-dependent kinase 2	TRCN0000197236
NM_001258	CDK3 sh1	Cyclin-dependent kinase 3	TRCN0000230929
NM_000075	CDK4 sh1	Cyclin-dependent kinase 4	TRCN0000196698
	CDK4 sh2	Cyclin-dependent kinase 4	TRCN0000010520
NM_004935	CDK5 sh1	Cyclin-dependent kinase 5	TRCN0000195513
	CDK5 sh2	Cyclin-dependent kinase 5	TRCN0000194974
NM_001259	CDK6 sh1	Cyclin-dependent kinase 6	TRCN0000039747
	CDK6 sh2	Cyclin-dependent kinase 6	TRCN0000039746
	CDK6 sh3	Cyclin-dependent kinase 6	TRCN0000194893
	CDK6 sh4	Cyclin-dependent kinase 6	TRCN0000055435
NM_001799	CDK7 sh1	Cyclin-dependent kinase 7	TRCN0000000592
	CDK7 sh2	Cyclin-dependent kinase 7	TRCN0000196306
NM_001260	CDK8 sh1	Cyclin-dependent kinase 8	TRCN0000196702
	CDK8 sh2	Cyclin-dependent kinase 8	TRCN0000199980
NM_001261	CDK9 sh1	Cyclin-dependent kinase 9	TRCN0000000495
	CDK9 sh2	Cyclin-dependent kinase 9	TRCN0000000497
NM_003674	CDK10 sh1	Cyclin-dependent kinase 10	TRCN0000199232
NM_052987	CDK10 sh2	Cyclin-dependent kinase 10	TRCN0000001822
NM_024011	CDK11A sh1	Cyclin-dependent kinase 11A	TRCN0000006991
	CDK11A sh2	Cyclin-dependent kinase 11A	TRCN0000006992
NM_016507	CDK12 sh1	Cyclin-dependent kinase 12	TRCN0000001795
	CDK12 sh2	Cyclin-dependent kinase 12	TRCN0000001798
NM_003718	CDK13 sh1	Cyclin-dependent kinase 13	TRCN0000000704
NM_012395	CDK14 sh1	Cyclin-dependent kinase 14	TRCN0000002366
	CDK14 sh2	Cyclin-dependent kinase 14	TRCN0000002367
NM_139158	CDK15 sh1	Cyclin-dependent kinase 15	TRCN0000002096
	CDK15 sh2	Cyclin-dependent kinase 15	TRCN0000002097
NM_033018	CDK16 sh1	Cyclin-dependent kinase 16	TRCN0000197222
	CDK16 sh2	Cyclin-dependent kinase 16	TRCN0000010251
NM_002595	CDK17 sh1	Cyclin-dependent kinase 17	TRCN0000196448
	CDK17 sh2	Cyclin-dependent kinase 17	TRCN0000194654
NM_002596	CDK18 sh1	Cyclin-dependent kinase 18	TRCN0000006333
	CDK18 sh2	Cyclin-dependent kinase 18	TRCN0000006335
NM_015076	CDK19 sh1	Cyclin-dependent kinase 19	TRCN0000003140
NM_ 178432	CDK20 sh1	Cyclin-dependent kinase 20	TRCN0000199977
	CDK20 sh2	Cyclin-dependent kinase 20	TRCN0000199297
NM_004196	CDKL1 sh1	Cyclin-dependent kinase- like 1	TRCN0000006072
	CDKL1 sh2	Cyclin-dependent kinase- like 1	TRCN0000006073
NM_016508	CDKL3 sh1	Cyclin-dependent kinase-like 3	TRCN0000002376
	CDKL3 sh2	Cyclin-dependent kinase-like 3	TRCN0000002377
XM_293029	CDKL4 sh1	Cyclin-dependent kinase-like 4	TRCN0000021520
	CDKL4 sh2	Cyclin-dependent kinase-like 4	TRCN0000021521
NM_007056	SFRS16 sh1	serine/arginine-rich splicing factor 16	TRCN0000286219
	SFRS16 sh2	serine/arginine-rich splicing factor 16	TRCN0000286220
NM_198102	TRA2A sh1	transformer 2 alpha homolog	TRCN0000293989

	TRA2A sh2	transformer 2 alpha homolog	TRCN0000286623
NM_004593	TRA2B sh1	transformer 2 beta homolog	TRCN0000314984
	TRA2B sh2	transformer 2 beta homolog	TRCN0000314919
NM_011358	SFRS2 sh1	serine/arginine-rich splicing factor 2	TRCN0000000109
	SFRS2 sh2	serine/arginine-rich splicing factor 2	TRCN0000000084
NM_133477	SYNP2 sh1	synaptopodin 2	TRCN0000140276
	SYNP2 sh2	synaptopodin 2	TRCN0000138984
NM_080743	SFRS12 sh1	serine/arginine-rich splicing factor 12	TRCN0000151704
	SFRS12 sh2	serine/arginine-rich splicing factor 12	TRCN0000151194
NM_030751	ZEB1 sh1	zinc finger E-box binding homeobox 1	TRCN0000364631
	ZEB1 sh2	zinc finger E-box binding homeobox 1	TRCN0000017565
NM_001455	FOXO3a sh1	Forkhead O transcription factor 3a	TRCN0000010334
	FOXO3a sh2	Forkhead O transcription factor 3a	TRCN0000040098
	FOXO3a sh3	Forkhead O transcription factor 3a	TRCN0000040099
	FOXO3a sh4	Forkhead O transcription factor 3a	TRCN0000235488
	FOXO3a sh5	Forkhead O transcription factor 3a	TRCN0000235489
NM_007631	Cyc D1 sh1	Cyclin D1	TRCN0000295873
NM_001760	Cyc D3 sh1	Cyclin D3	TRCN0000003828
NM_001184	ATR sh1	Ataxia-telangiectasia Rad3-related	TRCN0000196538
	sh-ctrl	control	SHC002

Table 1 Table 1 reports the shRNAs used in this work. Ref seq indicates GenBank accession number, TRC indicates The RNA Consortium target sequence number.

Number	*Tumor*	*Histotype*	*Grade*	*CT/Neoadjuvant*	*TNM*
4	Primary	Mucinous	Borderline		pT3N1c
6	Primary	Serous	G3		pT2N1M1
7a	Primary	Serous	G3		pT3cN1
7b	Primary	Serous	G3		pT3cN1
8a	Primary	Serous	G3		pT3N0M1
8a1	Primary	Serous	G3		pT3N0M1
11	Primary	Serous	G3		pT3cNx
14	Primary	Serous	Borderline		pT3aNo
15	Primary	Serous	G2		pT3cN1M1
18	Primary	Serous	G1		pT2b
21	Primary	Serous	G3		pT3c
22a	Primary	Serous	G3		pT3Nx
22b	Primary	Serous	G3		pT3Nx
23a	Primary	Serous	G3		pT3cN1
23b	Primary	Serous	G3		pT3cN1
24	Primary	Serous	G3		pT3cNx
27a	Primary	Serous	G3		pT3cN1
28a	Primary	Serous	G3		pT3cN1M1
29	Primary	Serous	G3		pT3cNx
30	Primary	Serous	G3		pT3cNo
31	Primary	Serous	G3		pT3cN1
34	Primary	Serous	G3		pT3b
35a	Primary	Serous	G3		pT3cN1
37	Primary	Serous	G3		pT3c
38a	Primary	Serous	G3		pT2cN1M1
38b	Primary	Serous	G3		pT2cN1M1
40	Primary	Serous	G2		pT3cN0M1
41	Primary	Serous	G3		pT3cN1
42	Primary	Serous	G3		pT3c
43	Primary	Serous	G3		pT3b
51	Primary	Serous	G2/3		pT3c
51asc	Primary	Serous	G2/3		pT3c
57a	Primary	Serous	G2		pT3c
57b	Primary	Serous	G2		pT3c
56	Primary	Serous	G3		pT2c
60	Primary	Serous	G3		pT3cN1
63	Primary	Serous	G3		pT1cNx
64	Primary	Serous	G3		pT3cN1
71a	Primary	Serous	G3		pT3cN1
71b	Primary	Serous	G3		pT3cN1
73	Primary	Serous	G3		pT1cN1
76	Primary	Serous	G3		pT3c
79	Primary	Serous	G2		pT2c
80	Primary	Serous	G3		pT3cN1M1
83	Primary	Serous	G3		pT3cN1
84	Primary	Serous	G3		pT3bN0

86a1	Primary	Serous	G3		pT3c
86a4	Primary	Serous	G3		pT3c
86b	Primary	Serous	G3		pT3c
88a	Primary	Serous	G3		pT3cM1
88c	Primary	Serous	G3		pT3cM1
9	Primary	Serous	n.a.	Yes	ypT2aN0
26	Primary	Serous	n.a.	Yes	ypT3cN1
44a1	Primary	Serous	G3	Yes	ypT3cNx
44a2	Primary	Serous	G3	Yes	ypT3cNx
52	Primary	Serous	G3	Yes	ypT2bN1
59	Primary	Serous	G3	Yes	ypT3c
77	Primary	Serous	n.a.	Yes	pT3c
81	Primary	Serous	n.a.	Yes	pT3cN1M1
91a	Primary	Serous	n.a.	Yes	ypT3c
67	Recurrence	Serous	n.a.		
68	Recurrence	Serous	n.a.		
69	Recurrence	Serous	n.a.		
70	Recurrence	Serous	n.a.		
72	Recurrence	Serous	n.a.		

Table 2: Histo-pathological and clinical data of ovarian cancer patients. Table 2 reports grade, histotype and chemotherapy (when applied) of primary and recurrent tumor samples analyzed in Figure 21 (*n.a.: not available).

Primer	*Sequence 5' – 3'*
CDK6 R31C *forward*	GAAGGTGTTCAAGGCCTGCGACTTGAAGAACGGAGG
CDK6 R31C *reverse*	CCTCCGTTCTTCAAGTCGCAGGCCTTGAACACCTTC
CDK6 D163N *forward*	GACAAATAAAACTCGCTAACTTCGGCCTTGCCCGCATC
CDK6 D163N *reverse*	GATGCGGGCAAGGCCGAAGTTAGCGAGTTTTATTTGTC
FOXO3a S294A *forward*	CTCCAAGTGGCCTGGCGCCCCCACGTCACGCAGCAGTG
FOXO3a S294A *reverse*	CTCACTGCTGCGTGACGTGGGGGCGCCAGGCCACTTGGAG
FOXO3a S344A *forward*	GATGATGCGCCTCTCGCGCCCATGCTCTACAGCAGC
FOXO3a S344A *reverse*	GCTGCTGTAGAGCATGGGCGCGAGAGGCGCATCATC
FOXO3a S325A *forward*	GTGGCCGCCTGGCGCCCATCATGGC
FOXO3a S325A *reverse*	GCCATGATGGGCGCCAGGCGGCCAC
FOXO3a S325E *forward*	GTGGCCGCCTGGAGCCCATCATGGC
FOXO3a S325E *reverse*	GCCATGATGGGCTCCAGGCGGCCAC
FOXO3a NT *forward*	GGATCCATGGCAGAGGCACCGGCT
FOXO3a CT *reverse*	GCGGCCGCTCAGCCTGGCACCCAG
FOXO3a CT1 *forward*	GGATCCCGGAACGTGATGCTTCGCAAT
FOXO3a CT3 *forward*	GGATCCACCAGCTCCTTTAACAGCACGGT
FOXO3a CT4 *forward*	GGATCCCTCTACAGCAGCTCAGCCAGC
FOXO3a CT5 *forward*	GGATCCGCCAGCACAGTCAGTGGCCGC
FOXO3a CT6 *forward*	GGATCCGCTGACGACAGTCCCTCCCAG
FOXO3a CT7 *forward*	GGATCCGTGGAACTGCCACGGCTGACT
FOXO3a (345-674) delta *forward*	AAGCTTCCCATGCTCTACAGCAGC
FOXO3a (1-314) delta *reverse*	AAGCTTATTGGTGCGTGAACGGAA
ATR promoter -1200/-1000 *forward*	AACATAGCAAGACCTTGTCTCTA
ATR promoter -1200/-1000 *reverse*	ACTCTGTTGTTCAGGTTCTAGAG
ATR promoter -1000/-800 *forward*	AAGACAATGTATCTAACAAAAAAAA
ATR promoter -1000/-800 *reverse*	GAAAAAAGTGATGGAATGACAGCC
ATR promoter -600/-400 *forward*	TGCGGATGCCCGTAATGGTG
ATR promoter -600/-400 *reverse*	TCTGAGAGATACAGGCCAAAAG
ATR promoter -400/-200 *forward*	AAGAGGGACAAGAGCGGTGG
ATR promoter -400/-200 *reverse*	AAGCCTGGGAGGCACAGAGA
ATR promoter -200/0 *forward*	GAGAACAGCAGAGTCTGGCC
ATR promoter -200/0 *reverse*	GCCGCTACTGGCCCCGCTT
ATR promoter -1000/-805 *reverse*	AAGTGATGGAATGACAGCCAAATA
ATR promoter -890/-710 *forward*	ATGACAGAGTGGTGTTCAAGGC
ATR promoter -890/-710 *reverse*	AAGTTATGTAGTTAATCACTCAAAGTC
ATR promoter -739/-510 *forward*	CATGACTTTGAGTGATTAACTACA
ATR promoter -739/-510 *reverse*	AATATTTGAAAATGGGGTTGGAAT

Table 3: Sequence data of the primers used for site-directed mutagenesis of FOXO3 and CDK6 cDNAs, to generate FOXO3 deletion mutants, and for ATR promoter fragments' amplification.

Movies' legends

Movie 1

MDAH cells treated with CBDCA for 16 hours and then recorded for additional 20 hours

Movie 2

MDAH cells treated with PD for 16 hours and recorded for additional 20 hours

Movie 3

MDAH cells treated with CBDCA for 16 hours and then treated with PD and recorded for additional 20 hours. Transient expression of EGFP-Histone H1 protein was used to visualize cell nuclei.

Movie 4

MDAH cells treated with CBDCA for 16 hours and then recorded for additional 20 hours. Transient expression of EGFP-Histone H1 protein was used to visualize cell nuclei.

Movie 5

MDAH cells treated with CBDCA for 16 hours and then treated with PD and recorded for additional 20 hours. Transient expression of EGFP-Histone H1 protein was used to visualize cell nuclei.

RESULTS

3.1 CDK6 silencing sensitizes ovarian cancer cells to platinum.

Before to perform our screening analysis we treated MDAH 2774 cells with increasing doses of carboplatinum (CBDCA) (Fig. 1A) for 16 hours to identify the appropriate dose to use in screening experiments. Thus, performing a loss-of-function shRNAs approach, we targeted the 23 human CDKs (Fig. 1B and Table 1) (Malumbres et al., 2009) using two different shRNAs for each CDK, to test if one or more CDK specifically participates in the response to platinum of MDAH cells, used as a model of HGEOC. Taking advantage from this approach we identified CDK6 as the gene that once knocked-down, most significantly reduced cell viability in CBDCA treated cells in 5 independent experiments (Fig. 1C). To confirm screening results we have extended the analysis to four different CDK6 shRNAs. Interestingly we found that in cell viability experiments (Fig. 2A) the extent of CDK6 knock-down paralleled the efficacy of CBDCA to induce MDAH cell death and we further observed that silencing of CDK6 in untreated cells, indicated by black bars in figure 2A had minimal effect on cell viability. We also investigated whether the silencing of the CDK6-homologue, CDK4, could alter cells sensitivity to CBDCA. We did not observe changes in cell viability in CDK4 silenced cells upon platinum treatment (Fig. 2B), confirming screening results, and excluding CDK4 involvement in platinum mediated cell death. CDK6 knock-down effect was recapitulated in other HGEOC cell lines such as OVCAR8 and SKOV3, in which CDK6 silencing decreased both cis-Platinum (CDDP) (Fig. 3A) and CBDCA (Fig. 3B) half maximal inhibitory concentration (IC50) from 2- to 20-fold, depending on the drug and the cell line used.

3.2 CDK6 kinase activity protects HGEOC cells from platinum-induced cell death *in vitro*.

Based on the notions that CDK4 and CDK6 share most but not all phosphorylation targets (Anders et al., 2011) and that CDK6 plays also kinase-independent roles (Kollmann et al., 2013), we verified if the kinase activity of CDK6 participated in the regulation of platinum response. We overexpressed CDK6 wild type ($CDK6^{WT}$), CDK6 dominant negative ($CDK6^{D163N}$) mutant and CDK6 constitutively active ($CDK6^{R31C}$) mutant in OVCAR8 and MDAH cells (that express low and high levels of CDK6 respectively) (Fig. 4A and 4B). The dominant negative carries a mutation in the ATP binding pocket, whereas the constitutive active carries a mutation making it unable to bind p16/INK4 inhibitor. In both OVCAR8 and MDAH models, the expression of $CDK6^{D163N}$ reduced the survival of platinum treated cells mimicking the results obtained with CDK6 knockdown (Fig. 4C and 4D) and in OVCAR8 cells, $CDK6^{R31C}$ expression protected from CBDCA induced death (Fig. 4C).

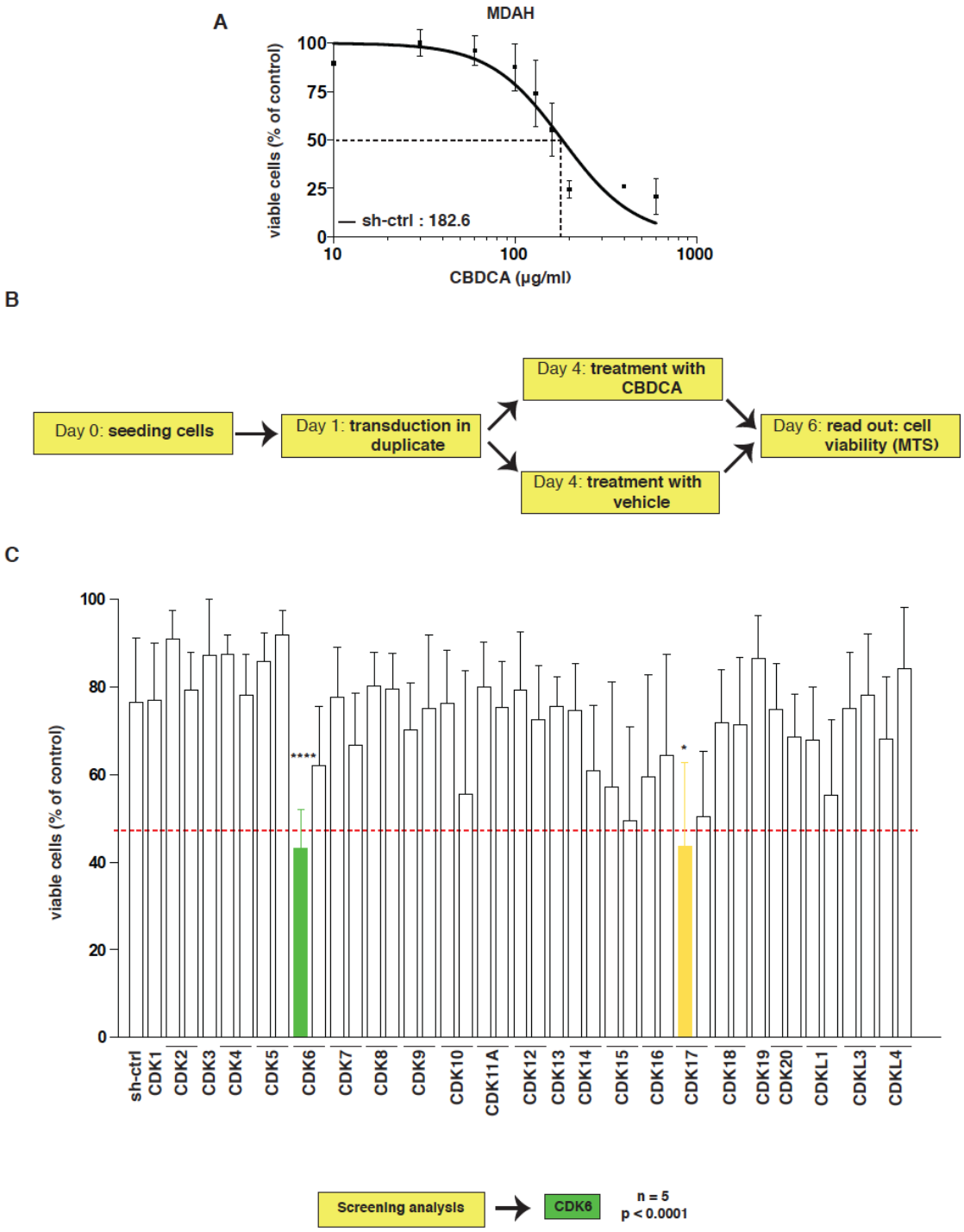

Figure 1: CDK6 knock-down sensitizes HGEOC cells to platinum induced cell death. A) Dose response curve on MDAH 2774 cells transduced with control (ctrl) shRNA and treated with increasing doses of CBDCA for 16 hours. **B)** Experimental design of the loss-of-function screening. **C)** Screening results: data represent the mean ± SD of five independent experiments performed in triplicate and are expressed as survival ratio between CBDCA treated and untreated cells. Red line indicates the pre specified cut off of significance that corresponds to the double of the standard deviation observed in sh-ctrl. Significance was calculated using the student t-test.

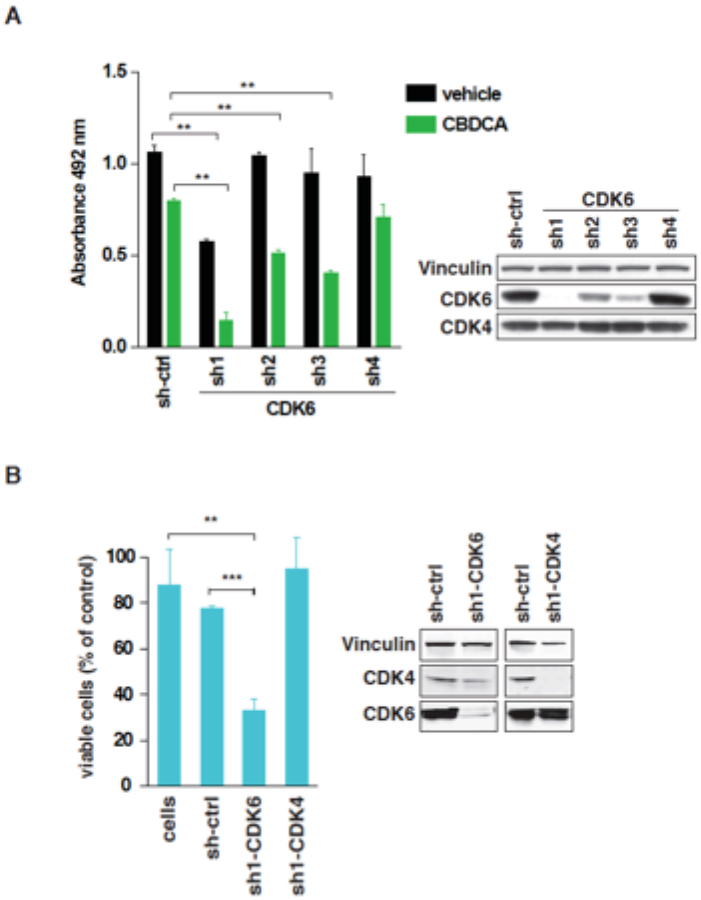

Figure 2: Validation of screening results. A) Graph reports the viability of MDAH cells transduced with ctrl and CDK6 shRNAs and then treated with CBDCA. The corresponding cell lysates were then analyzed by western blot (hereafter WB). Statistical significance was calculated using t-test. **B)** Graph reports the viability of MDAH cells transduced with ctrl, CDK6 and CDK4 specific shRNAs and then treated with CBDCA. Results are expressed as survival ratio between of CBDCA treated and untreated cells. The corresponding cell lysates were then analyzed by WB. Statistical significance was calculated using t-test.

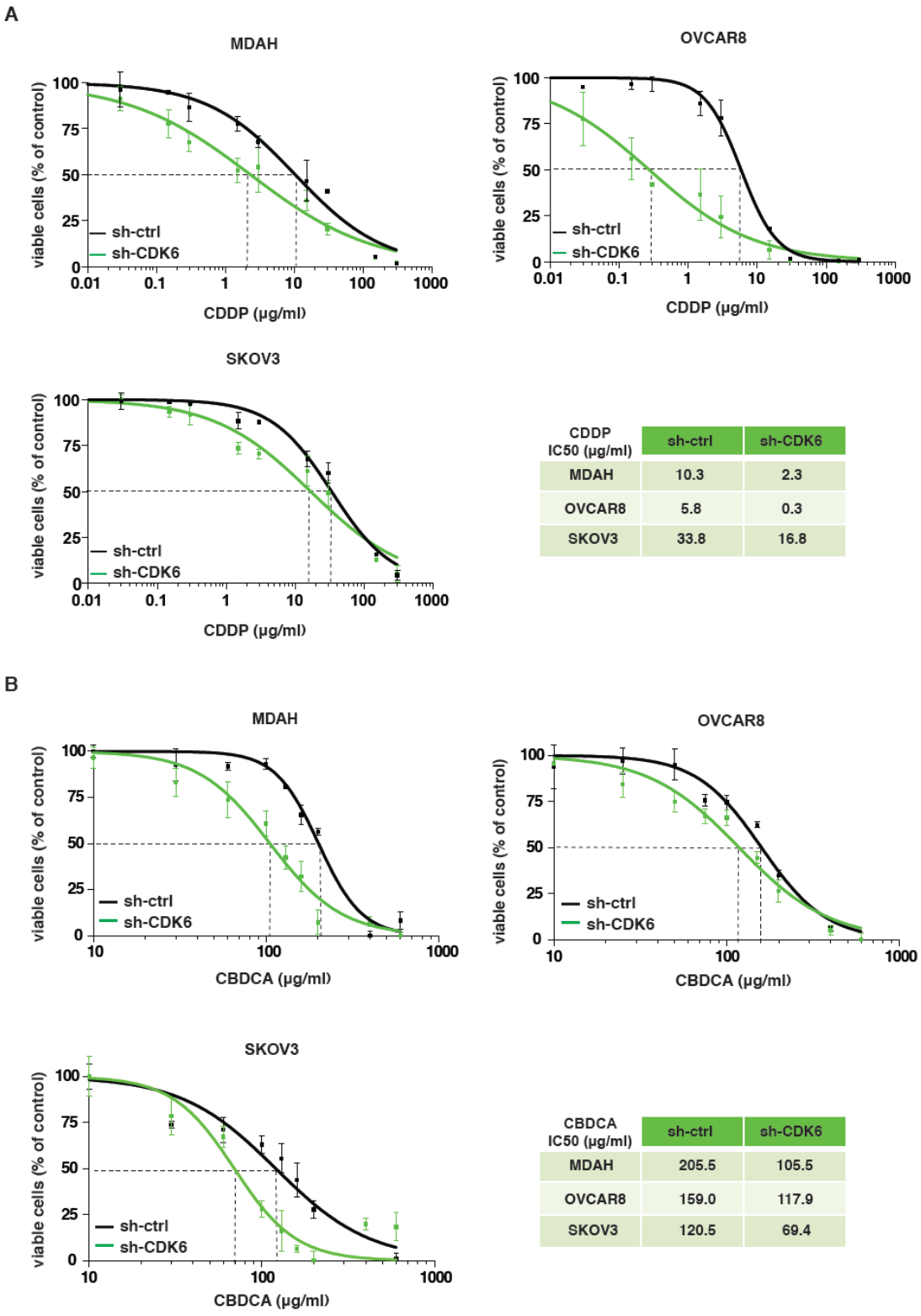

CDDP IC50 (µg/ml)	sh-ctrl	sh-CDK6
MDAH	10.3	2.3
OVCAR8	5.8	0.3
SKOV3	33.8	16.8

CBDCA IC50 (µg/ml)	sh-ctrl	sh-CDK6
MDAH	205.5	105.5
OVCAR8	159.0	117.9
SKOV3	120.5	69.4

Figure 3: CDK6 knock-down decreases CDDP and CBDCA IC50. A-B) CDDP (A) and CBDCA (B) dose response curves for the indicated HGEOC cell lines transduced with control (ctrl) or CDK6-specific shRNAs. Results are expressed as percentage of viable cells respect to untreated cells and the resulted IC50 are reported in the tables.

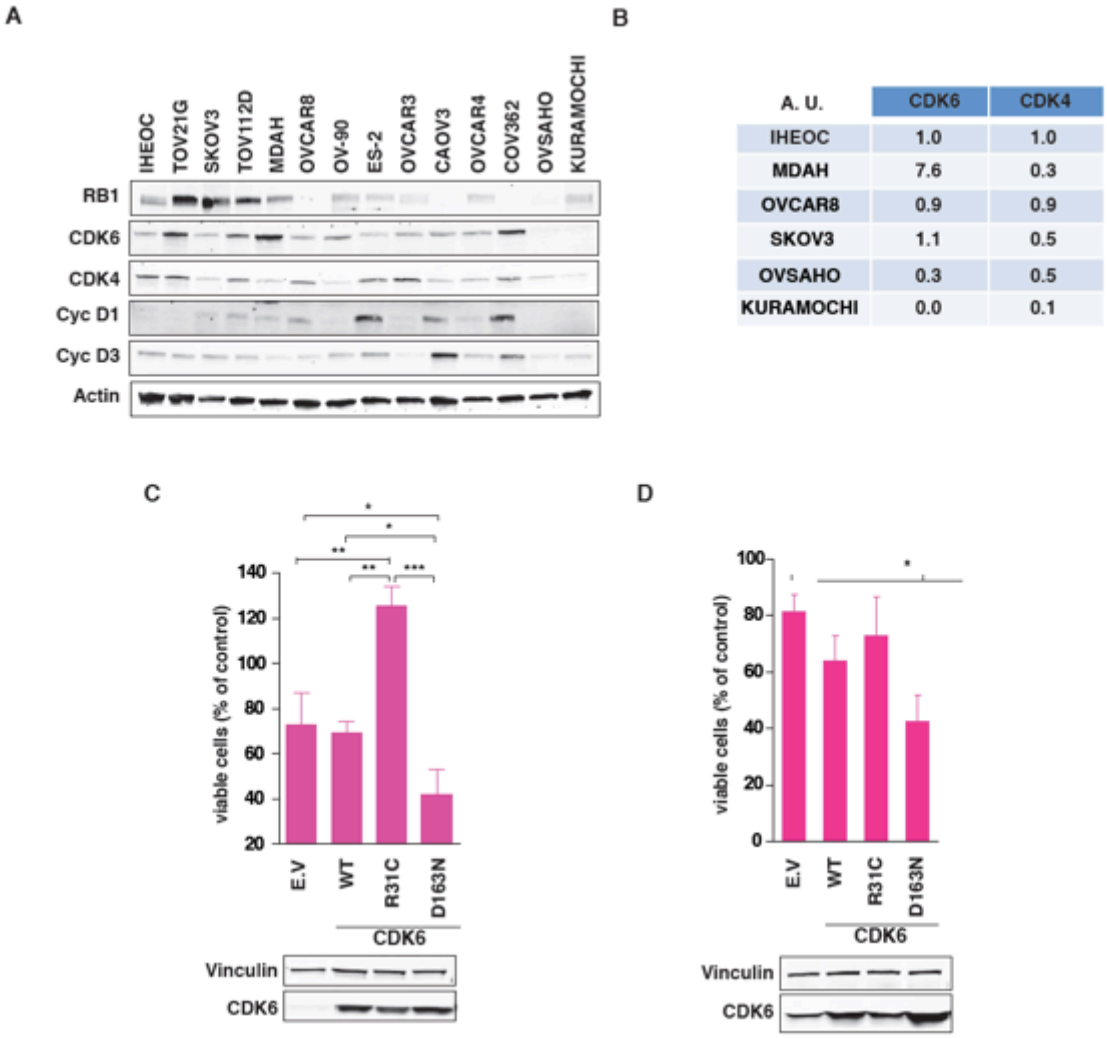

Figure 4: CDK6 kinase activity is necessary to prevent platinum-induced cell death in HGEOC. A) WB analyzing the expression of the indicated proteins in immortalized human epithelial ovarian cells (IHEOC) and in a panel of HGEOC cell lines. **B)** Quantification of CDK6 and CDK4 expression in the indicated HGEOC cell lines used for experimental analyses, compared with immortalized human epithelial ovarian cells (IHEOC). A.U. Arbitrary Unit. **C-D)** Cell viability in OVCAR8 (C) and MDAH (D) cells transfected with CDK6 wild type (WT), CDK6 constitutively active (R31C), CDK6 dominant negative (D163N) mutants or empty vector (E.V.) and treated with CBDCA. Results are expressed as survival ratio between of CBDCA treated and untreated cells. The corresponding OVCAR8 and MDAH cell lysates were then analyzed by WB. Actin and Vinculin were used as loading control. Significance was calculated using student t-test.

These results confirm the idea that CDK6 kinase activity is necessary to prevent cell death upon platinum treatment. To further confirm the involvement of CDK6 kinase activity in platinum mediated cell death, we treated a panel of HGEOC cell line with PD0332991 (hereafter PD) a specific CDK4/CDK6 kinase activity inhibitor (Toogood et al., 2005), to identify the suboptimal dose to use in combination with platinum (Fig. 5A). We then tested this compound in MDAH cells using two different schedules in combination with platinum and we observed that PD sensitized MDAH cells to CBDCA, especially when PD was administered to the cells after platinum, but not before (Fig. 5B). To verify the efficacy of PD treatment we valuated the phosphorylation status of RB1, the inhibition of CDK4/CDK6 results in fact in a decreasing of RB-pS780. In accord with previous observation (Konecny et al., 2011), we found that CDK6 levels did not correlate with the efficacy of PD in reducing HGEOC cell survival when used as single agent, in fact OVCAR8 and SKOV3 that show a similar CDK6 expression level (Fig. 4A-B), respond differently to PD treatment as single agent (Fig. 5A). Yet, CDK6 expression was necessary to mediate the effects of PD on platinum sensitivity, since PD had no effects on platinum sensitivity of KURAMOCHI and OVSAHO cells that express low/undetectable levels of CDK6 (Fig. 4A-B, 5C-D) or in MDAH cells stably silenced for CDK6 (Fig. 5E). These observations were also confirmed using time-lapse microscopy. MDAH cells treated with CBDCA and the specific CDK4/6 inhibitor PD alone or in combination, underwent massive cell death only when the combination CBDCA+PD was used (Movie 1, 2 and 3). CBDCA+PD treatment induced apoptosis in a higher number of cells respect to CBDCA alone, as demonstrated by the appearance of nuclear condensation and fragmentation and cell blebbing, looking at cells transfected with GFP-tagged Histone H1 to visualize cell nuclei in higher magnification movies (Movie 4 and 5). To test if inhibition of CDK6 kinase activity could impair the re-growth of platinum resistant clones (Sonego et al, manuscript in preparation) we performed a clonogenic assay. We seeded different combination of MDAH parental and resistant cells to mimic the HGEOC tumor heterogeneity and in these conditions we tested the efficacy of PD in increasing platinum mediated cell death (Fig. 6A and 6B). Interestingly we found that CDDP+PD combination was significantly more effective in preventing the re-growth of platinum resistant subclones.

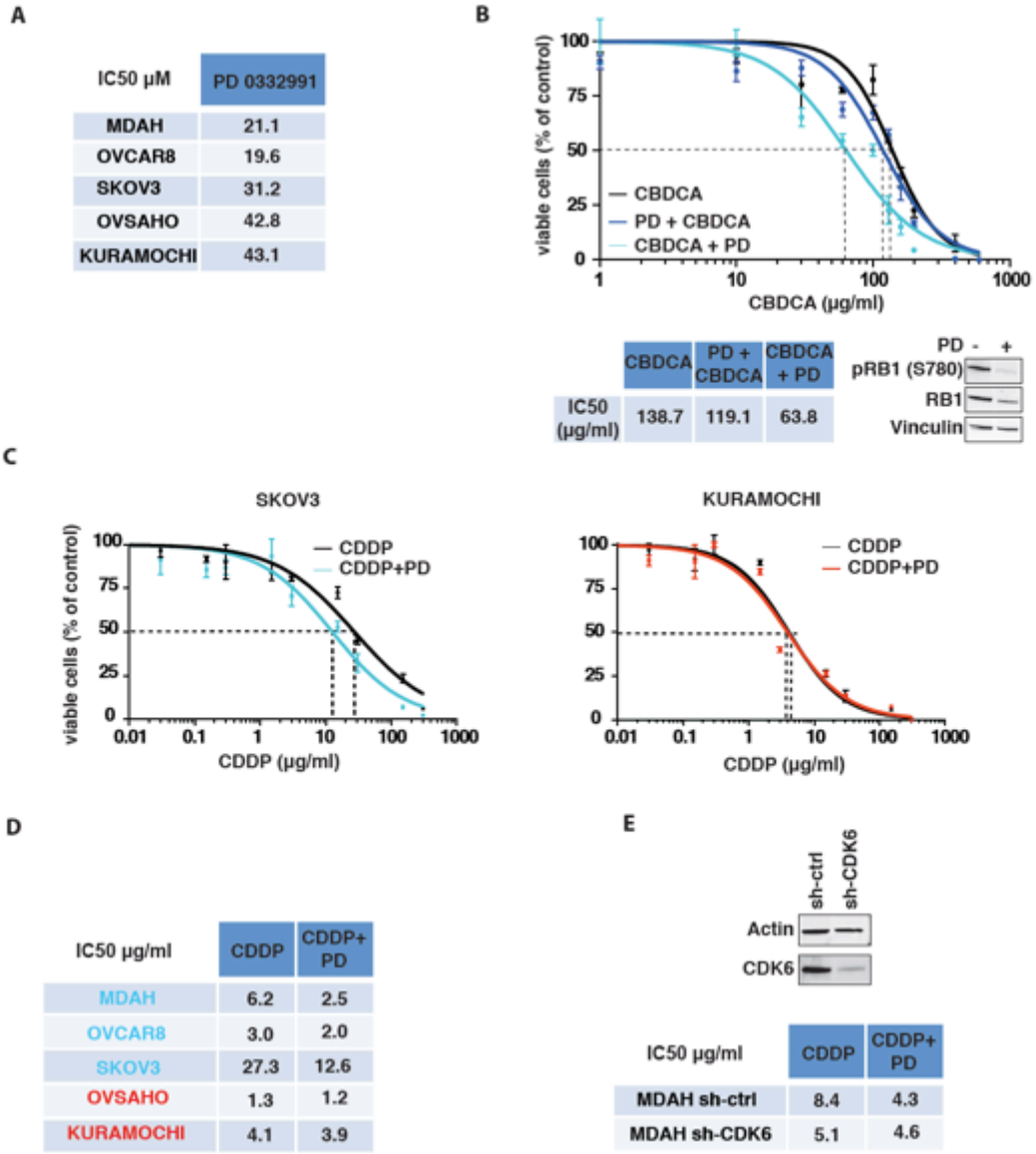

Figure 5: PD0332991 sensitizes HGEOC cells to platinum induced cell death *in vitro.* A) Table summarizing the calculated PD0332991 (PD) IC50 (µM) in the indicated HGEOC cell lines. **B)** Dose response curves of MDAH cells treated with 8 μ M PD and increasing doses of CBDCA using different schedules. In the inset is reported the expression and phosphorylation status of RB1. **C-D)** Dose response curve of SKOV3 and KURAMOCHI cells (C) treated with increasing doses of CDDP and with or without the appropriate concentration of PD (half dose of IC50 reported in figure A). Table reports the IC50 (D). **E)** MDAH cells stable silenced with ctrl and CDK6 shRNAs and then treated with CDDP alone or in the presence of PD. Table reports the calculated IC50. Cell lysates were analyzed by WB to confirm CDK6 silencing. Actin and vinculin were used as loading control.

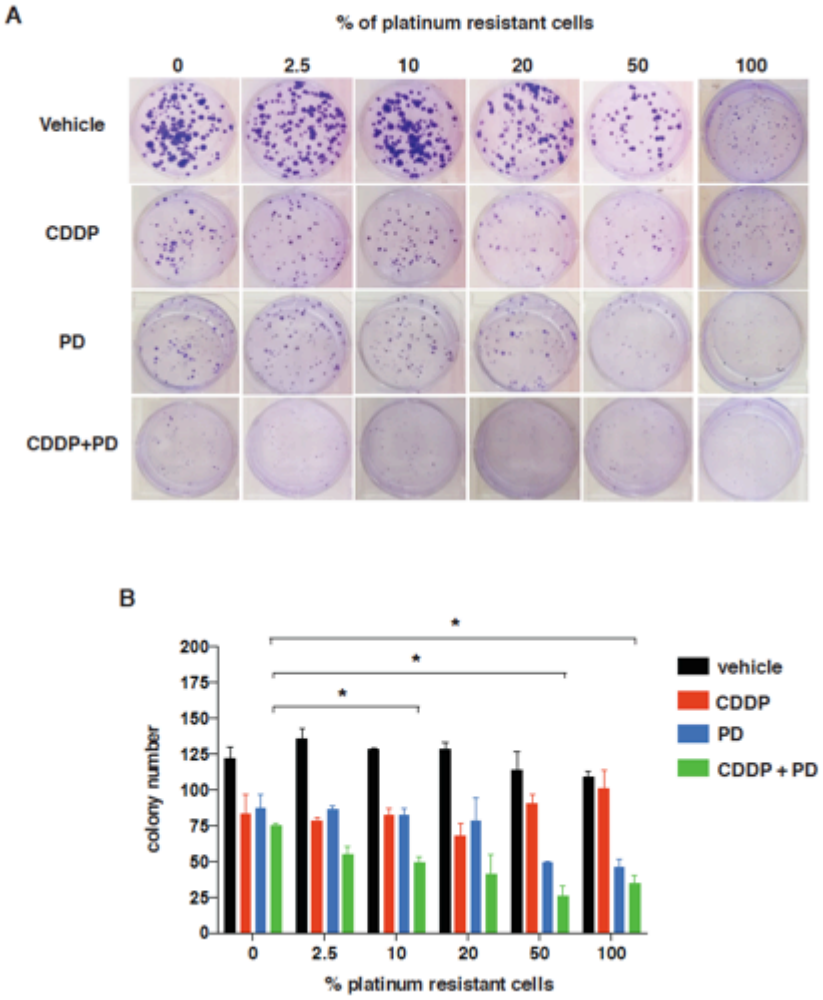

Figure 6: CDDP + PD0332991 combination sensitizes clonal growth of HGEOC cells. A) Crystal violet staining of colony assay performed using MDAH platinum resistant clones plated with parental cells in different proportions and treated with vehicle, CDDP, PD or CDDP + PD. **B)** Colony assay quantification graphed as number of colony formation. Statistical significance was calculated using t-test.

3.3 The CDK6 inhibitor PD0332991 increases platinum efficacy, also *in vivo.*

We next tested whether our *in vitro* observations could be recapitulated *in vivo*, using MDAH cells subcutaneously injected in nude mice. When tumors reached approx 50mm^3, we treated mice with CBDCA, PD or CBDCA+PD (Fig. 7A). In this setting, the sequential administration of CBDCA+PD, as indicated by the green line, significantly reduced tumor growth while the single treatments had minor effects (CBDCA red line, PD blue line) (Fig. 7B). Immunofluorescence analyses were used to evaluate the efficacy of the treatments in explanted tumors (Fig. 7C). γH2AX-pS139 staining (a marker of damaged DNA) and CDK4/6-dependent RB1 phosphorylation (pS780 staining) were used as readout of CBDCA and PD activity, respectively. As expected from the tumor volumes, the combination CBDCA+PD resulted the most effective in increasing γH2AX-pS139 and decreasing RB1-pS780 expression (Fig. 7B and 7D), with a consequent reduced proliferation, assessed by Ki67 staining (Fig. 7G). Similar results were observed using CDK6 silenced cells. We transduced MDAH cell with sh-ctrl and sh-CDK6, 48 hours post transduction we have injected these cells on the flank of the mice (sh-ctrl on the right, sh-CDK6 on the left) to assess if knock-down of CDK6 could impair tumor growth. We observed that tumor grown from sh-CDK6 MDAH cells responded significantly better than those grown from control cells to CBDCA (Fig. 8A) and displayed increased γH2AX-pS139 expression as already observed in nude mice treated with CDDP+PD (Fig. 8B and 7F). Noteworthy, CDK6 knock-down did not significantly impact on the expression of RB1-pS780 (Fig. 8B), raising the hypothesis that in platinum-treated HGEOC cells CDK6 is more implicated in the control of the DNA damage response than in cell proliferation via RB regulation.

3.4 CDK6 activity is mainly involved in DNA damage response than in cell proliferation.

To investigate the possibility that CDK6 could be more implicated in DNA damage response respect to cell cycle regulation, we evaluated the expression of CDK6 in a panel of HGEOC, by which we observed that CDK6 is predominantly expressed in the cytoplasm (Fig. 9A) and that silencing of CDK6 in MDAH cells did not alter the extent of nuclear RB1-pS780 expression (Fig. 9B), while it strongly increased the expression of γH2AXpS139 in cells exposed to CBDCA and allowed to recover for up to 8 hours (Fig. 9C and 9D). Accordingly, CDK6 knock-down did not substantially alter the proliferation of MDAH and OVCAR8 cells as it can be observed in growth curves (Fig. 9E-F) and FACS analysis of cell cycle distribution (Fig. 9G).

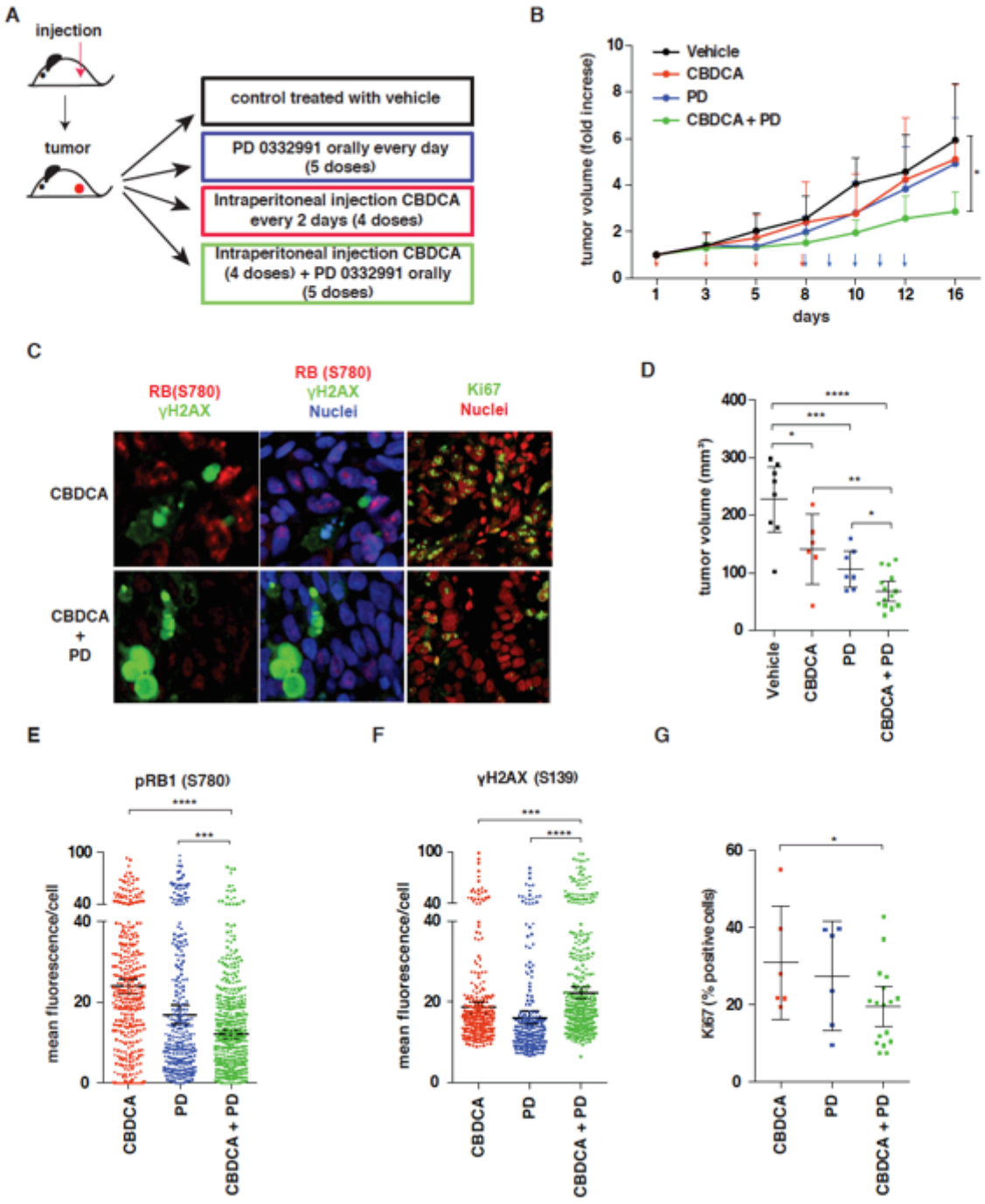

Figure 7: PD0332991 sensitizes HGEOC cells to platinum induced cell death *in vivo* A) Schematic design of *in vivo* experiments with MDAH xenografts testing the efficacy of CBDCA and PD treatments alone or in combination. **B)** Analysis of tumor growth of *in vivo* experiments described in A. Red and blue arrows indicate the days of CBDCA and PD treatment, respectively. **C)** Immunofluorescence analyses of pRB1 and γ H2AX and Ki67 expression in tumors explanted from mice treated with CBDCA (top) or with CBDCA + PD (bottom). **D)** Analysis of tumor volume of *in vivo* experiments described in A. **E-F)** Quantification of pRB1 (E) and γ H2AX (F) expression evaluated as mean fluorescence per cell in tumors explanted from mice treated as indicated. **G)** Quantification Ki67 expression evaluated as percent of positive cells in tumors explanted from mice treated as indicated. Significance was calculated using the student t-test.

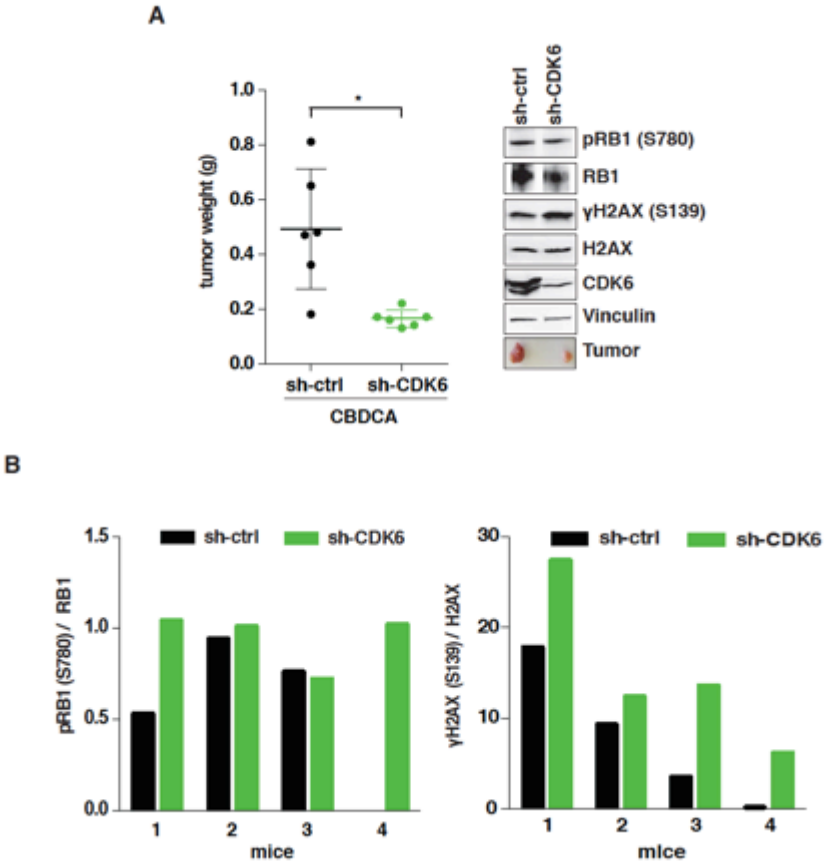

Figure 8: CDK6 knockdown sensitizes HGEOC cells to platinum induced cell death *in vivo* A) MDAH transduced with ctrl or CDK6 shRNAs were subcutaneously injected (sh-ctrl right flank and sh-CDK6 left flank) in nude mice then treated with CBDCA. Tumor volume was determined as end point and reported in the scattered dot plot. On the right typical WB analyses of RB1 and H2AX expression and phosphorylation in tumors explanted from one mouse injected as described in (A) and treated with CBDCA after tumor appearance. Vinculin was used as loading control. The macroscopic aspect of explanted tumors is shown in the bottom panel. **B)** Graphs reported the normalized quantification obtained by densitometric scanning of the blots, of phosphorylation levels of RB1 (left) and H2AX (right) of tumors explanted from 4 different mice treated as described in (A). Significance was calculated using the student t-test.

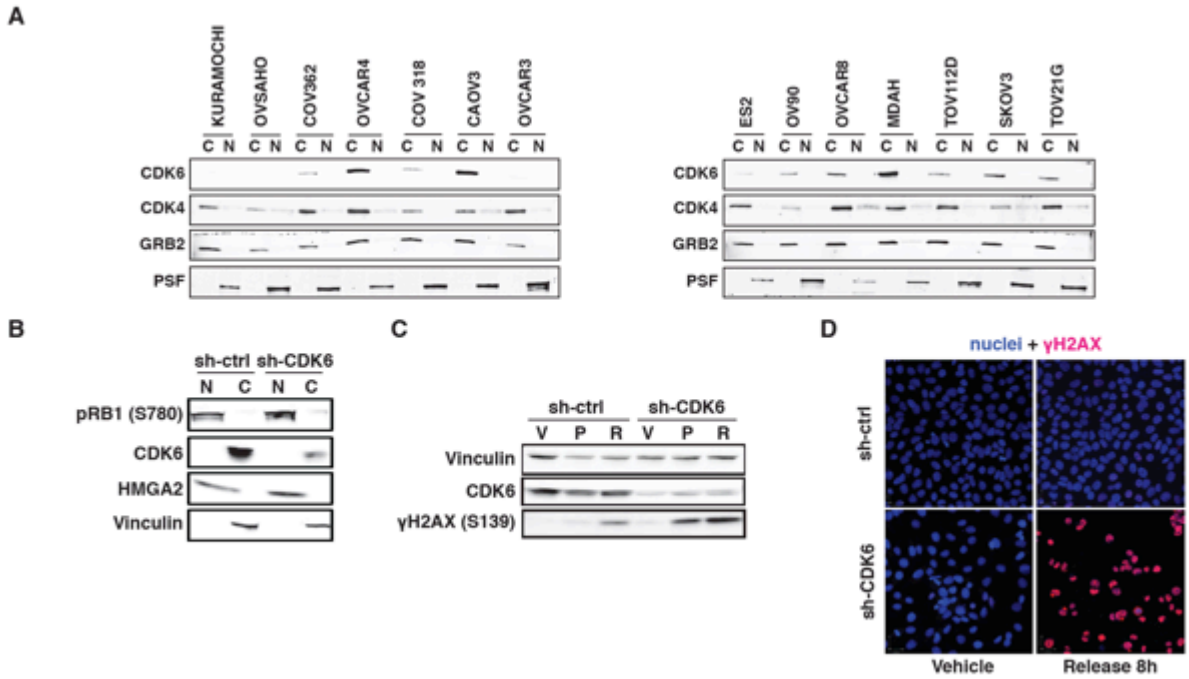

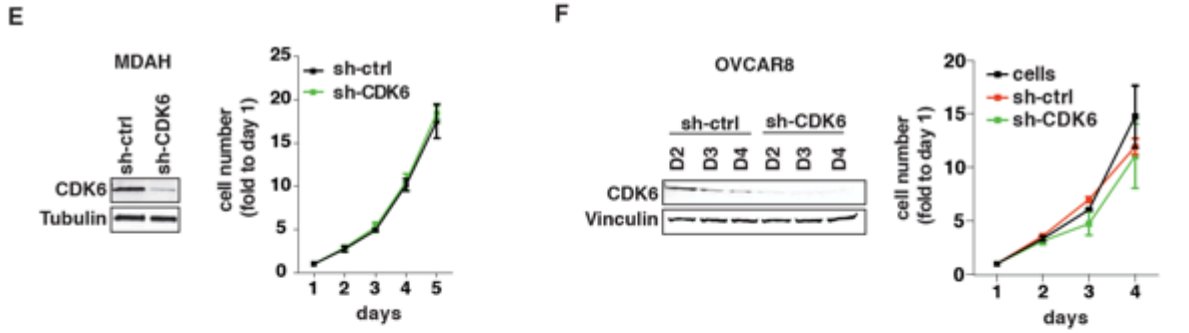

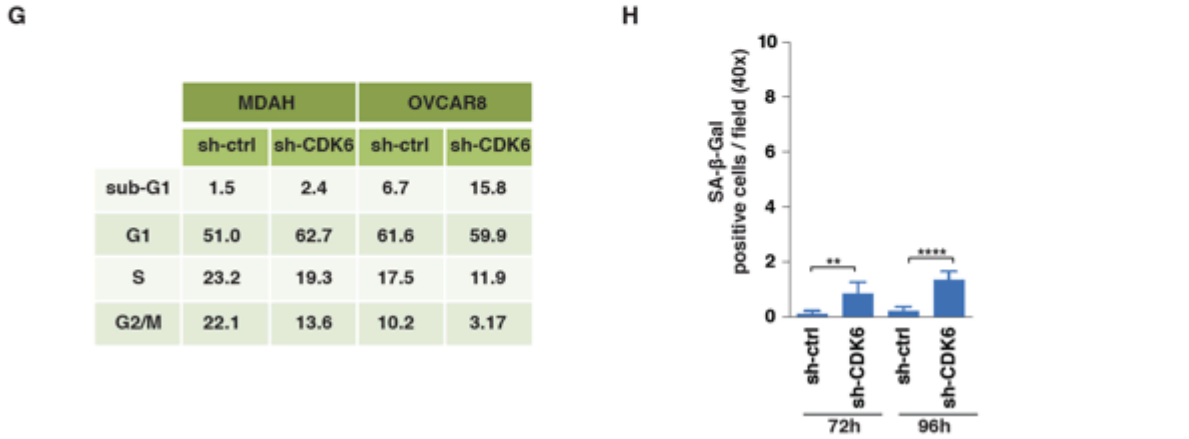

	MDAH		OVCAR8	
	sh-ctrl	sh-CDK6	sh-ctrl	sh-CDK6
sub-G1	1.5	2.4	6.7	15.8
G1	51.0	62.7	61.6	59.9
S	23.2	19.3	17.5	11.9
G2/M	22.1	13.6	10.2	3.17

Figure 9: CDK6 activity is involved in the control of the DNA damage response. A) Expression of CDK4 and CDK6 in the nuclear (N) or cytoplasmic (C) fractions of the indicated HGEOC cell lines. **B)** WB evaluating the expression of pRB1 and CDK6 in the nuclear (N) or cytoplasmic (C) fractions of MDAH cells transduced as indicated. **C)** WB evaluating the expression of γH2AX and CDK6 in MDAH cells transduced and treated as indicated. V= vehicle, P= CBDCA 16 hours, R= 8 hours release after platinum. **D)** Immunofluorescence analysis evaluating the expression of γH2AX (red) in MDAH treated as in C. Nuclei were stained with propidium iodide (blue). **E-F)** Growth curve in MDAH (E) and OVCAR8 (F) cells silenced with the indicated shRNAs. Lysates were analyzed by WB. **G)** Cell cycle distribution of MDAH and OVCAR8 cells transduced with the indicated shRNA and analyzed by FACS analyses. **H)** SA-β-Galactosidase assay in MDAH cells transduced as indicated and stained 72 and 96 hours post transduction. Results are graphed as percentage of positive cells/field counted using 40x magnification. GRB2, PSF, HGMA2, vinculin and tubulin were used as loading and fraction purity control.

Moreover the low percentage of β-Gal positive cells indicates that CDK6 knock-down had a limited impact on the induction of cell senescence (Fig. 9H), a proposed anti-tumoral mechanism of CDK4/6 inhibition in RB1 proficient cells (Anders et al., 2011; Choi et al., 2012)

3.5 FOXO3 is a CDK6-specific target able to modulate the sensitivity of HGEOC to platinum.

Data collected so far suggested that CDK6, but not CDK4, protected from platinum-induced cell death by phosphorylating, more likely in the cytoplasm, one (or more) specific target that could eventually regulate the DDR in EOC cells. Based on this hypothesis, we analyzed the recently identified panel of CDK6-specific phosphorylation targets (Anders et al., 2011). By applying criteria deriving from the above data, we selected nine proteins that were poorly phosphorylated by CDK4 and were phosphorylated by CDK6 at higher level than RB1 (Fig. 10A). Using a loss-of-function screening (Fig. 10B), we identified the transcription factor FOXO3 (also known as FOXO3a) as the only CDK6 tested target involved in the response to platinum in HGEOC cells (Fig. 10C). These data were confirmed first, with five different FOXO3-specific shRNAs (Fig. 11A) and second, by a dose response curve using the specific FOXO3 shRNAs that have given better results in term of IC50 reduction (Fig. 11B). To ascertain these observations we performed rescue experiments overexpressing FOXO3 in CDK6 knockdown cells by which we observed a complete overcame of the increased cell death induced by platinum in CDK6 silenced cells (Fig. 11C), strongly supporting the notion that FOXO3 acted downstream to CDK6 in regulating the platinum response in HGEOC cells.

3.6 Cyclin D3/CDK6 complex binds and phosphorylates FOXO3 in platinum treated cells.

We observed that FOXO3 was expressed in the majority of tested HGEOC cell lines, both in the nucleus and the cytoplasm (Fig. 11D-F). To verify whether CDK6 binds FOXO3 we performed a co-immunoprecipitation experiments, by which we have demonstrated that endogenous CDK6 interacted with FOXO3 in platinum-treated but not in untreated cells (Fig. 12A). Under the same conditions, CDK6 co-precipitated with both Cyclin D1 and D3 (Fig. 12A). CDK4 and Cyclin D1 failed to associate with FOXO3, both in treated and untreated cells (Fig. 12B-C), while Cyclin D3 bound FOXO3 in platinum-treated cells (Fig. 12C). Accordingly, only the knock-down of Cyclin D3 was able to increase the sensitivity of MDAH cells to platinum (Fig. 12D), supporting the possibility that in HGEOC cells treated with platinum the Cyclin D3/CDK6 complex regulates cell survival via the binding to FOXO3.

A

UniProKB SWISS-PROT	PR-score (%) CDK4-D1	PR-score (%) CDK6-D3
SFRS16_HUMAN Q8N2M8	3	304
TRA2A_HUMAN Q13595	12	264
TRA2B_HUMAN P62995	5	259
FOXO3_HUMAN O43524	5	147
SFRS2-HUMAN Q01130	1	134
SYNP2_HUMAN Q9UMS6	5	115
SRR35_HUMAN Q8WXF0	2	107
ZEB1_HUMAN P37275	4	104
RB_HUMAN P06400	100	100

B

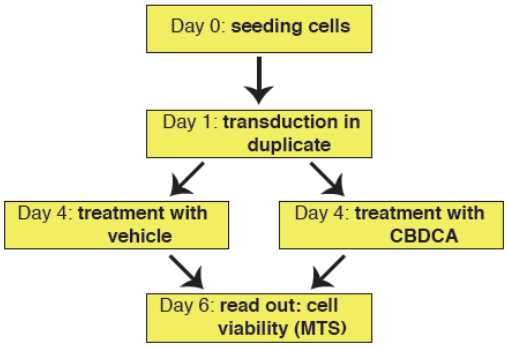

C

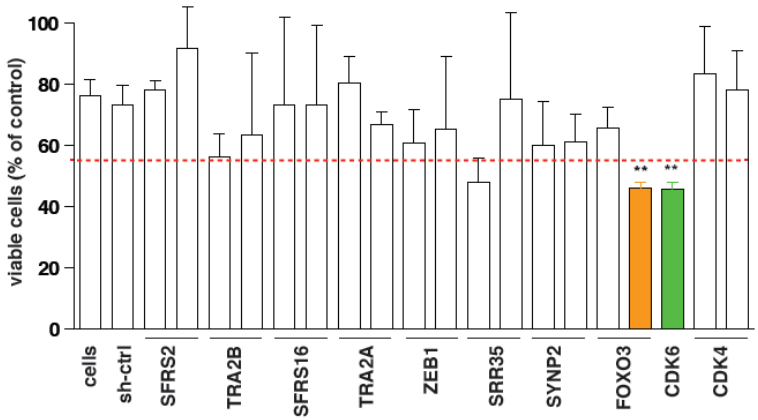

Figure 10: FOXO3 is a CDK6 phosphorylation target that controls platinum sensitivity in HGEOC cells. A) Table reports CDK6 specific phosphorylation targets ordered by their PR-score (adapted from Anders L et al. 2011). PR-score is the normalized phosphorylation levels of the different protein respect to RB used as positive control (PR=100). **B)** Experimental design of loss-of-function screening performed on MDAH cells silencing specific CDK6 phosphorylation targets. **C)** Loss-of-function screening results targeting the specific phosphorylation targets of CDK6: data represent the mean ± SD of 3 independent experiments performed in triplicate graphed as described in Figure 1C. Significance was calculated using the student t-test.

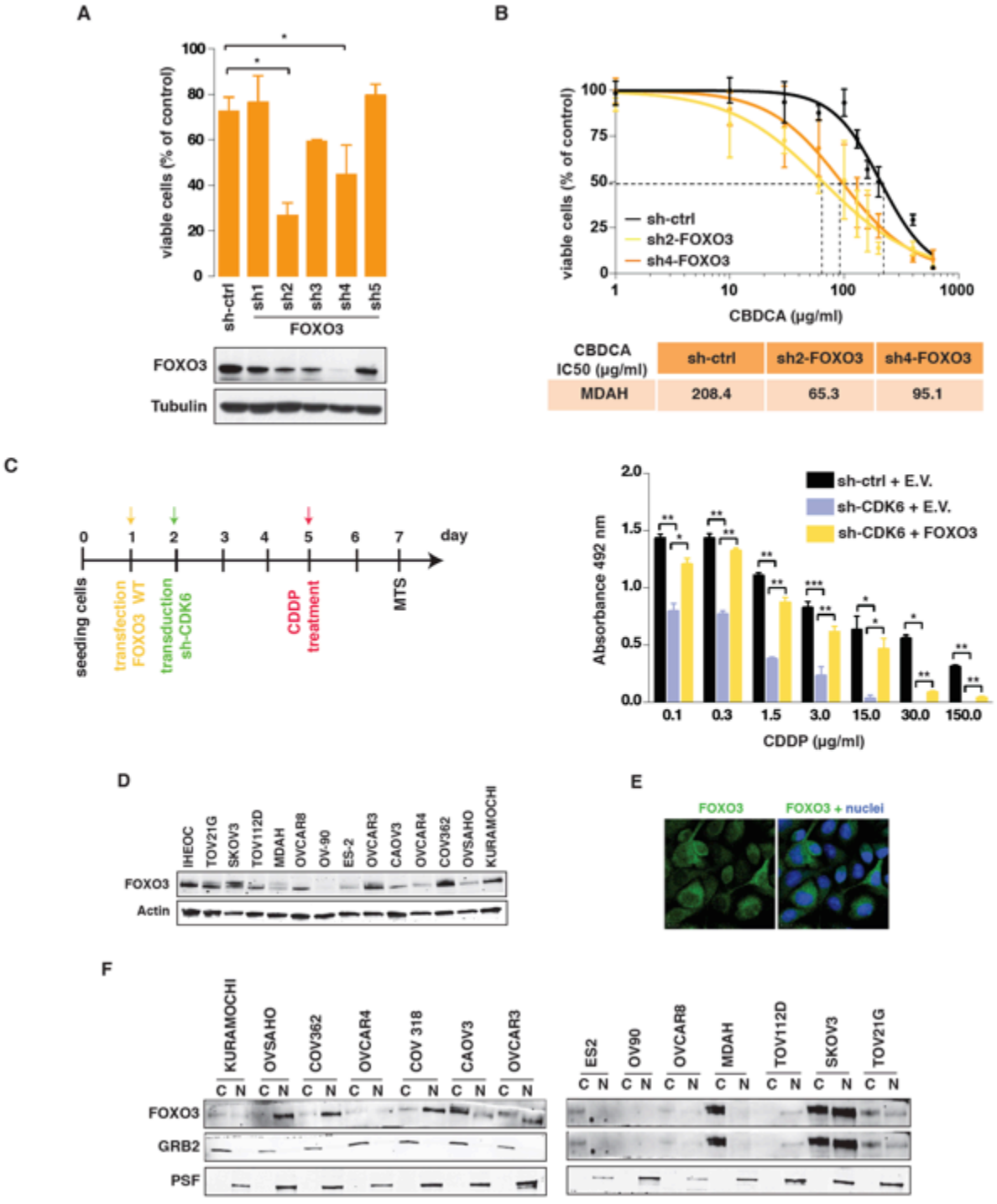

Figure 11: FOXO3 silencing sensitizes HGEOC cells to platinum induced cell death *in vitro*. **A)** Graph reporting MDAH cell viability in cells transduced with the indicated shRNAs and then treated with CBDCA. The corresponding cell lysates were then analyzed by WB. **B)** CBDCA dose response curves for MDAH cell lines transduced with control (ctrl) or FOXO3-specific shRNAs. Results are expressed as percentage of viable cells respect to untreated cells and the resulted IC50 is reported in the table. **C)** On the left, time line of the experiment. The graph reports cell viability of cells transfected as indicated and treated with increasing concentration of CDDP. Significant differences were calculated by t-test. **D)** Expression of FOXO3 in HGEOC cell lines. **E)** Immunofluorescence analysis of FOXO3 (green) in MDAH cells. Nuclei were stained with propidium iodide (blue) **F)** Expression of CDK4 and CDK6 in the nuclear (N) or cytoplasmic (C) fractions of the indicated HGEOC cell lines. Actin, tubulin, PSF and GRB2 expression were used as loading control and fraction purity. Significance was calculated using the student t-test.

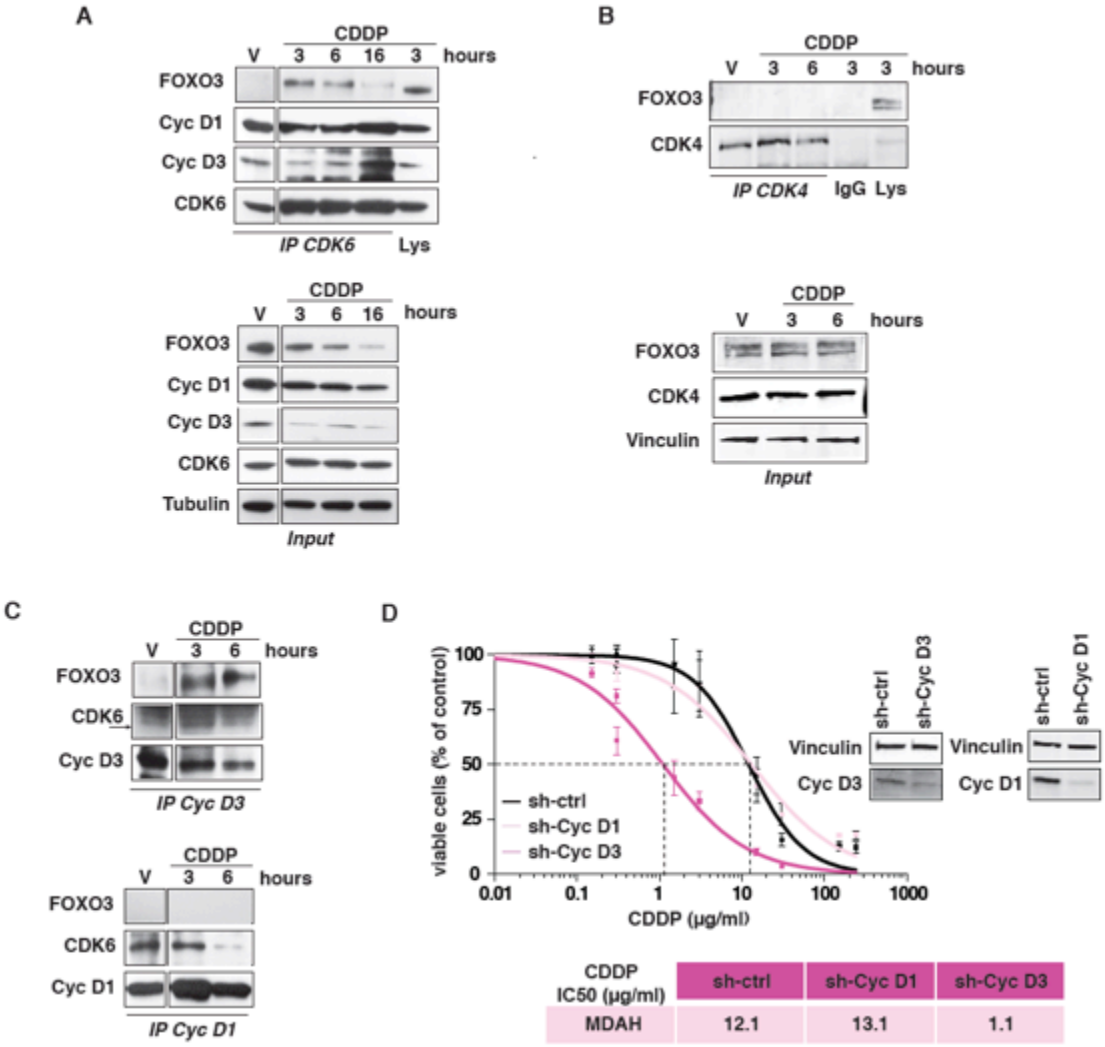

Figure 12: Cyclin D3/CDK6 complex binds FOXO3 in platinum treated cells. A) Co-Immunoprecipitation (IP) analysis of endogenous CDK6 from MDAH cells treated with vehicle (V) or with 50 μM CDDP for the indicated times. IPs were evaluated by WB for the presence of FOXO3, CDK6, Cyclin D1 and D3. In the lower panels, expression of the same proteins in the corresponding lysates (Input) is reported. **B)** Co-IP analysis of endogenous CDK4 (upper panels) from MDAH cells treated with vehicle (V) or with CDDP for 3 or 6 hours. IPs were evaluated for the presence of FOXO3 and CDK4. In the lower panels the expression of the same proteins in the lysates (Input) is reported. **C)** Co-IP analysis of endogenous Cyclin D3 (upper panels) and Cyclin D1 (lower panels) with FOXO3 and CDK6 in MDAH cells treated as in (A). **D)** Dose response curve on MDAH cells transduced with control (ctrl), Cyclin D1 or Cyclin D3 shRNAs and treated with increasing doses of CDDP for 16 hours. IC50 is reported in the table. WB analyses showing the expression of Cyclin D1 and D3 in transduced cells. Vinculin and tubulin were used as loading control.

In line with these results, *in vitro* kinase assay confirmed that CDK6/Cyclin D3 was able to phosphorylate the full-length FOXO3 recombinant protein (Fig. 13A) and *in silico* analyses with the GPS3.0 prediction software available online (http://gps.biocuckoo.org/) indicated that CDK6 could potentially phosphorylate eight serines in FOXO3 (Fig. 13B). Using several deletion mutants (Fig. 13C), we next mapped the region phosphorylated by the Cyclin D3/CDK6 complex between aminoacids 315 and 344 (Fig. 13D and 14A-B). Within this region S325 and S344 are predicted targets of CDK6 (13B). Both S325 and S344 are surface-exposed residues (Fig. 14B) located in an intrinsically disordered region (blue line in 14B), therefore both fulfilling the requirements of phosphorylable residues. Point mutation of S325 and/or S344 to alanine demonstrated that S325 is the residue preferentially phosphorylated by Cyclin D3/CDK6, *in vitro* (14C-D). Location of amino acids above the disordered (0.50 DC, dotted blue line) and surface exposure cut off (0.25 EC, dotted orange line) indicates whether they fall in an intrinsically disordered (blue line) and surface exposed region (orange line).

3.7 CDK6 regulates FOXO3 stability and nuclear localization.

Phosphorylation of FOXO3 mainly affects protein stability and subcellular localization (Tzivion et al., 2011; Yang and Hung, 2009). Using cycloheximide (CHX) to block de novo protein synthesis, we observed that CDK6 knockdown decreased FOXO3 stability, particularly in platinum-treated cells (Fig. 15A). To verify if S325 phosphorylation could be implicated in the regulation of FOXO3 stability, we generated the FOXO3 non phosphorylable ($FOXO3^{S325A}$) and pseudo-phosphorylated ($FOXO3^{S325E}$) mutants and expressed them or the wild type protein ($FOXO3^{WT}$), in MDAH cells. In untreated cells, $FOXO3^{WT}$, $FOXO3^{S325A}$, and $FOXO3^{S325E}$ displayed similar half-life. However, when cells were treated with platinum $FOXO3^{S325E}$ was more stable than $FOXO3^{WT}$, while $FOXO3^{S325A}$ was more rapidly degraded (Fig. 15B). Accordingly, the inhibition of ubiquitin mediated proteasomal degradation, using MG132, abrogated these differences, suggesting that phosphorylation on Serine 325 is necessary to prevent FOXO3 proteasome-mediated degradation (Fig. 15C). To deeper investigate this point we overexpressed $FOXO3^{WT}$, $FOXO3^{S325A}$, and $FOXO3^{S325E}$, in combination with HA-Ubiquitin constructs. After CDDP treatment we immunoprecipitated lysates using an anti-HA antibody and blotted with an anti-GFP antibody by which we observed that the three mutants were differently ubiquitinated. In particular we found that $FOXO3^{WT}$ was less ubiquitinated than $FOXO^{3S325A}$ and more ubiquitinated respect to $FOXO3^{S325E}$ (15D), suggesting that S325 phosphorylation could prevent the ubiquitin-mediated degradation of FOXO3.

A

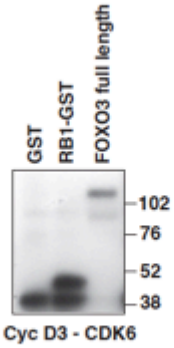

B

Pos.	Peptide	Score CDK6	Score CDK4
7	*MAEAPASPAPLSPL	10.167	11.471
12	PASPAPLSPLEVELD		9.118
43	QRPELQASPAKPSGE		5.941
110	PGGQDPGSGPATAAG		6.059
173	ITRAIESSPDKRLTL	11.667	
209	SSAGWKNSIRHNLSL	7.833	
294	QLSKWPGSPTSRSSD		10
325	STVSGRLSPIMASTE	10.333	6.353
344	QDDDAPLSPMLYSSS	8.667	9.235
446	SLNSLRQSPMQTIQE	13.333	
574	SAKHQQQSPVSQSMQ	13.333	5.235
666	FTGAKQASSQSWVPG	7	

C

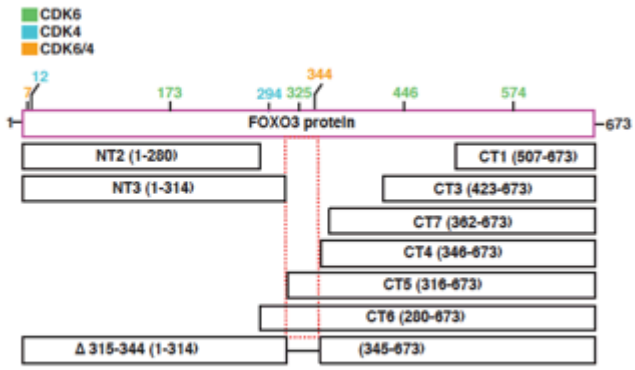

D

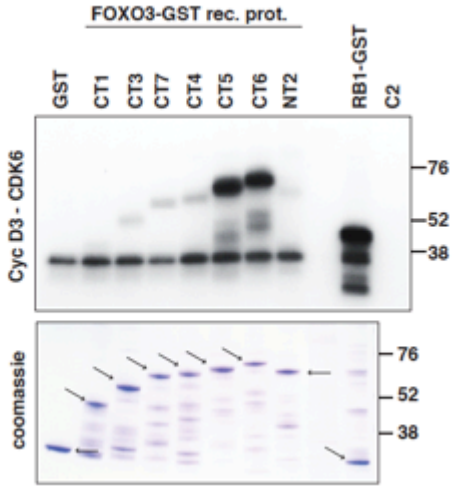

Figure 13: Cyclin D3/CDK6 complex phosphorylates FOXO3 in platinum treated cells. **A)** *In vitro* phosphorylation assay performed using recombinant Cyclin D3-CDK6 complex using GST-RB1 fragment and FOXO3 full length as substrates. **B)** *In silico* analysis of potentially phosphorylated sites on FOXO3 by CDK6/4. Pos. indicates the position in which the potentially phosphorylated serine is located. Peptide reports the sequence of the potentially phosphorylated peptide. The score indicate the probability of CDK6 or CDK4 to phosphorylate each residue. At higher score corresponds higher probability of phosphorylation. **C)** Schematic representation of FOXO3 phosphorylation sites and deletion mutants (NT: N-terminus, CT: C-terminus). Sites predicted to be phosphorylated by CDK6, CDK4 or both CDKs with a score higher than 9, are reported in green, light blue and orange, respectively. **D)** *In vitro* phosphorylation assays performed using recombinant Cyclin D3-CDK6 complex with the indicated FOXO3 deletion mutants and GST-RB1 was used as positive control. On the bottom of kinase assay, the coomassie staining of companion gel loaded with the same amount of recombinant proteins used in the kinase assay (C2: kinase reaction mix). Arrows indicate expected molecular weight of each recombinant fragment in the corresponding coomassie staining.

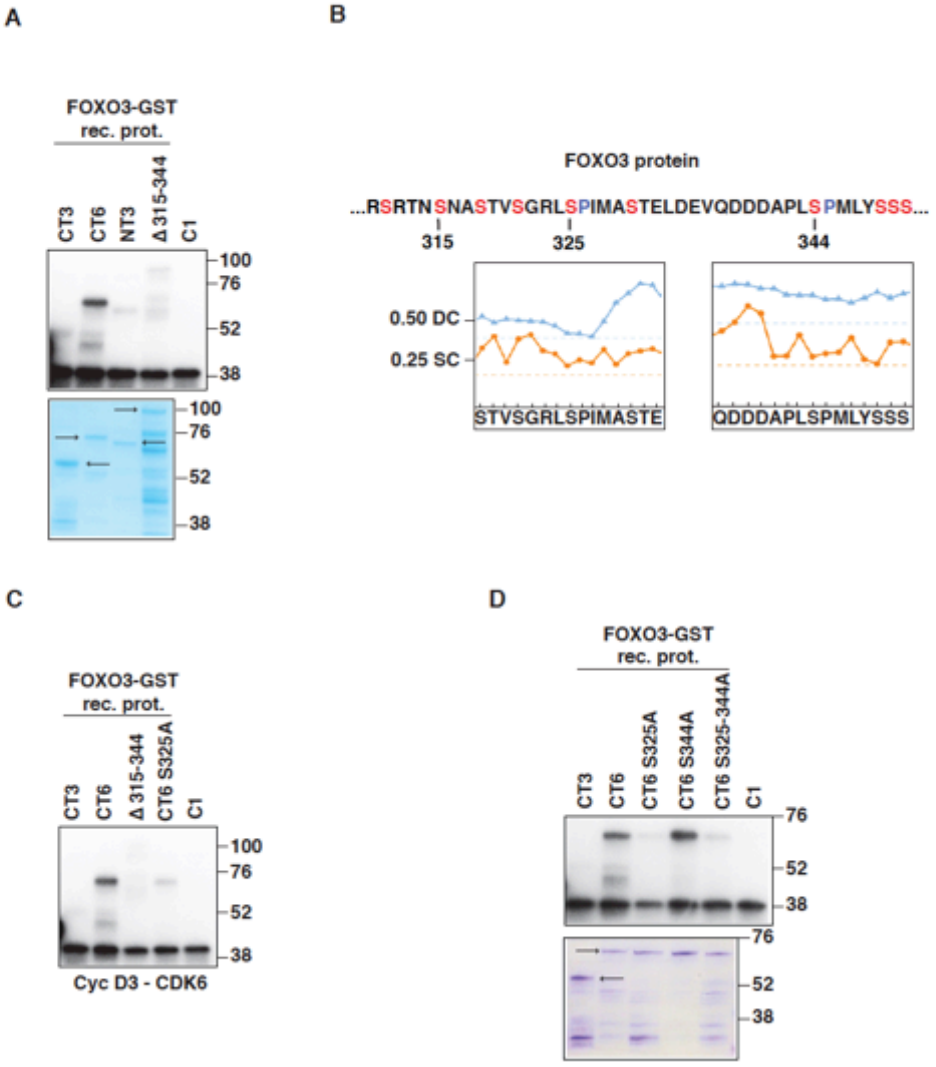

Figure 14: Cyclin D3/CDK6 complex phosphorylates FOXO3 on Serine 325. A) *In vitro* phosphorylation assays performed using recombinant Cyclin D3-CDK6 complex with the indicated FOXO3 deletion mutants. On the bottom of kinase assay, the coomassie staining of companion gel loaded with the same amount of recombinant proteins used in the kinase assay. **B)** Aminoacid sequence of FOXO3 region (residues 318-351) phosphorylated by CDK6 *in vitro* as experimentally determined using FOXO3 deletion mutants. In the lower plots is reported the disorder (blue line) and the surface exposure (orange line) of the two peptides containing S325 (left) and S344 (right). **C-D)** *In vitro* phosphorylation assays performed using recombinant Cyclin D3-CDK6 complex with the indicated FOXO3 deletion mutants carrying or not the point mutations S325A and/or S344A. GST-RB1 was used as positive control. On the bottom of kinase assay, the coomassie staining of companion gel loaded with the same amount of recombinant proteins used in the kinase assay. (C1: Control 1= kinase reaction mix plus recombinant Cyclin D3-CDK6, C2: kinase reaction mix and arrows indicate expected molecular weight of each recombinant fragment).

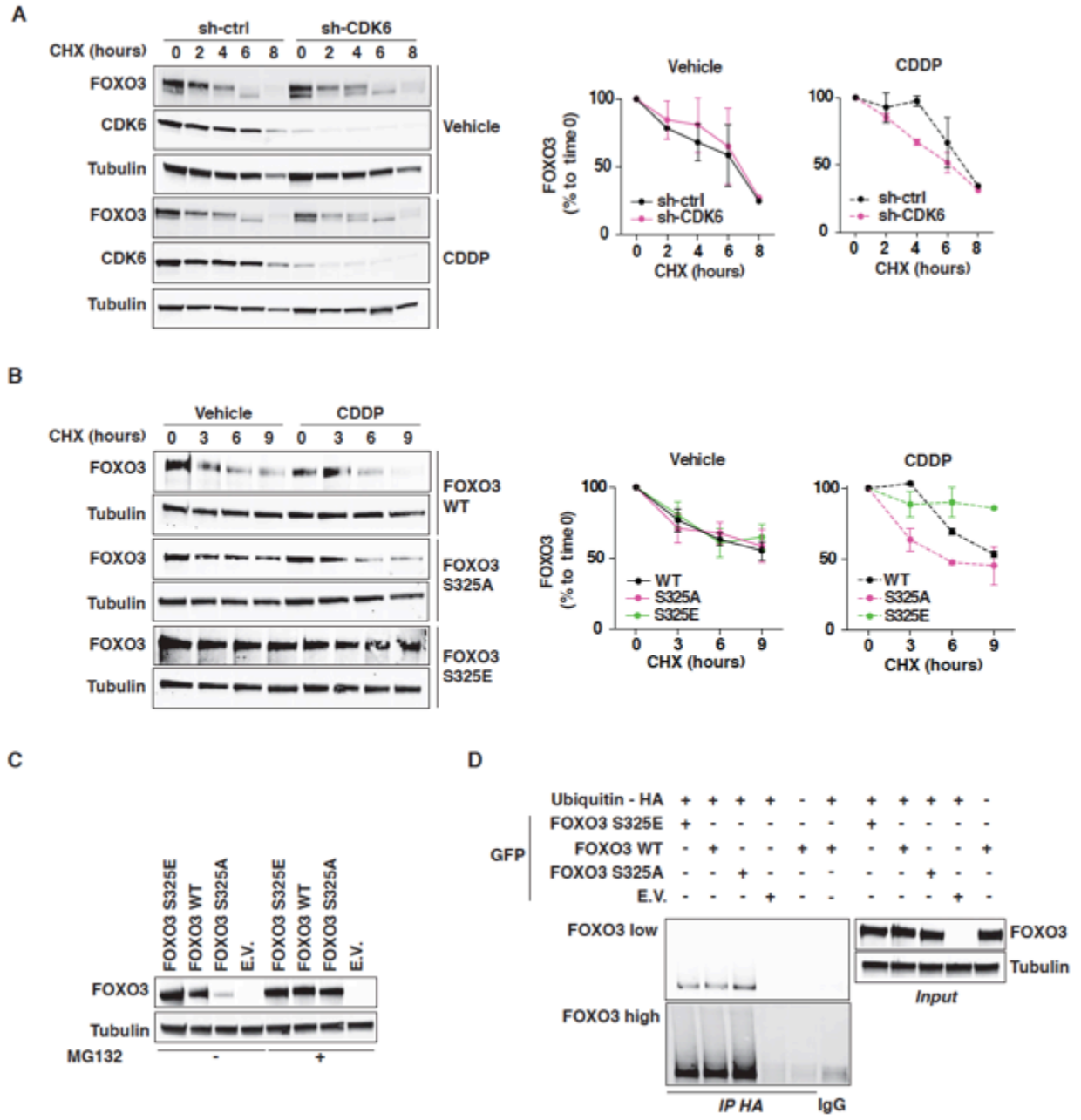

Figure 15: CDK6-mediated phosphorylation regulates FOXO3 stability following platinum treatment. A) Expression of FOXO3 in MDAH cells transduced with control (ctrl) or CDK6 shRNAs treated with vehicle or CDDP for 3 hours and then released in cycloheximide (CHX) containing medium for the indicated times. Graphs on the right report the densitometric quantification of the blot expressed as % of remaining FOXO3 (respect to T0) normalized to tubulin. **B)** Expression of $FOXO3^{WT}$, $FOXO3^{S325A}$ and $FOXO3^{S325E}$, in MDAH treated with vehicle or CDDP for 3 hours and then released in CHX containing medium for the indicated times. Graphs on the right report the densitometric quantification of the blots expressed as described in (A). Data represent the mean ± SD of three experiments. **C)** WB analysis evaluating the $FOXO3^{WT}$, $FOXO3^{S325A}$ and $FOXO3^{S325E}$ expression in 293 cells transfected with the indicated vectors and treated with CDDP for 3 hours in the presence or not of MG132. **D)** WB analysis evaluating $FOXO3^{WT}$, $FOXO3^{S325A}$ and $FOXO3^{S325E}$ ubiquitination in cells transfected with the indicated vectors and treated with CDDP for 3 hours in the presence of MG132. IgG indicates the IP with control antibody. Low and high indicate longer and shorter exposure time of the same blot. The expression of FOXO3 proteins in cells transfected as indicated is reported in the right panels. Tubulin was used as loading control (Input).

We confirmed these results by quantifying the mean GFP fluorescence/cell in cells untreated or treated with platinum and released. Under these conditions, the mean fluorescence/cell of $FOXO3^{WT}$ slightly increased following platinum treatment, while the expression of $FOXO3^{S325A}$ significantly decreased (Fig. 16A-B). Immunofluorescence analyses pointed out that $FOXO3^{WT}$, but not $FOXO3^{S325A}$, translocated into the nucleus after platinum treatment (Fig. 16A and 16C). This evidence was also confirmed by differential extraction of nuclear and cytoplasmic proteins (Fig. 16D), supporting the possibility that FOXO3 phosphorylation by CDK6 following platinum treatment could mediate FOXO3 nuclear translocation. Accordingly, also endogenous FOXO3 translocated to the nucleus following platinum treatment and this event was prevented by the concomitant inhibition of CDK6, using PD (Fig. 16E). Finally, we observed that overexpression of $FOXO3^{WT}$ and $FOXO3^{S325E}$, but not of $FOXO3^{S325A}$, overcame the increased cell death induced by platinum in CDK6-silenced cells (Fig. 17A-B), supporting the notion that the regulatory mechanism above described had functional consequences in HGEOC cells.

3.8 CDK6 controls platinum induced cell death by regulating ATR via FOXO3.

In HGEOC cells the response to platinum mainly relays on the activation of ATM and ATR kinases (Kelland, 2007; Maréchal and Zou, 2013; Siddik, 2003). In platinum treated cells, we observed that CDK6- or FOXO3–silencing induced a downregulation of ATR expression (Fig. 18A). The effect of CDK6-silencing on ATR was mediated by FOXO3, since it was rescued in CDK6-silenced FOXO3-overexpressing cells (Fig. 18B). ATR expression was also reduced *in vivo* in tumor xenografts from mice treated with CBDCA+PD, but not with either drugs used alone (Fig. 18C), confirming the relevance of this regulation in the *in vivo* context. Using *in silico* analysis, we identified 3 putative binding sites of FOXO3 in the ATR promoter, located in positions -915-908, -752-745 and -704-697, respect to the transcription start site (TSS) (Fig. 19A). Chromatin immunoprecipitation (ChIP) experiments in cells overexpressing FLAG-FOXO3 or control vector, demonstrated that FOXO3 bound the region of ATR promoter between -1000-800 from TSS that contains the -915-908 putative binding site (Fig. 19B). We next performed ChIP experiments in cells treated or not with platinum and then released for 3 hours (Fig. 19C). Under these conditions, endogenous FOXO3 binds ATR promoter in the same region (-915-908) and the binding significantly increased after platinum treatment (Fig. 19C). In accord, platinum treatment induced the expression of ATR mRNA within 2 hours and this increase was hampered in CDK6- and FOXO3-silenced cells (Fig. 19D).

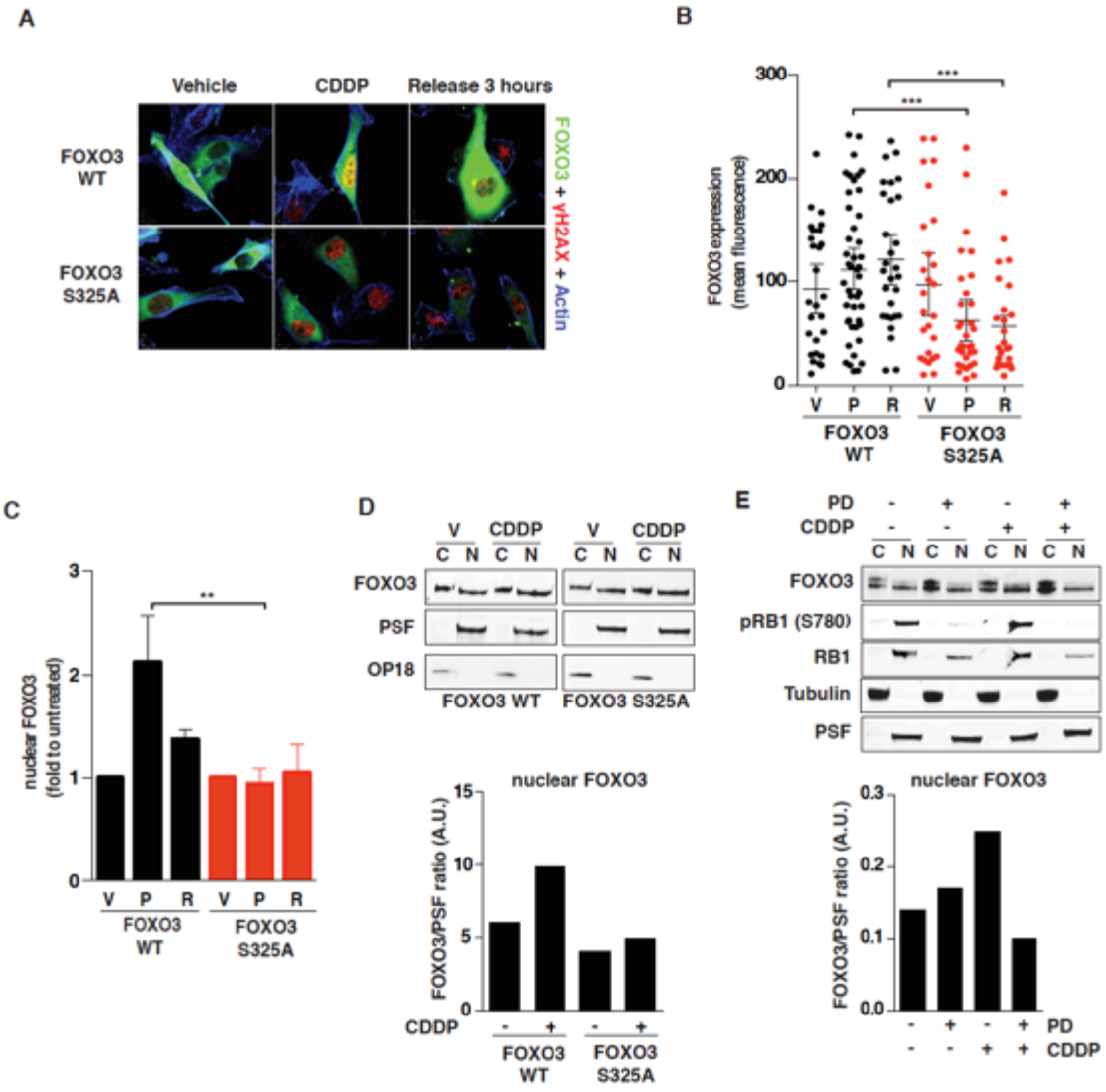

Figure 16: S325 phosphorylation regulates FOXO3 expression and nuclear translocation following platinum treatment. A) Immunofluorescence evaluating the expression and localization of GFP-FOXO3^{WT} and GFP-FOXO3^{S325A} (green) and γ H2AX (S139) phosphorylation (red) in MDAH cells treated with vehicle or CDDP for 3 hours and released for 3 hours. Phalloidin was used to visualize F-actin (blue). **B-C)** Quantification of FOXO3^{WT} and FOXO3^{S325A} expression (B) and localization (C) evaluated as mean fluorescence per cell (B) or fold induction over untreated cells (B), in cells treated as indicated in (A) **D)** Expression FOXO3^{WT} and FOXO3^{S325A} protein in the nuclear (N) and cytoplasmic (C) fractions of MDAH cells treated with vehicle or CDDP for 3 hours. In the lower graph is reported the normalized quantification of nuclear (i.e. FOXO3/PSF ratio) fractions of FOXO3 obtained by densitometric scanning of the blots. **E)** Expression of FOXO3 in the nuclear (N) and cytoplasmic (C) fractions of MDAH cells treated or not with CDDP and PD as indicated. In the lower graph is reported the quantification graphed as described in (D). V = vehicle; P = CDDP 3 hours; R = 3 hours release after platinum A.U = Arbitrary Unit. Tubulin, PSF and OP18 expression were used as controls of loading and fraction purity. Significance was calculated using the student t-test.

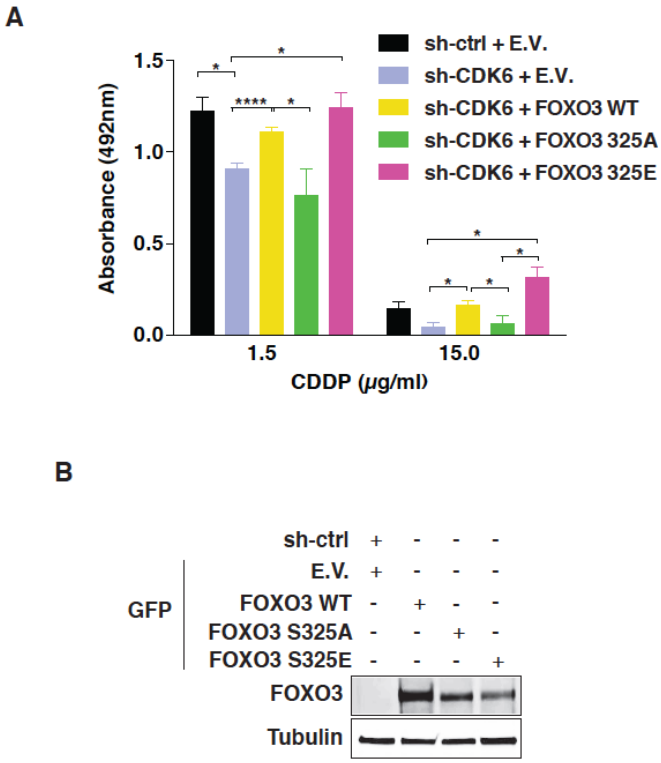

Figure 17: Overexpression of FOXO3^{WT} and FOXO3^{S325E} overcome sh-CDK6 phenotype. A) Graph reports viability of cells transfected with E.V., FOXO3^{WT}, FOXO3^{S325A} and FOXO3^{S325E}, transduced with control (ctrl) and CDK6 shRNAs treated with increasing concentration of CDDP as described in the figure (11C). **B)** WB analyses evaluating the expression of FOXO3^{WT}, FOXO3^{S325A} and FOXO3^{S325E} EGFP-tagged proteins in MDAH cells transfected as indicated in the experiment described in A. Tubulin was used as loading control. Significance was calculated using the student t-test.

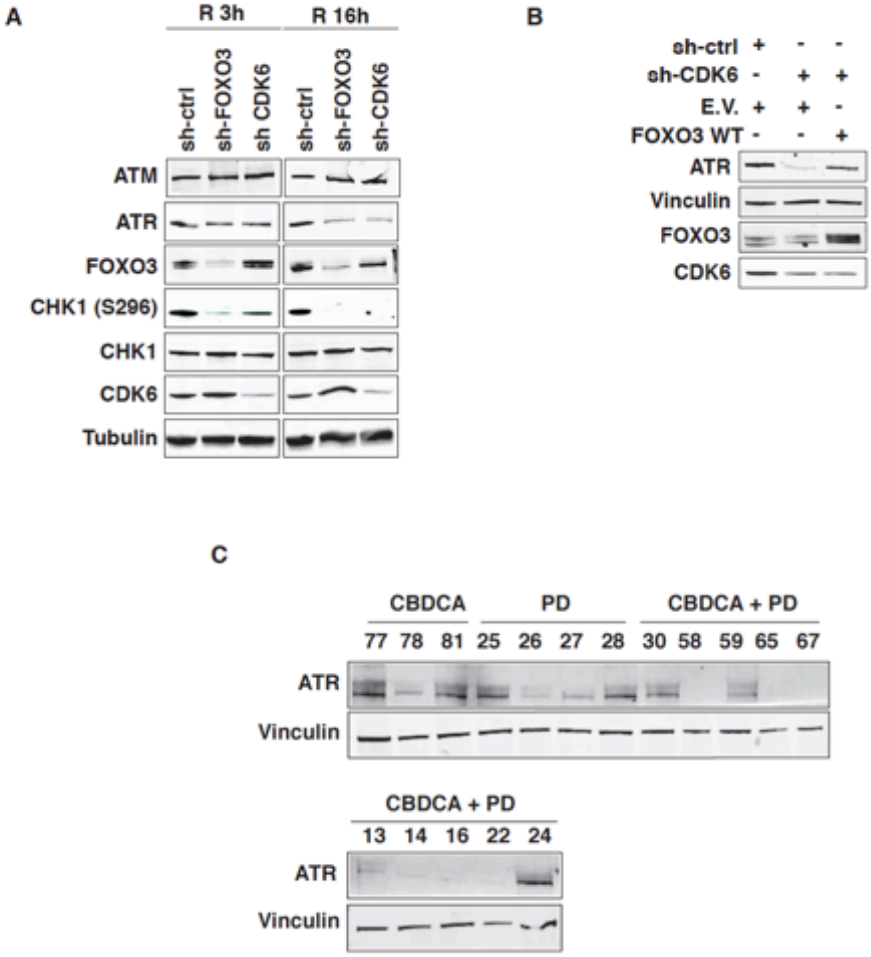

Figure 18: CDK6 and FOXO3 regulate ATR expression in platinum treated cells. A) MDAH cells were transduced with the indicated sh-RNAs treated for 3 hours with CDDP and then released for 3 or 16 hours (R 3h and R 16h). Cell lysates were analyzed by WB. **B)** MDAH cells were transduced with the control (ctrl) or CDK6 sh-RNAs and transfected with $FOXO3^{WT}$ as indicated. Cell lysates were analyzed by WB. **C)** ATR expression in tumors explanted from mice treated as indicated. Tubulin and Vinculin were used as loading controls.

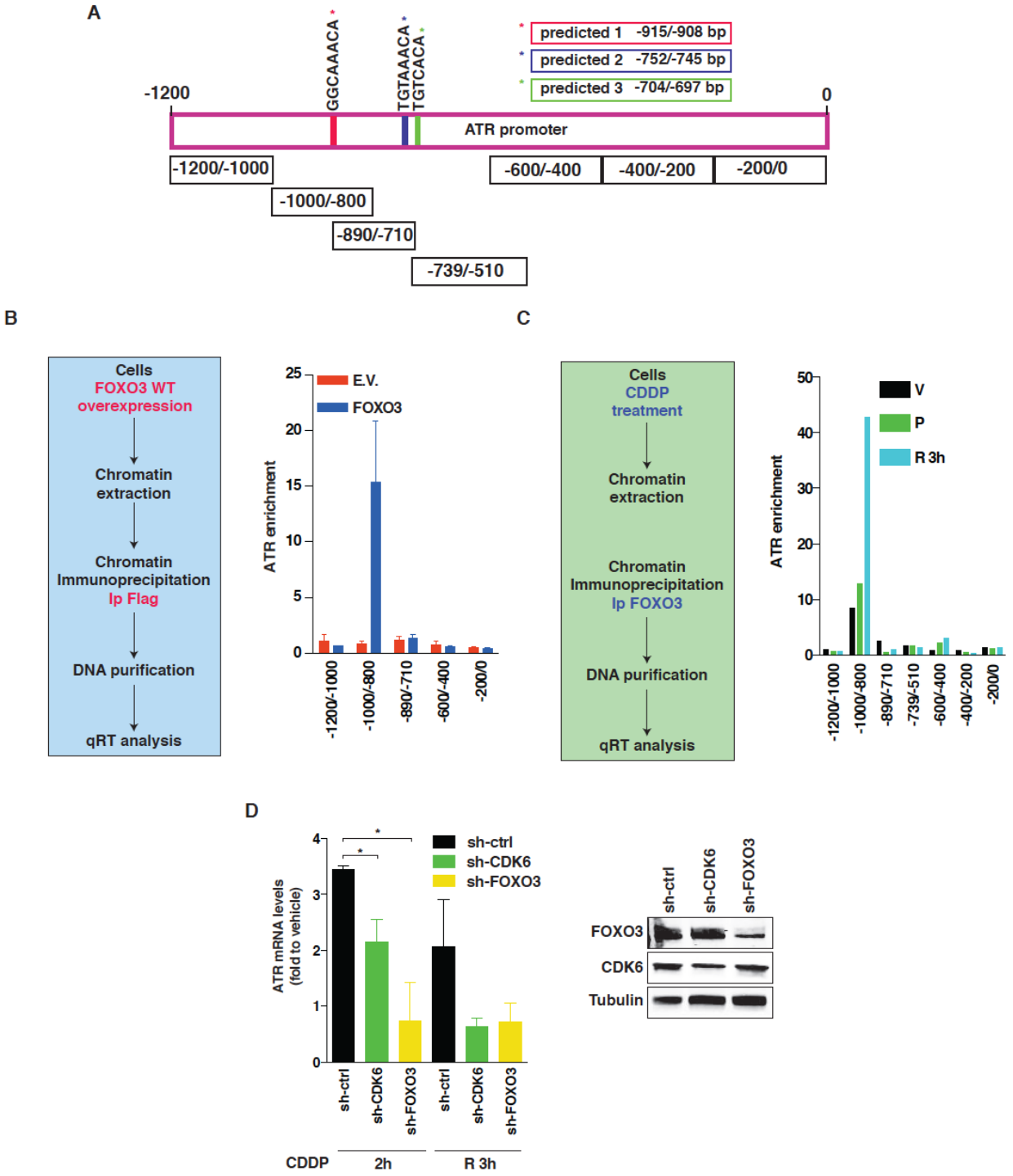

Figure 19: FOXO3 binds to ATR promoter. A) Schematic representation of ATR promoter showing the 3 putative FOXO3 binding sites (colored bars). On the bottom are reported the different amplified regions of ATR promoter. **B-C)** ChIP analysis in cells transfected with empty vector (E.V.) or FLAG-FOXO3 (B) and ChIP analysis on cells treated with vehicle or CDDP and release for 3 hours (C). V = Vehicle, P = CDDP 3 hours, R 3h = 3 hours release post platinum. Data are expressed as fold enrichment respect to control IgG. Box on the left reports the experimental design. **D)** Expression of ATR mRNA in MDAH cells transduced with the indicated shRNAs and then treated with CDDP for 2 hours (2h) or treated with CDDP and then allowed to repair for 3 hours (R3). Data are expressed as fold respect to the same cells treated with vehicle at the same time point. On the right the expression of FOXO3 and CDK6 in control and silenced cells is reported. Significance was calculated using the student t-test.

3.9 Impairment of CDK6/FOXO3/ATR pathway induces Premature Chromatin Condensation.

The above data demonstrated that, following platinum treatment, FOXO3 binds the ATR promoter eventually regulating ATR transcription. It is known that, in response to DNA damage, ATR phosphorylates and activates the CHK1 protein, which, in turn, blocks cell cycle progression and allows for the proper DNA repair mechanisms to operate (Nghiem et al., 2001; Siddik, 2003). In the absence of both CDK6 and FOXO3, the activity of CHK1 was markedly reduced, as demonstrated by the decrease in CHK1 S296 phosphorylation (Fig. 18A). As expected, ATR knock-down confirmed that the phosphorylation of CHK1 at S296 relied on ATR expression (Fig. 20A). ATR and its downstream target CHK1, but not ATM, are both necessary to prevent the so-called premature chromosome condensation (PCC). PCC is a hallmark for mammalian cells that begin mitosis before completing DNA replication and is invariably followed by apoptotic cell death (Nghiem et al., 2001). The role of ATR and CHK1 in preventing PCC is particularly relevant when S phase is prolonged by pharmacological treatments, such as platinum, in the absence of a functional p53 (Nghiem et al., 2001).

We thus tested whether PCC was involved in the mechanism of cell death induced by CDK6 silencing. Video time-lapse analyses of CBDCA-treated MDAH cells (harboring the $p53^{R273H}$ mutant protein) clearly showed that cells underwent nuclear condensation before dying, mostly when CDK6 activity was inhibited by PD (Movie 4 and 5). We next measured the number of normal mitosis and PCC in MDAH cells treated with platinum and silenced, or not, for CDK6, FOXO3 or ATR. In control cells, platinum induced only a mild reduction of mitotic figures respect to untreated cells, with no signs of PCC (Fig. 20B-D). In contrast, cells treated and silenced either for CDK6, FOXO3 or ATR displayed more than 70% of total mitoses categorized as PCC (Fig. 20B-D). These data were confirmed looking at the percentage of PCC in metaphase spreads in control and CDK6 silenced MDAH cells, showing an increase in PCC over time in CDK6-silenced cells, which paralleled the decreased expression of CDK6 protein (Fig. 20E-F).

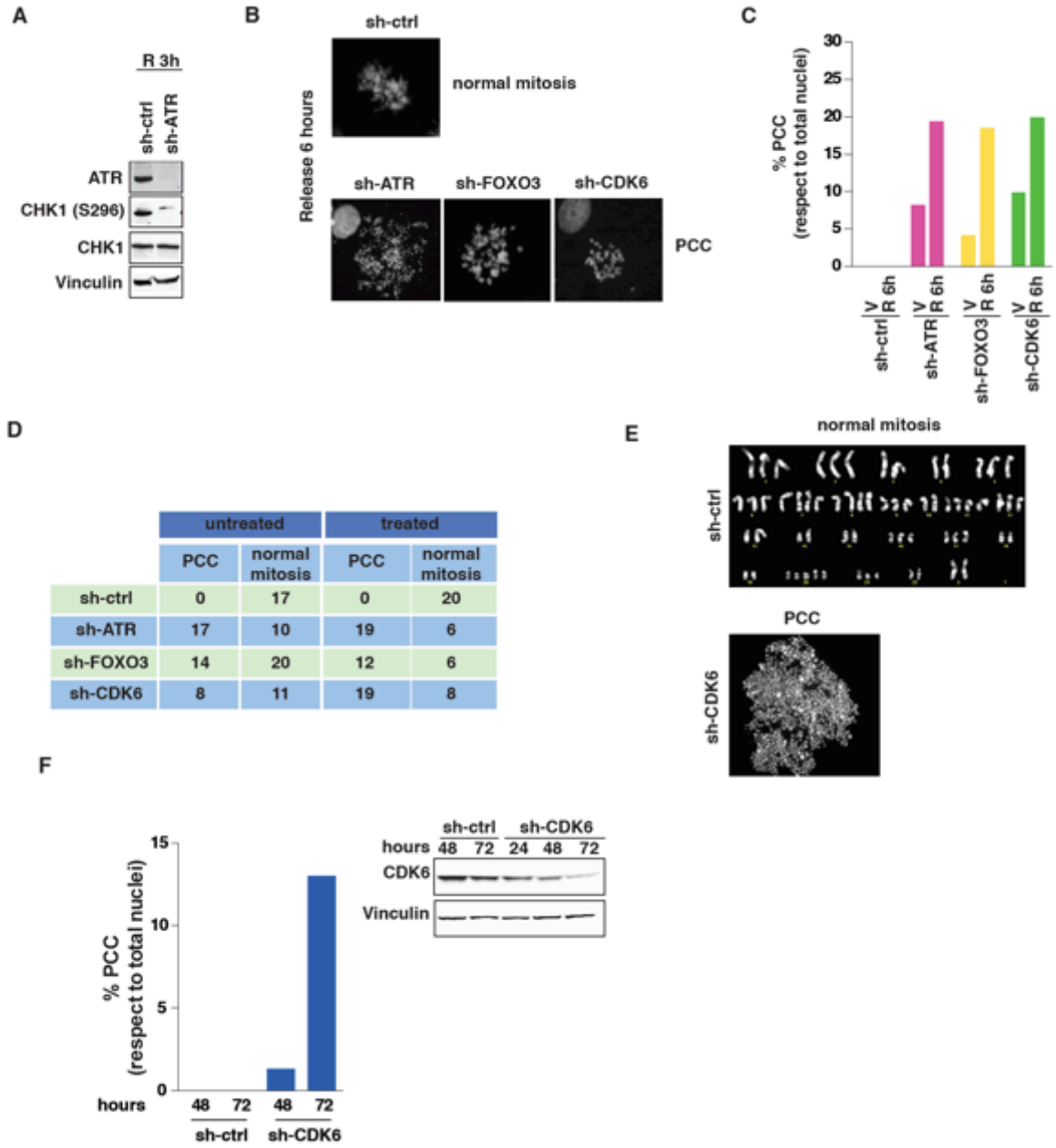

Figure 20: FOXO3 controls ATR transcription preventing premature chromosome condensation. **A)** MDAH transduced with the control (ctrl) or ATR sh-RNAs and then treated with CDDP and released for 3 hours (R). Cell lysates were analyzed by western blot. Vinculin was used as loading control. **B)** Typical images of normal mitosis or PCC events observed in MDAH cells transduced with control (ctrl), CDK6, FOXO3 or ATR sh-RNAs and then treated CDDP and released for 6 hours. **C)** Percentage of PCC (respect total nuclei) in MDAH cells treated or not as in (B). V= cells treated with vehicle, R= release. **D)** Table reporting the number of normal mitosis and PCC scored in cells treated or not as in (B). **E-F)** Mitotic spreads of MDAH cells transduced with control (ctrl) or CDK6-specific shRNAs (E). Graph (F) shows PCC events graphed as in (C).

3.10 CDK6 and FOXO3 predict the survival of HGEOC patients.

To verify if the *in vitro* data were relevant and consistent with the human pathology, we first analyzed the expression of CDK6, Cyclin D1 and Cyclin D3 in HGEOC primary samples collected in our Institute (Table 2). Immunohistochemistry analyses demonstrated that CDK6 is generally well expressed in primary HGEOC, particularly in the cytoplasm of tumor cells (Fig. 21A). Western blot analyses also showed that Cyclin D3 was the D-type cyclin preferentially expressed in primary HGEOC (Fig. 21B). More importantly, when we analyzed HGEOC samples collected from patients who already received platinum-based therapy, Cyclin D1 was generally not expressed while Cyclin D3 expression was maintained and readily co-precipitated with CDK6 (Fig. 21C-D). In the same tumors the expression of CDK6, FOXO3 and ATR significantly and positively correlated (Fig. 21E), overall supporting the possibility that the Cyclin D3/CDK6 complex played a role in the platinum response also *in vivo* by regulating FOXO3 expression. These observations prompted us to verify if the high expression of CDK6 and/or FOXO3 could be used to identify primary HGEOC at higher probability to recur after the standard platinum treatment. To this aim, we interrogated the online tool OvMark (http://glados.ucd.ie/OvMark/index.html), an algorithm that integrates data from gene expression microarrays (14 datasets corresponding to ~17,000 genes in up to 2,129 samples) and detailed clinical data, to correlate clinical outcome with differential gene expression levels. Using OvMark, we found that high CDK6 or FOXO3 expression significantly predicted a shorter progression free and overall survival of HGEOC patients (Fig. 22A). The combination of FOXO3 and CDK6 both expressed at high levels, even better identified the group of patients with worse prognosis (Fig. 22B). As expected from our results, CDK4 did not have any prognostic value, neither in the whole population nor in the group of patients for which the information on platinum therapy was specifically annotated (Fig. 23A-B). When only this latter group of patients was considered, again the high expression of CDK6, FOXO3 alone, and even better the combination of the two, identified patients with worse prognosis (Fig. 23A-B).

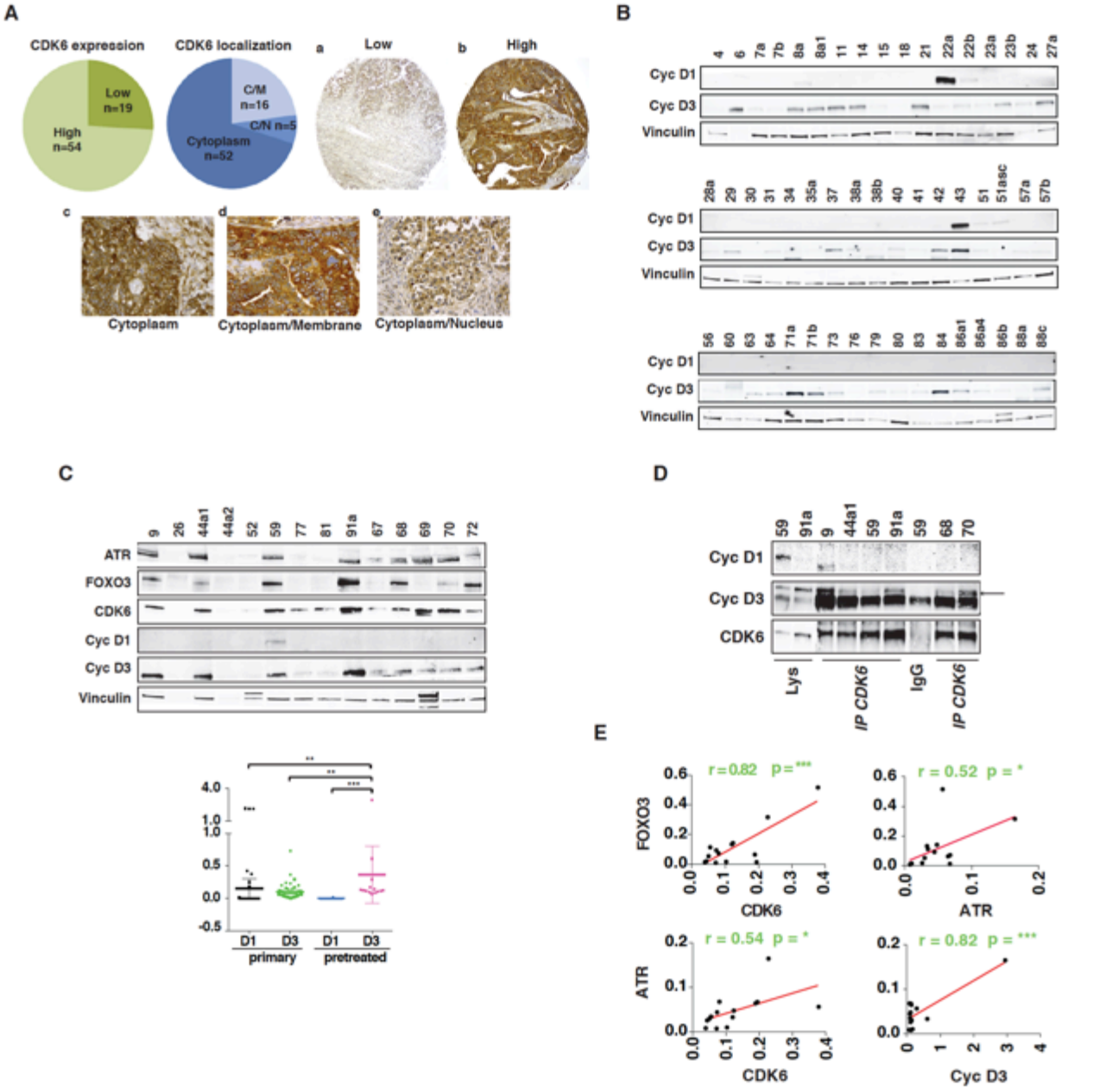

Figure 21: CDK6 expression in HGEOC samples from platinum-treated and untreated patients. A) Immunohistochemistry analyses of CDK6 expression (upper right a and b) and localization (lower c, d and e) in a panel of 73 patients. **B-C)** Expression of Cyclin D1/D3 in tumor samples obtained from patients with primary untreated (B) or platinum-treated EOC (C) (i.e. patients with recurrent disease or treated with neo-adjuvant chemotherapy). Tumor characteristics are described in Table 2. Lower graph (C) shows quantification of Cyclin D1/D3 expression in tumor samples described in B/C. Results are presented as scattered dot plot and represent the normalized expression respect to Vinculin used as loading control. Bars indicates mean ± 95% CI. **D)** Co-IP analysis of CDK6 with Cyclin D1 and D3 in the indicated human EOC tumors. IgG indicates IPs with a non-related Ab. Lys indicates lanes loaded with the corresponding cell lysates as controls proteins expression and molecular weight. **E)** Correlation analyses between FOXO3 and CDK6 or ATR expression (upper panels) or between ATR and CDK6 or CyclinD3 expression (lower panels) in samples from platinum treated patients (i.e. patients with recurrent disease or treated with neo-adjuvant chemotherapy).

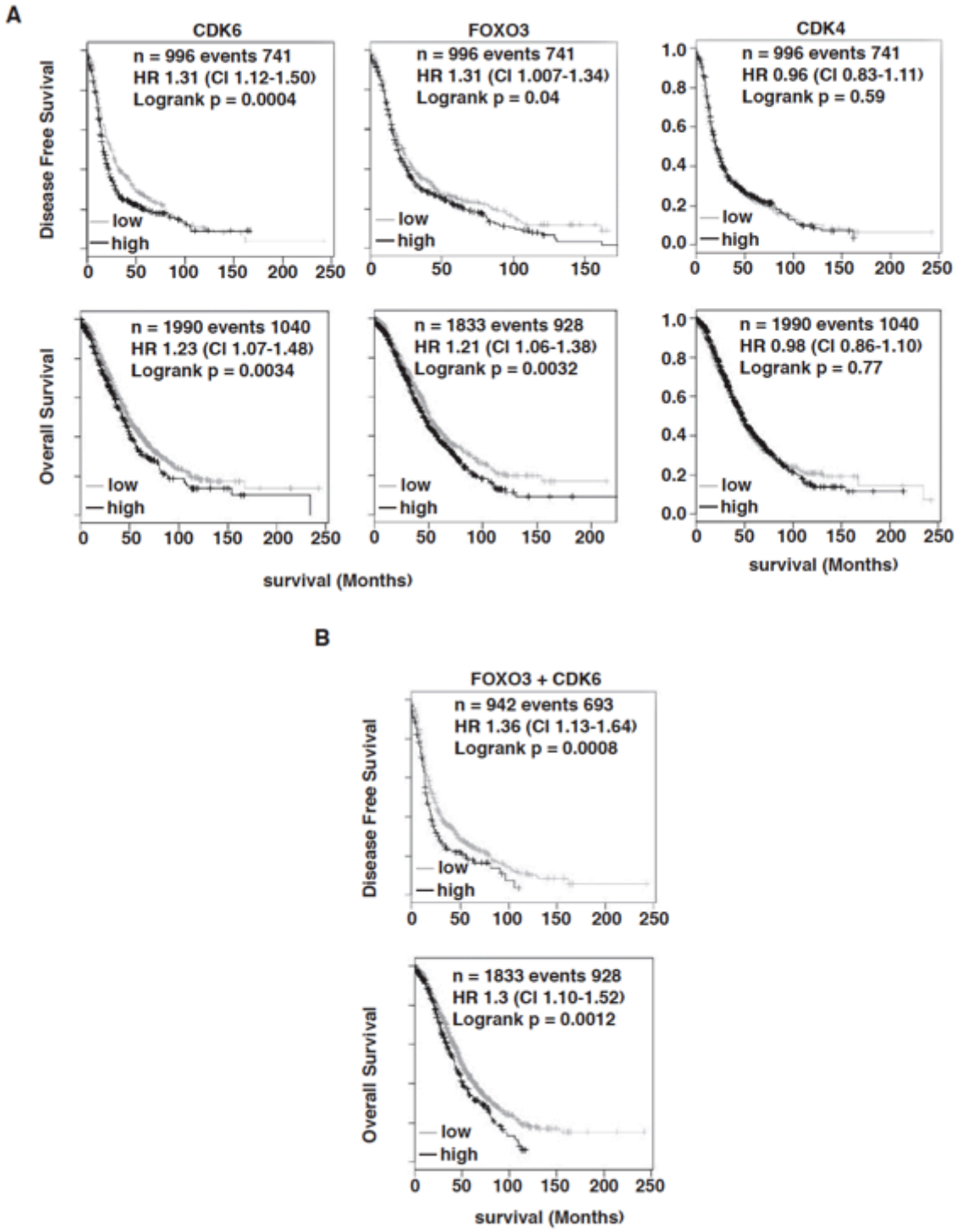

Figure 22: FOXO3 and CDK6 predict poor prognosis in EOC untreated patients. A-B) Kaplan Mayer survival curves evaluating the prognostic significance of CDK4, CDK6, FOXO3 (A) and of the combination of FOXO3 and CDK6 (B), as indicated, in predicting the Disease Free Survival (Upper panels) or the Overall Survival (OS) (Lower Panels) of EOC patients with the online tool Ovmark using a median cutoff. n= number of analyzed samples. HR = Hazard Ratio; CI = Confident Interval; Logrank = Logrank test evaluated the significance.

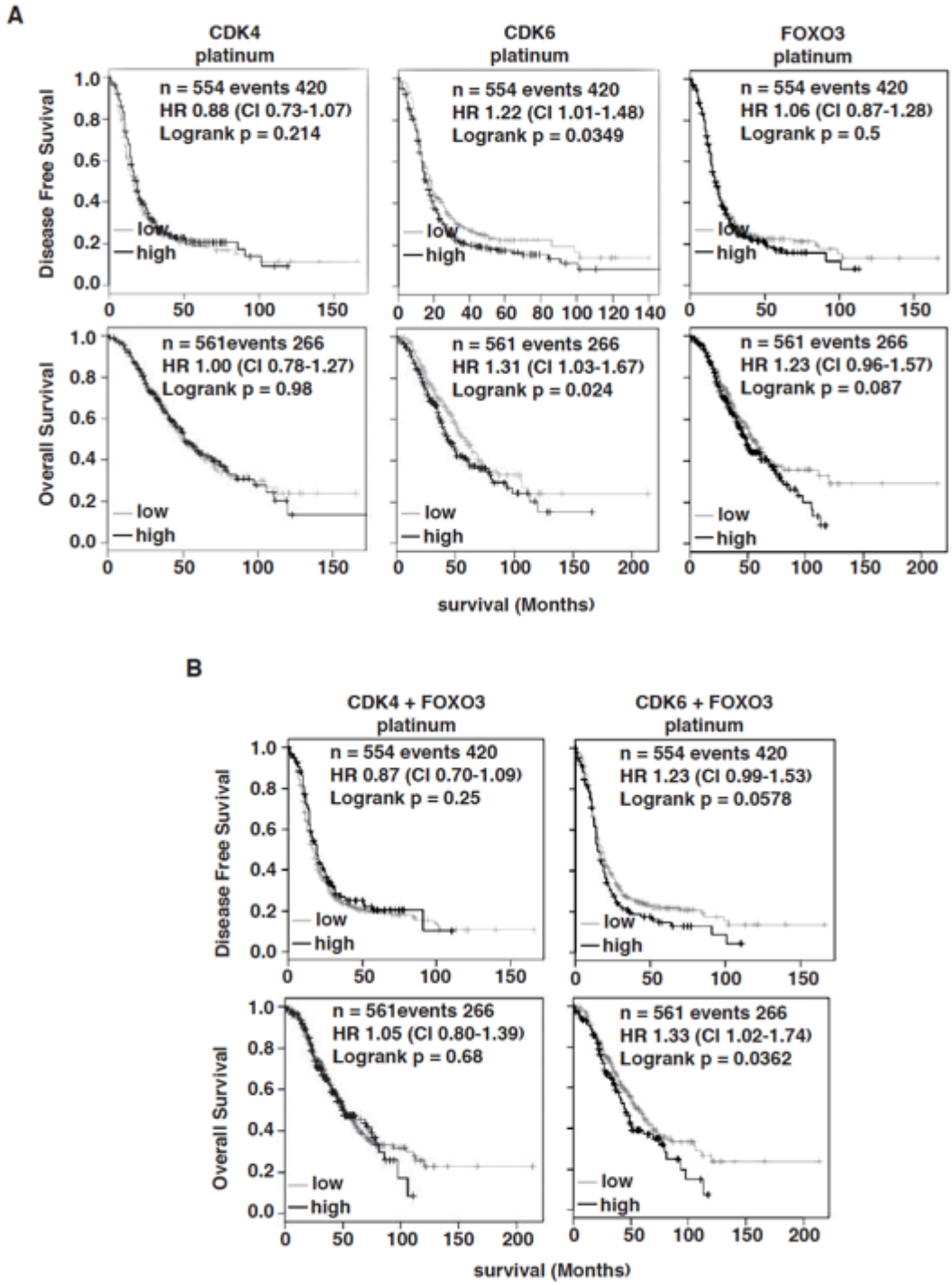

Figure 23: FOXO3 and CDK6 predict poor prognosis in EOC platinum- treated patients. A-B) Kaplan Mayer survival curves evaluating the prognostic significance of CDK4, CDK6, FOXO3 (A) and of the combination of FOXO3 and CDK6 or CDK4 (B), in the patients for which information of platinum treatment was specified in the datasets. Data were obtained as indicated in Fig. 22.

DISCUSSION

The prognosis of HGEOC patients mostly relies on the response to platinum-based therapy (Jayson et al., 2014), but most of the patients relapse and develop platinum resistant largely uncurable disease (Jayson et al., 2014). Clinical evidences regarding the combination between targeted therapies (i.e. PARP inhibitors) and standard chemotherapy show a significant improvement on the survival of patients carrying BRCA1/2 germline or somatic mutations (Oza et al., 2015). These findings open the way to consider combination therapies as a valid approach in HGEOC management, to prevent the emergence of resistant subclones that pre-exist at the beginning of tumor development. It has been already demonstrated that the employment of high-throughput screening based on RNA interference technology represents an interesting tool to identify undisclosed targets whose silencing impair cell survival in combination with chemotherapy (Arora et al., 2012; Lin et al., 2015). In this sense, the involvement of Cyclin-Dependent Kinases (CDKs) in several cellular mechanisms such as control of cell cycle progression, transcription and DNA repair make them an attractive target to investigate. For this reason using a loss-of function approach targeting the 23 members of the CDK family (Malumbres and Barbacid, 2009) we identified CDK6 as the one most significantly involved in the platinum-induced DNA damage. Together our results show that CDK6 protect HGEOC from DNA damage controlling FOXO3/ATR axis: in response to platinum CDK6 phosphorylates FOXO3 that in turn controls ATR expression, allowing cells to repair the DNA. CDK4 and CDK6 ability to phosphorylate the same targets (Anders et al., 2011) and the capacity to play in the same pathways (i.e cell cycle regulation) led us to verify if there was the involvement of CDK4 activity in platinum sensitization. Once verified that CDK4 knock-down does not impair cell growth upon platinum treatment, we confirmed screening results identifying CDK6 as the only CDK involved in platinum sensitivity. Our results perfectly match with several literature data that indicate discrete functions for CDK4 and CDK6, supporting a separated role for this two CDKs. Based on the evidence that CDK6 can exert its function dependently or independently from its kinase activity (Tigan et al., 2015) we proved the involvement of CDK6 kinase activity exploring the effect of CDK6 constitutively active and dominant negative mutants. Moreover the efficacy of CDK6 kinase activity inhibition harming cell viability was confirmed by the use of PD compound. In order to increment the efficiency of platinum treatment we investigated the significance of different schedule of treatment based on the combination between platinum and PD. In this sense, our *in vitro* and *in vivo* data pointed out that the sequential use of platinum followed by PD represents a treatment schedule that potentiates platinum efficacy. In light of our results, we can explain this effect in two ways. First, it is known that platinum exerts its anticancer activity in cycling cells, thus G1 cell cycle arrest induced by PD treatment antagonizes the cytotoxic effect of platinum making less effective the PD + platinum

schedule. Second, in HGEOC, CDK6 seems to be less involved in regulating cell cycle as demonstrated by the fact that inhibition of CDK6 results in an abnormal induction of PCC an event that leads to cell death because cells undergo to mitosis before having completed DNA replication (Nghiem et al., 2001). These suggestions are also supported by other groups, showing an increased EOC cell death when PD was administered with or after, but not before, platinum (Asghar et al., 2015; Konecny et al., 2011). The involvement of CDK6 kinase activity led us to exclude the role of CDK6 as direct transcriptional regulator (Kollmann et al., 2013; Placke et al., 2014), principally linked to a kinase-independent function. Active Cyclin D-type/CDK6 complexes enable to phosphorylate RB1 are localized principally into the nucleus, however CDK6 protein expression and cytoplasmic localization in HGEOC cells suggested a role of CDK6 that go beyond the properly regulation of cell cycle and RB1 phosphorylation, probably phosphorylating another target into the cytoplasm. This evidence agrees also with the fact that CDK6 knockdown did not impair RB1 phosphorylation status. By analyzing a panel of CDK6-specific phosphorylation targets (Anders et al., 2011) and selecting nine proteins that were poorly phosphorylated by CDK4 and were phosphorylated by CDK6 at higher level than RB1 we identified the transcription factor FOXO3 as a relevant downstream target of CDK6. In fact, FOXO3 knock-down using multiple shRNAs impairs cell viability in platinum treated HGEOC cells as CDK6 silencing, suggesting that they work along the same axis preventing platinum induced cell death. FOXO3 (Forkhead Box O3) is a transcription factor whose role is linked to several biological processes such as cell cycle, apoptosis, resistance to oxidative stress and metabolism, activating or inhibiting a number of downstream targets. FOXO3 activity depends on opposing signaling pathways that regulate its post-translational modification and among them, phosphorylation at different sites controls FOXO3 subcellular localization, protein stability and DNA-binding activity (Xie et al., 2012). For instance, AKT and SGK have been identified as the major enzymes for FOXO3 phosphorylation on Thr32, Ser253 and Ser318 able to induce FOXO3 nuclear exclusion (Brunet et al., 1999, 2001). Similarly results were described for ERK (Yang et al., 2008) and IKK (Hu et al., 2004) on different sites. Conversely, phosphorylation by MST1 disrupts FOXO3 binding to 14-3-3 proteins promoting its nuclear translocation (Lehtinen et al., 2006). CDK6 ability to bind and phosphorylate FOXO3 is not shared by CDK4, even if CDK4 and CDK6 bind the same D-type Cyclins to regulate G1 phase progression (Choi and Anders, 2014). Moreover Cyclin D3 ability to co-precipitate with FOXO3 under platinum treatment suggests that CDK6/Cyclin D3 could be the active binding complex able to phosphorylate FOXO3 and this evidence is further confirm by platinum-induced cell death upon Cyclin D3 knock-down. These results are not surprising because it is well accepted that CDK4 and CDK6 are characterized by discrete and non-overlapping functions due not only to differential

expression/localization of each CDKs or D-type Cyclins but also to differential binding ability of each complex (Anders et al., 2011; Choi and Anders, 2014; Grossel and Hinds, 2006a, 2006b; Kollmann et al., 2013; Malumbres et al., 2004). In line with these results *in silico* analysis identified on FOXO3 eight potentially serines residues that could be phosphorylated by CDK6 and by *in vitro* kinase assay we discovered that CDK6 phosphorylates FOXO3 on Ser325. In particular phosphorylation on this site is necessary to control FOXO3 stability and nuclear translocation in HGEOC cells. CDK6 knock-down in fact, results in decreasing of FOXO3 half-life upon platinum treatment and this is further confirmed in the same treatment conditions by $FOXO3^{S325A}$ increased ubiquitination and rapidly degradation, suggesting a role of CDK6 in preventing FOXO3 ubiquitin-mediated degradation. Even if the role FOXO3 is mainly linked to transcription of several apoptotic genes, not surprisingly we found that its role also correlates with DNA Damage Response. Literature data reports that after stress stimuli FOXO3 protects cells from DNA damage by a Gadd45-dependent mechanism (Tran et al., 2002) and more recently Tsai et al., described a direct interaction between FOXO3 and ATM upon DNA damage (Tsai et al., 2008). We found that FOXO3 phosphorylation on Ser325 is necessary to drive FOXO3 shuttling into the nucleus where, acting as transcription factor, it regulates ATR transcription upon DNA damage induced by platinum. Our results demonstrate that CDK6 or FOXO3 knock-down results in downregulation of ATR expression and taking advantage from *in silico* preliminary analysis and ChIP assay we demonstrated for the first time that FOXO3 binds to ATR promoter regulating its transcription. ATR (Ataxia-telangiectasia and Rad3-related) belongs to the PIKKs family, is early involved in the DDR and in complex with its partner ATRIP is activated following recruitment of RPA-coated ssDNA regions generated during the DSBs induced by platinum (Ciccia and Elledge, 2010; Cimprich and Cortez, 2008). ATR in turn phosphorylates, CHK1, which once activated phosphorylates a number of downstream targets. ATR inhibition by siRNA has been shown to sensitize tumor cells to cisplatin and carboplatin both *in vitro* and *in vivo* (Lewis et al., 2009) and this correlates with the evidence that ATR kinase activity is necessary to prevent PCC and cell death (Nghiem et al., 2001; Rybaczek and Kowalewicz-Kulbat, 2011). Accordingly, our results show that silencing of CDK6 or FOXO3 induces ATR downregulation, decreased CHK1 phosphorylation and increased platinum dependent-cell death via the induction of PCC (Figure 1). The role of ATR and CHK1 in preventing PCC is particularly relevant when S phase is prolonged by pharmacological treatments, such as platinum, in the absence of a functional p53 (Nghiem et al., 2001). The fact that HGEOC almost invariably carry p53 mutations (Cancer Genome Atlas Research Network, 2011; Jayson et al., 2014; Lim and Oliva, 2013; Shih and Kurman, 2004) strongly suggests that, at least in this type of tumors, the association of chemotherapy and CDK6

inhibitors could be particularly effective. To confirm our *in vitro* results, we have evaluated CDK6, Cyclin D3, FOXO3 and ATR expression in HGEOC samples from patients who already received chemotherapy, supporting in this way the possibility that Cyclin D3/CDK6 complex plays a role in platinum response. Moreover, using OvMark online tool we found that combination of FOXO3 and CDK6 both expressed at high levels identified the group of patients with worse prognosis. In this work we show that CDK6/FOXO3 axis is necessary to control the DNA damage response in HGEOC cells through the regulation of ATR/CHK1 pathway.

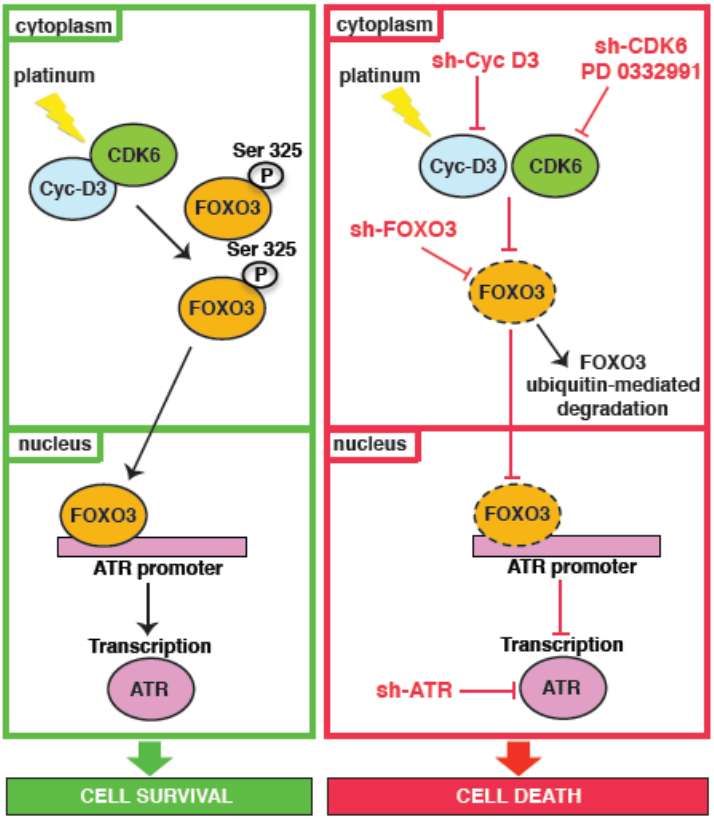

Figure 1: Proposed role of CDK6 in platinum sensitivity in HGEOC cells. Upon platinum treatment Cyclin D3-CDK6 binds and phosphorylate FOXO3, eventually regulating ATR expression. Inhibition of CDK6, FOXO3 or ATR may cause cell death via PCC in platinum treated cells.

This effect is highly reminiscent of the effects elicited on the related transcription factor FOXM1 that following CDK4/6 phosphorylation is stabilized and transactivated to prevent cancer cells to undergo senescence (Anders et al., 2011). Our results, in line with literature data, indicate that CDK6 is an important regulator of FOXO3, a member of FOXO family of transcription factors. Interestingly, Foxo3 knock-out in mice results in early depletion of functional ovarian follicles and in female sterility (Castrillon et al., 2003), further supporting a specific role for FOXO3 in ovarian cells and their response to external stimuli. In this work we identified a previously unknown

pathway that, in HGEOC cells prevents platinum induced cell death. In particular we discovered the specific CDK6 phosphorylation site on FOXO3 (Serine 325) and the role of this phosphorylation in terms of cell survival and response to platinum. In future studies, will be interesting to investigate in if FOXO3 S325 could be an actionable biomarker to predict platinum response. Finally we also demonstrated for the first time a role of FOXO3 as an ATR transcription factor upon phosphorylation by CDK6. Interestingly the link between CDK6 and DNA damage response (prevention from PCC) makes this pathway actionable and druggable and should be therefore further explored to improve response to platinum and prevent disease relapse in HGEOC patients.

Agarwal, R., and Kaye, S.B. (2003). **Ovarian cancer: strategies for overcoming resistance to chemotherapy.** *Nat Rev Cancer 3,* 502–516.

Alvarez-Calderon, F., Gregory, M., and DeGregori, J. (2013). **Using functional genomics to overcome therapeutic resistance in hematological malignancies.** *Immunol. Res. 55*, 100–115.

Anders, L., Ke, N., Hydbring, P., Choi, Y.J., Widlund, H.R., Chick, J.M., Zhai, H., Vidal, M., Gygi, S.P., and Braun, P. (2011). **A systematic screen for CDK4/6 substrates links FOXM1 phosphorylation to senescence suppression in cancer cells.** *Cancer Cell 20*, 620–634.

Arora, S., McCall, R., Cervantes, S.S., Young, L., Gonzales, I.M., Lal, D., Hinni, M.L., Hayden, R.E., and Azorsa, D.O. (2012). **Identification of sensitizers of platinum-based therapy in head and neck cancer using a functional genomics approach.** *Cancer Res. 72*, 5136–5136.

Asghar, U., Witkiewicz, A.K., Turner, N.C., and Knudsen, E.S. (2015). **The history and future of targeting cyclin-dependent kinases in cancer therapy.** *Nat. Rev. Drug Discov. 14*, 130–146.

Audeh, M.W., Carmichael, J., Penson, R.T., Friedlander, M., Powell, B., Bell-McGuinn, K.M., Scott, C., Weitzel, J.N., Oaknin, A., and Loman, N. (2010). **Oral poly (ADP-ribose) polymerase inhibitor olaparib in patients with BRCA1 or BRCA2 mutations and recurrent ovarian cancer: a proof-of-concept trial.** *The Lancet 376*, 245–251.

Baldassarre, G., Belletti, B., Nicoloso, M.S., Schiappacassi, M., Vecchione, A., Spessotto, P., Morrione, A., Canzonieri, V., and Colombatti, A. (2005). **p27(Kip1)-stathmin interaction influences sarcoma cell migration and invasion.** *Cancer Cell 7*, 51–63.

Belletti, B., Nicoloso, M., Schiappacassi, M., Chimienti, E., Berton, S., Lovat, F., Colombatti, A., and Baldassarre, G. (2005). **p27kip1 functional regulation in human cancer: a potential target for therapeutic designs.** *Curr. Med. Chem. 12*, 1589–1605.

Belletti, B., Pellizzari, I., Berton, S., Fabris, L., Wolf, K., Lovat, F., Schiappacassi, M., D'Andrea, S., Nicoloso, M.S., Lovisa, S., et al. (2010). **p27kip1 controls cell morphology and motility by regulating microtubule-dependent lipid raft recycling.** *Mol. Cell. Biol. 30*, 2229–2240.

Berton, S., Pellizzari, I., Fabris, L., D'Andrea, S., Segatto, I., Canzonieri, V., Marconi, D., Schiappacassi, M., Benevol, S., Gattei, V., et al. (2014). **Genetic characterization of p27(kip1) and stathmin in controlling cell proliferation in vivo.** *Cell Cycle 13*, 3100–3111.

Bowtell, D.D., Bohm, S., Ahmed, A.A., Aspuria, P.-J., Bast Jr, R.C., Beral, V., Berek, J.S., Birrer, M.J., Blagden, S., Bookman, M.A., et al. (2015). **Rethinking ovarian cancer II: reducing mortality from high-grade serous ovarian cancer.** *Nat Rev Cancer 15*, 668–679.

Braden, W., McClendon, A., and Knudsen, E. (2008). **Cyclin-dependent kinase 4/6 activity is a critical determinant of pre-replication complex assembly.** *Oncogene 27*, 7083–7093.

Brunet, A., Bonni, A., Zigmond, M.J., Lin, M.Z., Juo, P., Hu, L.S., Anderson, M.J., Arden, K.C., Blenis, J., and Greenberg, M.E. (1999). **Akt promotes cell survival by phosphorylating and inhibiting a Forkhead transcription factor.** *Cell 96*, 857–868.

Brunet, A., Park, J., Tran, H., Hu, L.S., Hemmings, B.A., and Greenberg, M.E. (2001). **Protein kinase SGK mediates survival signals by phosphorylating the forkhead transcription factor FKHRL1 (FOXO3a).** *Mol. Cell. Biol. 21*, 952–965.

Cancer Genome Atlas Research Network (2011). **Integrated genomic analyses of ovarian carcinoma.** *Nature 474*, 609–615.

Canzonieri, V., Barzan, L., Franchin, G., Vaccher, E., Talamini, R., Sulfaro, S., and Baldassarre, G. (2012). **Alteration of G1/S transition regulators influences recurrences in head and neck squamous carcinomas**. *J. Cell. Physiol. 227*, 233–238.

Castellarin, M., Milne, K., Zeng, T., Tse, K., Mayo, M., Zhao, Y., Webb, J.R., Watson, P.H., Nelson, B.H., and Holt, R.A. (2013). **Clonal evolution of high-grade serous ovarian carcinoma from primary to recurrent disease.** *J. Pathol. 229*, 515–524.

Castrillon, D.H., Miao, L., Kollipara, R., Horner, J.W., and DePinho, R.A. (2003). **Suppression of ovarian follicle activation in mice by the transcription factor Foxo3a.** *Science 301*, 215–218.

Chan, S.L., and Mok, T. (2010). **PARP inhibition in BRCA-mutated breast and ovarian cancers.** *The Lancet 376*, 211–213.

Chen, D., Law, M.E., Theis, J.D., Gamez, J.D., Caron, L.B., Vrana, J.A., Dogan, A., and Remstein, E.D. (2009). **Clinicopathologic features of CDK6 translocation-associated B-cell lymphoproliferative disorders.** *Am. J. Surg. Pathol. 33*, 720-729

Choi, Y., and Anders, L. (2014). **Signaling through cyclin D-dependent kinases.** *Oncogene 33*, 1890–1903.

Choi, Y.J., Li, X., Hydbring, P., Sanda, T., Stefano, J., Christie, A.L., Signoretti, S., Look, A.T., Kung, A.L., and von Boehmer, H. (2012). **The requirement for cyclin D function in tumor maintenance.** *Cancer Cell 22*, 438–451.

Ciccia, A., and Elledge, S.J. (2010). **The DNA Damage Response: Making It Safe to Play with Knives.** *Mol. Cell 40*, 179–204.

Cimprich, K.A., and Cortez, D. (2008). **ATR: an essential regulator of genome integrity.** *Nat. Rev. Mol. Cell Biol. 9*, 616–627.

Cooke, S.L., and Brenton, J.D. (2011). **Evolution of platinum resistance in high-grade serous ovarian cancer.** *Lancet Oncol. 12*, 1169–1174.

Copeland, N.A., Sercombe, H.E., Wilson, R.H.C., and Coverley, D. (2015). **Cyclin‐A–CDK2‐mediated phosphorylation of CIZ1 blocks replisome formation and initiation of mammalian DNA replication.** *J. Cell Sci. 128*, 1518–1527.

Esashi, F., Christ, N., Gannon, J., Liu, Y., Hunt, T., Jasin, M., and West, S.C. (2005). **CDK-dependent phosphorylation of BRCA2 as a regulatory mechanism for recombinational repair.** *Nature 434*, 598–604.

Falck, J., Forment, J.V., Coates, J., Mistrik, M., Lukas, J., Bartek, J., and Jackson, S.P. (2012). **CDK targeting of NBS1 promotes DNA‐end resection, replication restart and homologous recombination.** *EMBO Rep. 13*, 561–568.

Galluzzi, L., Senovilla, L., Vitale, I., Michels, J., Martins, I., Kepp, O., Castedo, M., and Kroemer, G. (2012). **Molecular mechanisms of cisplatin resistance.** *Oncogene 31*, 1869–1883.

Grossel, M.J., and Hinds, P.W. (2006a). **Beyond the cell cycle: a new role for Cdk6 in differentiation.** *J. Cell. Biochem. 97*, 485–493.

Grossel, M.J., and Hinds, P.W. (2006b). **From cell cycle to differentiation: an expanding role for cdk6.** *Cell Cycle 5*, 266–270.

Holmes, D. (2015). **Ovarian cancer: beyond resistance.** *Nature 527*, S217–S217.

Hu, M.C.-T., Lee, D.-F., Xia, W., Golfman, L.S., Ou-Yang, F., Yang, J.-Y., Zou, Y., Bao, S., Hanada, N., Saso, H., et al. (2004). **IκB Kinase Promotes Tumorigenesis through Inhibition of Forkhead FOXO3a.** *Cell 117*, 225–237.

Hu, M.G., Deshpande, A., Enos, M., Mao, D., Hinds, E.A., Hu, G., Chang, R., Guo, Z., Dose, M., and Mao, C. (2009). **A requirement for cyclin-dependent kinase 6 in thymocyte development and tumorigenesis.** *Cancer Res. 69*, 810–818.

Jayson, G.C., Kohn, E.C., Kitchener, H.C., and Ledermann, J.A. (2014a). **Ovarian cancer.** *The Lancet 384*, 1376–1388.

Kaufman, B., Shapira-Frommer, R., Schmutzler, R.K., Audeh, M.W., Friedlander, M., Balmaña, J., Mitchell, G., Fried, G., Stemmer, S.M., and Hubert, A. (2014). **Olaparib monotherapy in patients with advanced cancer and a germline BRCA1/2 mutation.** *J. Clin. Oncol. 33*, 244-250

Kelland, L. (2007). **The resurgence of platinum-based cancer chemotherapy.** *Nat. Rev. Cancer 7,* 573–584.

Kohrt, D., Crary, J., Zimmer, M., Patrick, A., Ford, H., Hinds, P.W., and Grossel, M.J. (2014). **CDK6 binds and promotes the degradation of the EYA2 protein.** *Cell Cycle 13*, 62–71.

Kollmann, K., Heller, G., Schneckenleithner, C., Warsch, W., Scheicher, R., Ott, R.G., Schäfer, M., Fajmann, S., Schlederer, M., and Schiefer, A.-I. (2013). **A kinase-independent function of CDK6 links the cell cycle to tumor angiogenesis**. *Cancer Cell 24*, 167–181.

Konecny, G.E., Winterhoff, B., Kolarova, T., Qi, J., Manivong, K., Dering, J., Yang, G., Chalukya, M., Wang, H.-J., and Anderson, L. (2011). **Expression of p16 and retinoblastoma determines response to CDK4/6 inhibition in ovarian cancer.** *Clin. Cancer Res. 17*, 1591–1602.

Larochelle, S., Merrick, K.A., Terret, M.-E., Wohlbold, L., Barboza, N.M., Zhang, C., Shokat, K.M., Jallepalli, P.V., and Fisher, R.P. (2007). **Requirements for Cdk7 in the assembly of Cdk1/cyclin B and activation of Cdk2 revealed by chemical genetics in human cells.** *Mol. Cell 25*, 839–850.

Lehtinen, M.K., Yuan, Z., Boag, P.R., Yang, Y., Villén, J., Becker, E.B., DiBacco, S., de la Iglesia, N., Gygi, S., and Blackwell, T.K. (2006). **A conserved MST-FOXO signaling pathway mediates oxidative-stress responses and extends life span.** *Cell 125*, 987–1001.

Lewis, K.A., Lilly, K.K., Reynolds, E.A., Sullivan, W.P., Kaufmann, S.H., and Cliby, W.A. (2009). **Ataxia telangiectasia and rad3-related kinase contributes to cell cycle arrest and survival after cisplatin but not oxaliplatin.** *Mol. Cancer Ther. 8*, 855–863.

Liang, K., Gao, X., Gilmore, J.M., Florens, L., Washburn, M.P., Smith, E., and Shilatifard, A. (2015). **Characterization of Human Cyclin-Dependent Kinase 12 (CDK12) and CDK13 Complexes in C-Terminal Domain Phosphorylation, Gene Transcription, and RNA Processing.** *Mol. Cell. Biol. 35*, 928–938.

Lim, D., and Oliva, E. (2013). **Precursors and pathogenesis of ovarian carcinoma.** *Pathol.-J. RCPA 45*, 229–242.

Lim, S., and Kaldis, P. (2013). **Cdks, cyclins and CKIs: roles beyond cell cycle regulation.** *Development 140*, 3079–3093.

Lin, M., Zhang, Y., Li, A., Tang, E., Peng, J., Tang, W., Lu, L., Xiao, Y., Wei, Q., and Yin, L. (2015). **High-throughput RNAi screening of human kinases identifies predictors of clinical outcome in colorectal cancer patients treated with oxaliplatin.** *Oncotarget 6*, 16774-16785

Lord, C.J., and Ashworth, A. (2013). **Mechanisms of resistance to therapies targeting BRCA-mutant cancers.** *Nat Med 19*, 1381–1388.

Malumbres, M., and Barbacid, M. (2005). **Mammalian cyclin-dependent kinases.** *Trends Biochem. Sci. 30*, 630–641.

Malumbres, M., and Barbacid, M. (2009). **Cell cycle, CDKs and cancer: a changing paradigm.** *Nat. Rev. Cancer 9*, 153–166.

Malumbres, M., Sotillo R., Santamaria D., Galàn J., Cerezo, A., Ortega, S., Dubus, P., and Barbacid, M. (2004). **Mammalian cells cycle without the D-type cyclin-dependent kinases Cdk4 and Cdk6.** *Cell 118*, 493–504.

Malumbres, M., Harlow, E., Hunt, T., Hunter, T., Lahti, J.M., Manning, G., Morgan, D.O., Tsai, L.-H., and Wolgemuth, D.J. (2009). **Cyclin-dependent kinases: a family portrait.** *Nat Cell Biol 11*, 1275–1276.

Maréchal, A., and Zou, L. (2013). **DNA damage sensing by the ATM and ATR kinases.** Cold Spring Harb. *Perspect. Biol.5,* a012716

Meyerson, M., and Harlow, E. (1994). **Identification of G1 kinase activity for cdk6, a novel cyclin D partner.** *Mol. Cell. Biol. 14*, 2077–2086.

Nemet, J., Jelicic, B., Rubelj, I., and Sopta, M. (2014). **The two faces of Cdk8, a positive/negative regulator of transcription.** *Biochimie 97*, 22–27.

Nghiem, P., Park, P.K., Kim, Y., Vaziri, C., and Schreiber, S.L. (2001). **ATR inhibition selectively sensitizes G1 checkpoint-deficient cells to lethal premature chromatin condensation.** *Proc. Natl. Acad. Sci. 98*, 9092–9097.

Nigg, E.A. (2001). **Mitotic kinases as regulators of cell division and its checkpoints.** Nat Rev *Mol Cell Biol 2*, 21–32.

Nijman, S.M.B. (2015). **Functional genomics to uncover drug mechanism of action.** *Nat Chem Biol 11*, 942–948.

Oza, A.M., Cibula, D., Benzaquen, A.O., Poole, C., Mathijssen, R.H., Sonke, G.S., Colombo, N., Špaček, J., Vuylsteke, P., and Hirte, H. (2015). **Olaparib combined with chemotherapy for recurrent platinum-sensitive ovarian cancer: a randomised phase 2 trial.** *Lancet Oncol. 16*, 87–97.

Patch, A.-M., Christie, E.L., Etemadmoghadam, D., Garsed, D.W., George, J., Fereday, S., Nones, K., Cowin, P., Alsop, K., Bailey, P.J., et al. (2015). **Whole–genome characterization of chemoresistant ovarian cancer.** *Nature 521*, 489–494.

Pathak, H., Zhou, Y., Sethi, G., Hirst, J., Schilder, R., Golemis, E., and Godwin, A. (2014). **A Synthetic Lethality Screen Using a Focused siRNA Library to Identify Sensitizers to Dasatinib Therapy for the Treatment of Epithelial Ovarian Cancer**. *PloS One 10*, e0144126

Placke, T., Faber, K., Nonami, A., Putwain, S.L., Salih, H.R., Heidel, F.H., Krämer, A., Root, D.E., Barbie, D.A., and Krivtsov, A.V. (2014). **Requirement for CDK6 in MLL-rearranged acute myeloid leukemia.** *Blood 124*, 13–23.

Prat, J. (2015). **Staging classification for cancer of the ovary, fallopian tube, and peritoneum: abridged republication of guidelines from the International Federation of Gynecology and Obstetrics (FIGO).** *Obstet. Gynecol. 126*, 171–174.

Ross, J.S., Ali, S.M., Wang, K., Palmer, G., Yelensky, R., Lipson, D., Miller, V.A., Zajchowski, D., Shawver, L.K., and Stephens, P.J. (2013). **Comprehensive genomic profiling of epithelial ovarian cancer by next generation sequencing-based diagnostic assay reveals new routes to targeted therapies.** *Gynecol. Oncol. 130*, 554–559.

Rybaczek, D., and Kowalewicz-Kulbat, M. (2011). **Premature chromosome condensation induced by caffeine, 2-aminopurine, staurosporine and sodium metavanadate in S-phase arrested HeLa cells is associated with a decrease in Chk1 phosphorylation, formation of phospho-H2AX and minor cytoskeletal rearrangements.** *Histochem. Cell Biol. 135*, 263–280.

Scheicher, R., Hoelbl-Kovacic, A., Bellutti, F., Tigan, A.-S., Prchal-Murphy, M., Heller, G., Schneckenleithner, C., Salazar-Roa, M., Zöchbauer-Müller, S., Zuber, J., et al. (2014). **CDK6 as a key regulator of hematopoietic and leukemic stem cell activation.** *Blood 125*, 90–101.

Schiappacassi, M., Lovat, F., Canzonieri, V., Belletti, B., Berton, S., Di Stefano, D., Vecchione, A., Colombatti, A., and Baldassarre, G. (2008). **p27Kip1 expression inhibits glioblastoma growth, invasion, and tumor-induced neoangiogenesis.** *Mol. Cancer Ther. 7*, 1164–1175.

Schwartz, G.K., and Shah, M.A. (2005). **Targeting the cell cycle: a new approach to cancer therapy.** *J. Clin. Oncol. 23*, 9408–9421.

Sethi, G., Pathak, H.B., Zhang, H., Zhou, Y., Einarson, M.B., Vathipadiekal, V., Gunewardena, S., Birrer, M.J., and Godwin, A.K. (2012). **An RNA interference lethality screen of the human druggable genome to identify molecular vulnerabilities in epithelial ovarian cancer.** *PloS One 7*, e47086

Shapiro, G.I. (2006). **Cyclin-dependent kinase pathways as targets for cancer treatment.** J. *Clin. Oncol. 24*, 1770–1783.

Sherr, C.J., and Roberts, J.M. (1999). **CDK inhibitors: positive and negative regulators of G1-phase progression.** *Genes Dev. 13*, 1501–1512.

Shih, I.-M., and Kurman, R.J. (2004). **Ovarian Tumorigenesis: A Proposed Model Based on Morphological and Molecular Genetic Analysis.** *Am. J. Pathol. 164*, 1511–1518.

Siddik, Z.H. (2003). **Cisplatin: mode of cytotoxic action and molecular basis of resistance.** *Oncogene 22*, 7265–7279.

Sonego, M., Schiappacassi, M., Lovisa, S., Dall'Acqua, A., Bagnoli, M., Lovat, F., Libra, M., D'Andrea, S., Canzonieri, V., Militello, L., et al. (2013). **Stathmin regulates mutant p53 stability and transcriptional activity in ovarian cancer.** *EMBO Mol. Med. 5*, 707–722.

Tan, T.Z., Miow, Q.H., Huang, R.Y., Wong, M.K., Ye, J., Lau, J.A., Wu, M.C., Hadi, L.H.B.A., Soong, R., and Choolani, M. (2013). **Functional genomics identifies five distinct molecular subtypes with clinical relevance and pathways for growth control in epithelial ovarian cancer.** *EMBO Mol. Med. 5*, 1051–1066.

Tigan, A.-S., Bellutti, F., Kollmann, K., Tebb, G., and Sexl, V. (2015). **CDK6 a review of the past and a glimpse into the future: from cell-cycle control to transcriptional regulation.** *Oncogene. (Epub ahead of print)*

Toogood, P.L., Harvey, P.J., Repine, J.T., Sheehan, D.J., VanderWel, S.N., Zhou, H., Keller, P.R., McNamara, D.J., Sherry, D., and Zhu, T. (2005). **Discovery of a potent and selective inhibitor of cyclin-dependent kinase 4/6.** *J. Med. Chem. 48*, 2388–2406.

Tran, H., Brunet, A., Grenier, J.M., Datta, S.R., Fornace, A.J., DiStefano, P.S., Chiang, L.W., and Greenberg, M.E. (2002). **DNA repair pathway stimulated by the forkhead transcription factor FOXO3a through the Gadd45 protein.** *Science 296*, 530–534.

Tsai, W.-B., Chung, Y.M., Takahashi, Y., Xu, Z., and Hu, M.C.-T. (2008). **Functional interaction between FOXO3a and ATM regulates DNA damage response.** *Nat. Cell Biol. 10*, 460–467.

Tzivion, G., Dobson, M., and Ramakrishnan, G. (2011). **FoxO transcription factors; Regulation by AKT and 14-3-3 proteins.** *Biochim. Biophys. Acta 1813*, 1938–1945.

Vecchione, A., Belletti, B., Lovat, F., Volinia, S., Chiappetta, G., Giglio, S., Sonego, M., Cirombella, R., Onesti, E.C., Pellegrini, P., et al. (2013). **A microRNA signature defines chemoresistance in ovarian cancer through modulation of angiogenesis.** *Proc. Natl. Acad. Sci. U. S. A. 110*, 9845–9850.

Waddell, N., Pajic, M., Patch, A.-M., Chang, D.K., Kassahn, K.S., Bailey, P., Johns, A.L., Miller, D., Nones, K., and Quek, K. (2015). **Whole genomes redefine the mutational landscape of pancreatic cancer.** *Nature 518*, 495–501.

Wiedemeyer, W.R., Dunn, I.F., Quayle, S.N., Zhang, J., Chheda, M.G., Dunn, G.P., Zhuang, L., Rosenbluh, J., Chen, S., and Xiao, Y. (2010). **Pattern of retinoblastoma pathway inactivation dictates response to CDK4/6 inhibition in GBM.** *Proc. Natl. Acad. Sci. 107*, 11501–11506.

Wohlbold, L., and Fisher, R.P. (2009). **Behind the wheel and under the hood: Functions of cyclin-dependent kinases in response to DNA damage.** *Checkp. Response DNA Damage 8*, 1018–1024.

Xie, Q., Chen, J., and Yuan, Z. (2012). **Post-translational regulation of FOXO.** *Biochim. Biophys. Acta. Sin. 44*, 897–901.

Xu, N., Libertini, S., Black, E., Lao, Y., Hegarat, N., Walker, M., and Gillespie, D. (2012). **Cdk-mediated phosphorylation of Chk1 is required for efficient activation and full checkpoint proficiency in response to DNA damage.** *Oncogene 31*, 1086–1094.

Yang, J.-Y., and Hung, M.-C. (2009). **A new fork for clinical application: targeting forkhead transcription factors in cancer.** *Clin. Cancer Res. 15*, 752–757.

Yang, J.-Y., Zong, C.S., Xia, W., Yamaguchi, H., Ding, Q., Xie, X., Lang, J.-Y., Lai, C.-C., Chang, C.-J., Huang, W.-C., et al. (2008). **ERK promotes tumorigenesis by inhibiting FOXO3a via MDM2-mediated degradation.** *Nat Cell Biol 10*, 138–148.

Yata, K., and Esashi, F. (2009). **Dual role of CDKs in DNA repair: to be, or not to be.** *DNA Repair 8*, 6–18.

Zegerman, P. (2015). **Evolutionary conservation of the CDK targets in eukaryotic DNA replication initiation.** *Chromosoma 3*, 309-321.

PUBLICATIONS

1. **"Stathmin regulates mutant p53 stability and transcriptional activity in ovarian cancer."**
   Sonego M, Schiappacassi M, Lovisa S, **Dall'Acqua A**, Bagnoli M, Lovat F, Libra M, D'Andrea S, Canzonieri V, Militello L, Napoli M, Giorda G, Pivetta B, Mezzanzanica D, Barbareschi M, Valeri B, Canevari S, Colombatti A, Belletti B, Del Sal G, Baldassarre G.
   EMBO Mol Med. 2013 May

2. **"SUMOylation regulates p27Kip1 stability and localization in response to TGFβ."**
   Lovisa S, Citro S, Sonego M, **Dall'Acqua A**, Ranzuglia V, Berton S, Colombatti A, Belletti B, Chiocca S, Schiappacassi M, Baldassarre G.
   J Mol Cell Biol. 2015 Oct

3. **" CDK6 phosphorylates FOXO3 to prevent platinum-induced cell death in epithelial ovarian cancer cells."**
   Alessandra Dall'Acqua, Maura Sonego, Ilenia Pellizzari, Ilenia Pellarin, Vincenzo Canzonieri, Sara D'Andrea, Sara Benevol, Roberto Sorio, Giorgio Giorda, Loredana Militello, Daniela Califano, Gennaro Chiappetta, Joshua Armenia, Barbara Belletti, Monica Schiappacassi, and Gustavo Baldassarre.
   Submitted

Vorrei fare un ringraziamento speciale a tutte le persone che mi hanno permesso di raggiungere questo importante traguardo…

A Marco, ai miei genitori e mia sorella Francesca, per avermi sostenuto, sopportato e insegnato che nella vita non bisogna mai farsi sopraffare dalle proprie insicurezze.

Alla Dott.ssa Monica Schiappacassi e al Dott. Gustavo Baldassarre per avermi insegnato tutto ciò che ho imparato in questi anni, per avermi dato l'opportunità di seguire questo progetto e per avermi spronato a dare il massimo.

A tutto lo SCICC LAB per i suggerimenti e discussioni costruttive durante i Lab meeting, per il supporto tecnico, morale e soprattutto perché dietro ad un "bel lavoro" c'è anche il sostegno di chi, con te, condivide il bancone, il posto sotto cappa o l'ansia di una presentazione.